Scholar Commons
USF University of South Florida

University of South Florida
Digital Commons @ University of South Florida

USF Tampa Graduate Theses and Dissertations | USF Graduate Theses and Dissertations

July 2021

Preparation and Characterization of Single Layer Conducting Polymer Electrochromic and Touchchromic Devices

Sharan Kumar Indrakar
University of South Florida

Follow this and additional works at: https://digitalcommons.usf.edu/etd

Part of the Chemical Engineering Commons, Materials Science and Engineering Commons, and the Polymer Chemistry Commons

Scholar Commons Citation

Indrakar, Sharan Kumar, "Preparation and Characterization of Single Layer Conducting Polymer Electrochromic and Touchchromic Devices" (2021). *USF Tampa Graduate Theses and Dissertations.*
https://digitalcommons.usf.edu/etd/9685

This Dissertation is brought to you for free and open access by the USF Graduate Theses and Dissertations at Digital Commons @ University of South Florida. It has been accepted for inclusion in USF Tampa Graduate Theses and Dissertations by an authorized administrator of Digital Commons @ University of South Florida. For more information, please contact scholarcommons@usf.edu.

Preparation and Characterization of Single Layer Conducting Polymer Electrochromic and Touchchromic Devices

by

Sharan Kumar Indrakar

A dissertation submitted in partial fulfillment
of the requirements for the degree of
Doctor of Philosophy
Department of Electrical Engineering
College of Engineering
University of South Florida

Major Professor: Elias Stefanakos, Ph.D.
Arash Takshi, Ph.D.
Sylvia Thomas, Ph.D.
Ashok Kumar, Ph.D.
Sesha Srinivasan, Ph.D.

Date of Approval:
July 02, 2021

Keywords: Electrochromism, Touchchromism, Composite Gel, Polyaniline, Asymmetric Electrode

Copyright © 2021, Sharan Kumar Indrakar

Dedication

This thesis is wholeheartedly dedicated to my beautiful parents who have raised me to be the person I am today, my family who believed in the richness of learning, my friends who supported and encouraged me.

Lastly, I dedicate this thesis to mother nature. Thank you for being a constant source of motivation and inspiration.

Acknowledgments

My deep gratitude goes first to Dr. Elias Stefanakos, who expertly guided me through my Ph.D. degree and who shared the excitement of five years of discovery. His unwavering enthusiasm for nanochemistry kept me constantly engaged with my research. I am thankful to Dr. Stefanakos for his professional guidance and encouragement for all these years. I am honored to be one of his students.

I am also thankful to the Ph.D. committee members - Dr. Arash Takshi, Dr. Sylvia Thomas, Dr. Ashok Kumar, and Dr. Sesha Srinivasan - for their valuable suggestions and for helping me reach my goal. I have learned many lessons under their mentorship, which would be helpful forever in my life. A special appreciation and thanks go to Dr. Manoj Ram and Dr. Arash Takshi for their keen interest in this study at every stage of my research. Their prompt inspiration, timely suggestions with kindness, and dynamics have enabled me to complete my thesis.

In addition, I would like to thank the Electrical Engineering Department and Material Science Department for allowing me to use the laboratory facilities, Florida Polytechnic University for technical support, and the USF staff who helped me through these years.

My appreciation also extends to my friends Deena Martina, Anil Kumar, and Sriram Konakanchi, whose encouragement has been valuable. Many thanks to all my colleagues in the CERC group at USF and UNT Denton. Sai Rohit and Nandita Ghodki, thank you very much for your time. Special thanks to Sai Bharadwaj for making me feel at home during my time at USF and helping me survive all the stress.

Above all I am indebted to my parents, whose values have helped me grow with age.

Table of Contents

List of Tables iv

List of Figures v

Abstract ix

Chapter 1: Introduction 1
1.1 Background 1
1.2 Research Objectives 3
1.3 Scope of the Research Work 4

Chapter 2: Literature Review 6
2.1 Chromatic Devices 6
2.1.1 Touch Chromism 7
2.1.2 Color Change Mechanism of the Touchchromic Device and Energy Band Diagram 8
2.1.3 Electrochromism 12
2.1.4 Multi-Layer Organic EC Devices 12
2.2 Conjugated Polymers 13
2.3 Polypyrrole 15
2.4 Polythiophene 16
2.5 Polyaniline 17
2.5.1 Introduction 17
2.5.2 Polymerization Mechanism 18
2.5.3 Morphology of Polyaniline 18
2.5.4 Applications of Polyaniline 19

Chapter 3: Electrochemical Materials and Methods Used for Fabrication and Characterization of Devices 21
3.1 Introduction 21
3.2 Fabrication of Electrochromic Devices 22
3.3 Synthesis of PANI Film 23
3.4 Synthesis of Polyaniline and Dye Solution 24
3.5 Electrochemical Deposition of Conducting Polymer Composite 25
3.6 Preparation of Single Active Composite Gel Electrolyte 26
3.6.1 Preparation of PVA Gel 26
3.6.2 Preparation of Liquid Electrolyte 26
3.6.3 Preparation of (PVA+HCl+APS+PANI) Gel 26

3.7 Characterization 27
3.7.1 Cyclic Voltammetry 27
3.7.2 Chronopotentiometry 29
3.7.3 Electrochemical Impedance Spectroscopy 29
3.7.4 Scanning Electron Microscopy 29
3.7.5 Fourier Transform Infrared Spectroscopy 31
3.7.6 UV-Visible Spectroscopy 31

Chapter 4: Touchchromic Device Based on Nanocomposite Polymer-Dye Film 32
4.1 Background 32
4.2 Results and Discussion 32
4.3 Conclusions 42

Chapter 5: Single Active Layer Electrochromic Devices 43
5.1 Background 43
5.2 Methods 44
5.2.1 Preparation 44
5.2.2 Device Preparation and Measurements 45
5.3 Results and Discussion 45
5.3.1 Physical Characterization 45
5.3.2 Cyclic Voltametric and Spectroscopic Studies 48
5.3.3 Electrochemical Impedance Spectroscopy 51
5.4 Mechanism of Single Layer Based Electrochromism 53
5.5 Mechanism of Gelling the Single Layer EC Device 54
5.6 Conclusions 56

Chapter 6: Single Active Layer Electrochromic Device with Different Colors 57
6.1 Background 57
6.2 Materials and Methods 58
6.3 Results and Discussion 60
6.3.1 SEM Studies 60
6.3.2 UV-Vis Studies 61
6.3.3 UV-Visible Absorption of Composite Gel 63
6.3.4 Cyclic Voltammetry Studies 64
6.4 Observations 66
6.5 Conclusions 69

Chapter 7: Lower Power and Longer Lifetime Asymmetric Electrode Single Active Layer Electrochromic Devices 71
7.1 Background 71
7.2 Materials and Methods 71
7.2.1 Materials 71
7.2.2 Characterization 72
7.3 Results and Discussion 72
7.3.1 Cyclic Voltammetry Studies 72

7.3.2 Mechanism of Color Change 73
7.4 Conclusions 75

Chapter 8: Conclusion and Recommendations for Future Research 76
8.1 Conclusion 76
8.2 Recommendations for Future Research 77

References 78

Appendix A: Copyrights and Permissions 85

List of Tables

Table 2-1 Types of Chromism.....7

Table 4-1 Types of Electrolytes and Time of Color Change 41

Table 4-2 Rate of Color Change for Different Concentrations of KCl+APS Electrolyte.....42

Table 6-1 Experimental Conditions and Dye, Aniline, PVA Gel Required to Obtain Active One-Layer Electrochromic Material 59

Table 6-2 Chemical Structure of the Dyes and Pictures of their Reduced and Oxidized States, taken from Videos of EC devices Operating in the Voltage Range of -0.7 to 2 Volts.....59

List of Figures

Figure 1-1 World Energy Consumption by Source 1

Figure 1-2 Schematic Diagram of an EC window in (a) Transparent (b) Colored state; (c) Dimmable Electronic Window from Boeing 787 Dreamliner Airplane 2

Figure 2-1 Chromic Phenomena 6

Figure 2-2 Schematic of a Thin Film Structure for Color Change 8

Figure 2-3 Difference in Color Before and After Metal Touch 8

Figure 2-4 (a) The States of PANI with Electrolyte and Metal Contact, (b) The Metal Ion is Oxidized in the Presence of Oxidant and Acid, (c) the Formation of Pernigraniline to Leucoemeraldine with Metal Contact 9

Figure 2-5 The Mechanism of Color Change in the PANI System while in Contact with a Metal in the Presence of an Electrolyte 10

Figure 2-6 Band Diagrams of Individual Layers and Composite Smart Material Film 11

Figure 2-7 Schematic of EC Device 12

Figure 2-8 Multi-Layer Configuration of an Electrochromic Device 13

Figure 2-9 Chemical Structures of Various Conducting Polymers 14

Figure 2-10 Schematic Illustration of Applications of Conducting Polymers and their Composites 14

Figure 2-11 Structure of Polypyrrole 15

Figure 2-12 Structure of Polythiophene 16

Figure 2-13 Structure of Polyaniline 17

Figure 2-14 Aniline Polymerization Mechanism 19

Figure 2-15 SEM Micrograph of PANI 19

Figure 2-16 Applications of PANI 20

Figure 3-1 Fabrication of Electrochromic Device 22

Figure 3-2 Oxidation of Aniline in a Medium Containing Ammonium Persulfate and HCl 23

Figure 3-3 In-Situ Self-Assembly of Polyaniline Film 24

Figure 3-4 Chemical Preparation Process of PANI films 25

Figure 3-5 Electrochemical Synthesis of PANI Film (a) Under no Applied Voltage, and (b) Under Applied Voltage 25

Figure 3-6 Preparation of Single Active Layer Composite Gel Electrolyte 27

Figure 3-7 Structure of Polyaniline in (a) General Form, (b) Reduced Form, (c) Oxidized Form. 28

Figure 3-8 Typical Cyclic Voltammetry Curve of Polyaniline 29

Figure 3-9 Scanning Electron Microscopy 30

Figure 3-10 Fourier Transform Infrared Spectroscopy 30

Figure 3-11 UV-Visible Spectroscopy 31

Figure 4-1 UV-Visible Spectra of Chromatic Devices having a Polyaniline-Dye Active Layer treated with Various Electrolytes 33

Figure 4-2 UV-Visible Spectra of a Chromatic Device having a Polyaniline-Dye Active Layer treated with Magnesium Chloride ($MgCl_2$)+Ammonium Persulphate (APS) Electrolyte, both with and without Contact with a Metal. 34

Figure 4-3 UV-Visible Spectra for a Chromatic Device having a Polyaniline-Dye Active Layer and treated with Potassium Chloride (KCl)+APS Electrolyte, both with and without Contact with a Metal 35

Figure 4-4 UV-Visible Spectra for a Chromatic Device having a Polyaniline-Dye Active Layer treated with Sodium Chloride (NaCl)+APS Electrolyte, both with and without Contact with a Metal 35

Figure 4-5 Raman Spectra of a Chromatic Device having a Polyaniline-Dye Active Layer Deposited on a Silicon Substrate treated with Various Electrolytes 36

Figure 4-6 Fourier Transformed Infrared (FTIR) Spectra of a Chromatic Device having a Polyaniline-Dye Active Layer Deposited on a Silicon Substrate treated with Various Electrolytes 37

Figure 4-7 (A-F) are Scanning Electron Microscope (SEM) images of Chromatic Devices having Polyaniline-Dye Active Layers with and without treatment with an Electrolyte 39

Figure 4-8 (A-F) are Photographs Showing the Color Change of a Chromatic Device with a Polyaniline-Dye Active Layer treated with KCl+APS Electrolyte 40

Figure 5-1 (a) Schematic and Real Pictures of a Device with an All in One Active Layer (PVA+APS+MB+PANI) biased at 1.5 -2.0 V for the Colored State and at 0 - -0.5 V for the Transparent State; (b) UV-Vis Spectra of (1) PVA+APS, (2) PVA+APS+MB, (3) PVA+APS+PANI and (4) PVA+APS+PANI+MB (the inset in Figure (b) Shows the UV-Vis Spectra of the PVA+APS Film on Glass Plate) 46

Figure 5-2 SEM Pictures of the PVA +APS+MB, PVA+APS+PANI or PVA +APS+PANI+MB on FTO Coated Glass Plates Dried at Room Temperature 47

Figure 5-3 FTIR Spectra of (1) PVA+APS, (2) PVA+APS+MB, (3) PVA+APS+PANI and (4) PVA+APS+PANI+MB 47

Figure 5-4 CVs of EC Devices Containing EC gels as a Function of Scan Rate. Figure (a) for PVA+APS+MB; Figure (b) for PVA+APS+PANI and Figure (c) for PVA+APS+MB +PANI. 49

Figure 5-5 Chronoamperometric Plots of (a) PVA+APS+MB, (b) PVA+APS+ PANI, and (c) PVA+APS+PANI+MB in the Single Active Layer Device; and (d) Absorption Change by the PVA+APS+PANI+MB Active Layer at an Excitation Wavelength of 550 nm is Changed for -0.2V and 1.5 V for between two FTO Coated Glass Plates 50

Figure 5-6 The Spectro-Electrochemical Study of PVA+APS+MB+PANI Gel base EC Device at Potential (1) 1.7 V and (2) -0.7 V 51

Figure 5-7 (a) Magnitude and Phase of the PVA+APS+PANI+MB Device Impedance vs Frequency at a Biasing Voltage of 0.0 V (Transparent Color) and 2.0 V (Dark Color). (b) Experimental and Simulation Results for the Complex Impedance of the Device at 0.0 V 53

Figure 5-8 (a) The Gelling Process of PVA in HCl; (b) The PVA-gel in HCl with Ammonium Persulfate (APS) Oxidant Process; (c) Emeraldine Salt Forms in the Presence of HCl and APS after Polymerization of Aniline to Emeraldine salt; (d) Emeraldine Salt Changes to Pernigraniline due to the Presence of APS and Oxidized PVA in APS; (e) Coloration and Decoloration due to the Application of a Voltage across the Single PVA+HCl +APS+MB+PANI Layer 55

Figure 6-1 SEM Pictures of Single Layer Gels for Different Dyes: (a) No Dye; (b) Methyl Orange (MO); (c) Methyl Viologen (MV); (d) Eosin (EO); (e) Congo Red (CR); (f) Rhodamine Blue (RB); and (g) Methylene Blue (MB) 61

Figure 6-2 UV-Visible Absorption Spectra of Active Gel Layers Containing Different Dyes 62

Figure 6-3 UV-Vis Absorption Spectra for Single Gel Electrolyte Layers with Different Dyes at Applied Voltages of 1.7 and -0.7 Volts 63

Figure 6-4 Cyclic Voltammetry Results of Various Dyes in the (PVA +APS+PANI) Active Gel Layer.....65

Figure 6-5 Chrono-Amperometry Results of Active Layers in EC Devices.....65

Figure 6-6 Coloration and Decoloration of the (PVA+APS+ MO +PANI) Active Layer EC Device 67

Figure 6-7 Coloration and Decoloration of the Composite (PVA+APS+ CR +PANI) Active Layer EC Device 68

Figure 6-8 Chemical Structures explaining the Coloration and Decoloration of a Composite PVA+APS+ RB +PANI All in One Layer EC Device.....69

Figure 7-1 Systematic Representation of Symmetric and Asymmetric Electrochromic Device Configuration at Different Bias Voltages.....72

Figure 7-2 Cyclic Voltametric Analysis of Composite Gel PVA-HCl-APS-PANI with Symmetric and Asymmetric Electrode Device Configuration with a Scan Rate of 50 mV/s 73

Figure 7-3 Gelling process of the Composite Gel: a) The Gelling Chemical process of PVA in HCl; b) The PVA-HCl gel with Ammonium Persulfate (APS); c) The Interaction of PVA-HCl gel with APS and PANI after Polymerization; and d) Chemical Reactions in three Different Oxidation States of PANI 74

Abstract

Electrochromic devices (ECDs) have triggered great interest because of their potential applicability in energy-efficient buildings and low power display systems, including reflective type smart windows/mirrors and wearable-flexible devices. In the past decades, electrochromic technologies with different device structures and materials have been proposed. The idea of employing a simple device structure with a durable, cost effective electrolyte is crucial to designing and manufacturing high-performance ECDs. With this idea in mind, this thesis describes the various efforts to develop a simple ECD comprising of a composite single active layer gel electrolyte, sandwiched between two transparent conducting electrodes, lasting over 10,000 cycles with low power consumption. The research evolved through the development and testing of various ECD structures.

At first, a polymer composite dye-thin-film coated on a conducting substrate enabled a reversible color change from dark to transparent when the thin film was touched (touchchromic device) by a specific metal, without any other external excitation. The results showed that the coloration and decoloration depend upon the composition of the electrolyte, type of metals, film thickness, and the nature of the composite film. As simple as this idea may be, it turned out difficult to apply it to commercial devices.

In the second approach, a simple and potentially inexpensive electrochromic device was made, consisting of a single active composite gel layer placed between two transparent conducting fluorine-doped tin oxide glass plates. The single active layer gel electrolyte is a mixture of conducting polymer (polyaniline), polyvinyl alcohol (PVA), acid, oxidant, and synthetic dye. The

results showed color change in the ECDs from dark blue to transparent at an applied potential in the range of +1.5 V to – 1.5 V. The effects are explained in terms of the change in the chemical structure of the conducting polymer and synthetic dye at different bias voltages.

In the third approach, to obtain different colors, the gel was modified by adding different types of synthetic dyes to the single active PANI composite gel electrolyte. Polyvinyl alcohol, polyaniline, and ammonium persulfate intercalated with distinct synthetic dyes resulted in enhanced transmittance modulation and diverse colors at the oxidation and reduction peaks. The results showed that the redox characteristics of the dye greatly influence the overall oxidation and reduction potentials of the EC device's active gel layer.

Even though the single (all-in-one) active layer EC device is very attractive, for the case of water-based electrolytes it has exhibited a short lifecycle due to bubble formation when the applied voltage exceeds 1.23 volts (water electrolysis). This led to the concept of an asymmetric EC device. In the asymmetric electrode structure one of the fluorine-doped tin oxide electrodes was coated by a gold (Au) thin film. The results showed that asymmetric ECDs (two electrodes having different work functions) can operate within the smaller voltage window of -1 volt to +1 volt, requiring reduced operating power and overcoming the potential problem of bubble formation in the active ECD layer.

Chapter 1: Introduction

1.1 Background

In recent times, there has been a rapid increase in the demand and consumption of nonrenewable resources such as coal, gas, and oil as shown in figure 1-1. Moreover, this increase in energy consumption has led to the emission of harmful gases in the atmosphere leading to climate change. Global energy demand has tripled in the past 60 years, and is predicted to increase further in the next 20 years [1].

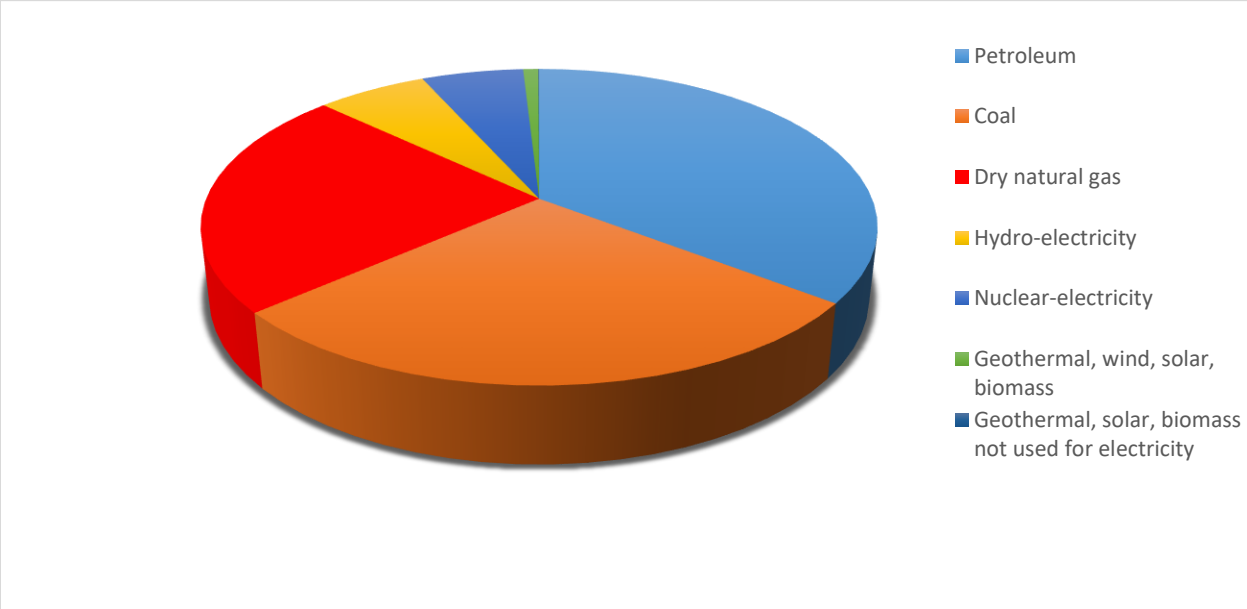

Figure 1-1 World Energy Consumption by Source.

Industrial and scientific communities have been coming together to address the energy crisis and develop novel techniques to overcome this issue. It is essential to promote and improve the rate of use of renewable resources and, at the same time, decrease the need for energy. For

instance, it has been found that energy losses through windows have been estimated to be in the range of 10-25% in residential buildings [2]. This suggests a need to improve the window properties according to the requirements of changing seasons to control the energy loss through windows.

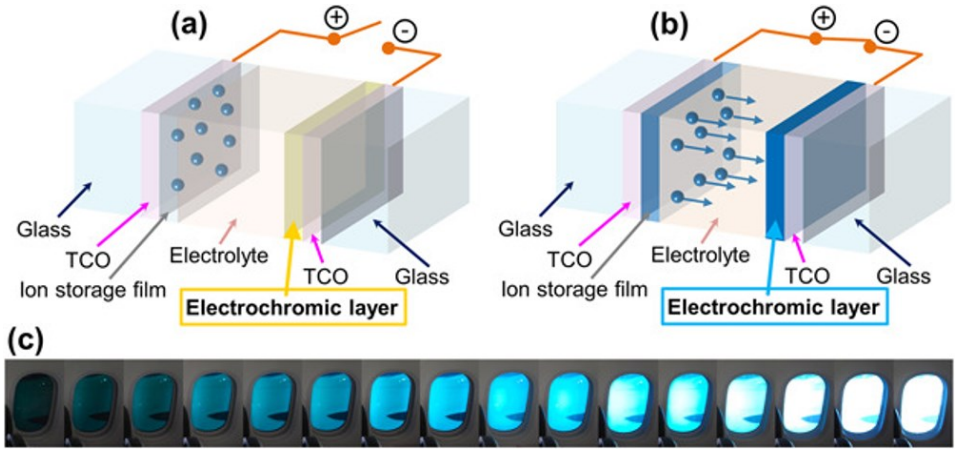

Figure 1-2 Schematic Diagram of an EC window in (a) Transparent (b) Colored state; (c) Dimmable Electronic Window from Boeing 787 Dreamliner Airplane [3]. By Mardare et al. © (2019) Wiley-VCH.

Electrochromic materials are a part of intelligent systems that can change their color upon the application of an external electric potential. Studies have shown [2,4] that electrochromic windows exhibit better energy efficiency. Various energy simulation studies [5–7] for office buildings have found that the energy consumption is reduced significantly when EC windows are used (figure 1-2)

Refurbishment of buildings with electrochromic windows is important for energy savings. Despite the advantages of using electrochromic materials in numerous practical applications, color change speed, ease of processing, electrolyte leakage, and device fabrication are pressing issues limiting their implementation in some practical applications. Therefore, there is a need to find new solutions and advancements to eliminate these drawbacks.

1.2 Research Objective

The main objective of this thesis is to develop a single active layer “all-in-one “gel electrolyte ECD that can be sandwiched between two fluorine doped tin oxide conductive substrates. The achievement of this objective has been pursued through the development and analysis of different ECD structures. The first ECD structure is composed of a polymer composite dye-thin -film coated on a conducting substrate. When touched (touch chromic) by a specific metal, the color changes from dark to transparent. Generally, such devices are easy to produce and have a low cost, however, their application is difficult.

The second ECD structure is composed of two electrodes containing a single active layer redox gel electrolyte. The electrolyte is made with a conducting polymer (polyaniline), polyvinyl alcohol (PVA), acid, oxidant, and dye synthesized by a chemical process.

The third ECD structure contains a redox-active single layer composite gel electrolyte and different synthetic dyes (i.e., methylene blue, methyl orange, methyl viologen, eosin, rhodamine b, and Congo red) to achieve different color ECDs.

All the above ECDs suffer from short lifetime due to bubble formation when the oxidizing voltage exceeds 1.23 volts (water electrolysis)

The fourth structure is a composite gel electrolyte placed between two electrodes having different surface work functions. The purpose of this device is to achieve lower power consumption and prevent bubble formation from water electrolysis in the gel layer. The two electrodes chosen for this task were two fluorine doped tin oxide coated on glass with one of the two coated with Gold (Au) (asymmetric electrodes).

The results presented in this dissertation are encouraging. Gel electrolytes are preferred over liquid electrolytes because of their lower cost and improved safety in practical devices.

Composite gels can enhance the transmittance modulation and provide a unique capability of a single layer. Asymmetric ECDs consume less power and operate for longer periods of time.

1.3 Scope of the Research Work

This research focuses on electrochromic devices composed of a single nanocomposite thin film gel electrolyte that consume minimum power, are cost effective and have long lifetime. The advancement of the research work is described in the following chapters.

Chapter 1 provides a brief overview of the energy consumption and commercial electrochromic windows operating at different modes, followed by information about the Research objective and organization of the dissertation.

Chapter 2 presents a literature review on chromism, followed by fundamental principles and configuration of Electrochromism and touch chromism and an investigation of different types of conjugated conducting polymers. The last part of chapter 2 is devoted to the polymerization mechanism and applications of polyaniline.

Chapter 3 focuses on the methodology and techniques used to evaluate the electrochemical materials and methods used to fabricate and test the ECDs.

Chapter 4 presents an innovative nanocomposite thin film electrochemically deposited on Fluorine doped tin oxide glass plate which enables reversible coloration and decoloration when touched by a specific metal (touch chromic).

Chapter 5 describes the use of a redox-active gel electrolyte as a single active layer for electrochromic device applications.

Chapter 6 applies the results of the previous chapters for the fabrication of electrochromic devices, with different synthetic dyes added to a conducting polymer (PANI), a water-soluble polymer polyvinyl alcohol (PVA), an oxidant, and acid.

Chapter 7 discusses a new asymmetric device obtained by replacing one of the electrodes with a gold (Au) plated glass electrode.

Chapter 8 concludes the study with the significant findings of the electrochromic devices with different redox-active gel electrolytes. This chapter also proposes recommendations for future work regarding the development of materials, fabrication process and electrochromic device applications.

Chapter 2: Literature Review

2.1 Chromatic Devices

Chromism can be defined as a process that induces a change, reversible or irreversible, in a material's color. Such color change can be brought about from various external stimuli such as temperature, pressure, electric field, light, and humidity many materials such as conjugated conducting polymers, dyes, oxides exhibit the chromic phenomenon. Recently, electrochromic devices have attracted significant attention in various applications such as color tunable glass windows, sensors, sunglasses, smart windows and molecular switches [8–12]. The color change occurs due to the flow of electrons in the electrolyte resulting in the oxidation/reduction of the specific materials. The different ways that light interacts with a material exhibiting the chromic phenomenon are shown in figure 2-1.

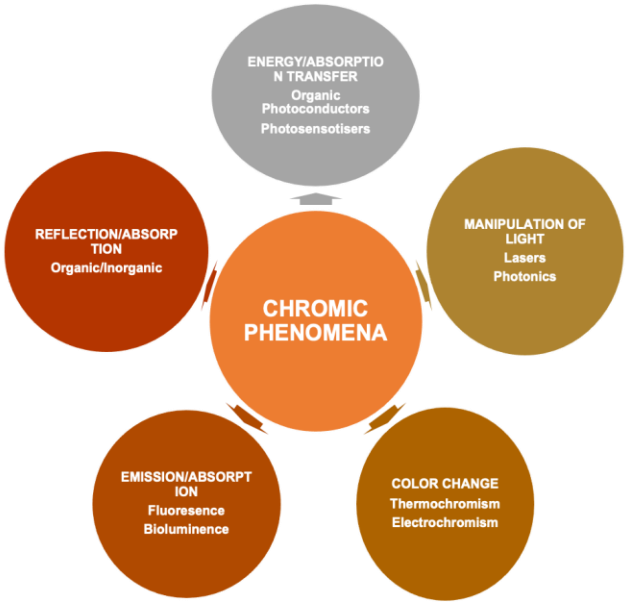

Figure 2-1 Chromic Phenomena

The color change depends on the applied external stimulus, and thus chromism can be described in various ways depending on different stimuli as shown in Table 2-1:

Table 2-1 Types of Chromism

Chromic Phenomena	**Stimuli**	**Reference**
Photochromism	Light	[13]
Thermochromism	Temperature	[14]
Electrochromism	Electrical current	[15]
Halochromism	pH Change	[16]
Magnetochromism	Magnetic field	[17]
Ionochromism	Ions	[18]
Tribochromism	Mechanically induced Friction	[19]
Biochromism	Biological sources	[20]

2.1.1 Touch Chromism

Touch chromic is a novel thin film-based nanocomposite layer device that changes color when the active polymer electrolyte is touched by a different metal (electrode), without any external excitation such as light, voltage, temperature, heat, etc. The building structure of the touch chromic device consists of a nanocomposite conducting polymer layer coated onto a fluorine-doped tin oxide (FTO) substrate as the chromic material, a liquid electrolyte and a metal pin used for the color change) as shown in figure 2-2. The coloration and decoloration depend on different types of composite film, film thickness, and the nature of the electrolyte. Figure 2-2 [21] shows the color change in the smart film when the metal pin is in contact and colorless when the pin is removed. The smart film changes color from green/blue to transparent and returns to its original color state upon removing the metal contact pin.

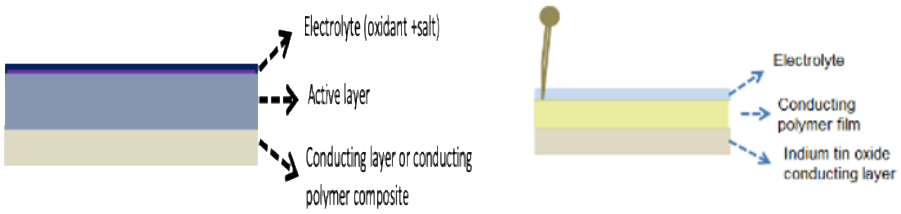

Figure 2-2 Schematic of a Thin Film Structure for Color Change [21]. By M. K. ram et al. © (2016) Elsevier.

Figure 2-3 shows pictures of the touch chromic device before and after metal contact. The liquid electrolyte can contain salt, oxidizer, and acid. The removal of the metal pin brings back the original color (figure 2-3).

Figure 2-3 Difference in Color Before and After Metal Touch

2.1.2 Color Change Mechanism of the Touchchromic Device and Energy Band Diagram

Figure 2-4a shows the doped structure of PANI in the electrolyte and contact with a metal pin. The doped form of Pernigraniline (PNB) is achieved by the presence of the electrolyte in PANI. The oxidant is the major contributor to the color change in the film when the conductive film is in contact with the electrolyte containing the oxidant APS and the acid [22]. The color of the film changes from purple to greenish to fade yellow with the metal contact. Figure 2-4 b helps understanding the color change mechanism. The reaction of the iron (+2) (Fe+2) state to the iron (+3) (Fe+3) oxidized state in the presence of the electrolyte [23]. The electron is released from the iron changing the PNB to the emeraldine and subsequently to the Leucoemeraldine (LEU) state of

the PANI. Figure 2-4 (c) shows the change of states of polymer and release of the electron in the presence of metal pin in contact. The metal contact is oxidized in the presence of acid and oxidant [24]. It releases electrons that combine with protons (hydrogen ions), reducing the PNB to its LEU form.

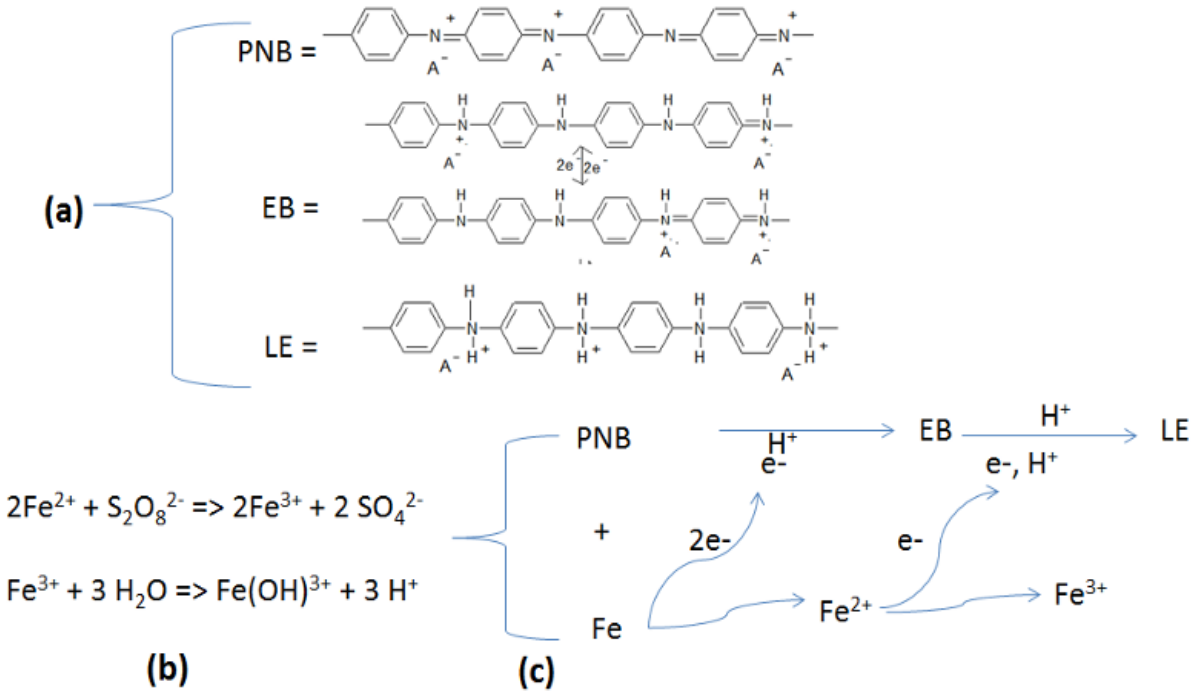

Figure 2-4 (a) The States of PANI with Electrolyte and Metal Contact. (b) The Metal Iron is Oxidized in the Presence of Oxidant and Acid, (c) the formation of Pernigraniline to Leucoemeraldine with Metal Contact [25]. By M. K. Ram et al. © USPTO.

The film goes back to its original color of PNB when the metal contact is removed. The structure of PANI from the doped form to the doped LEU is shown in figure 2-5. The coloration and de-coloration of the conductive film depend on the oxidation state of the conductive film, metal alloys were used to touch the electrolyte to produce the color change [26].

The color change mechanism can be explained using the energy bands and fermi levels of the individual components and the overall energy band diagram of the ECD structure [27]. The energy band structures of ITO, PANI, and gel electrolyte with and without the metal pin contact

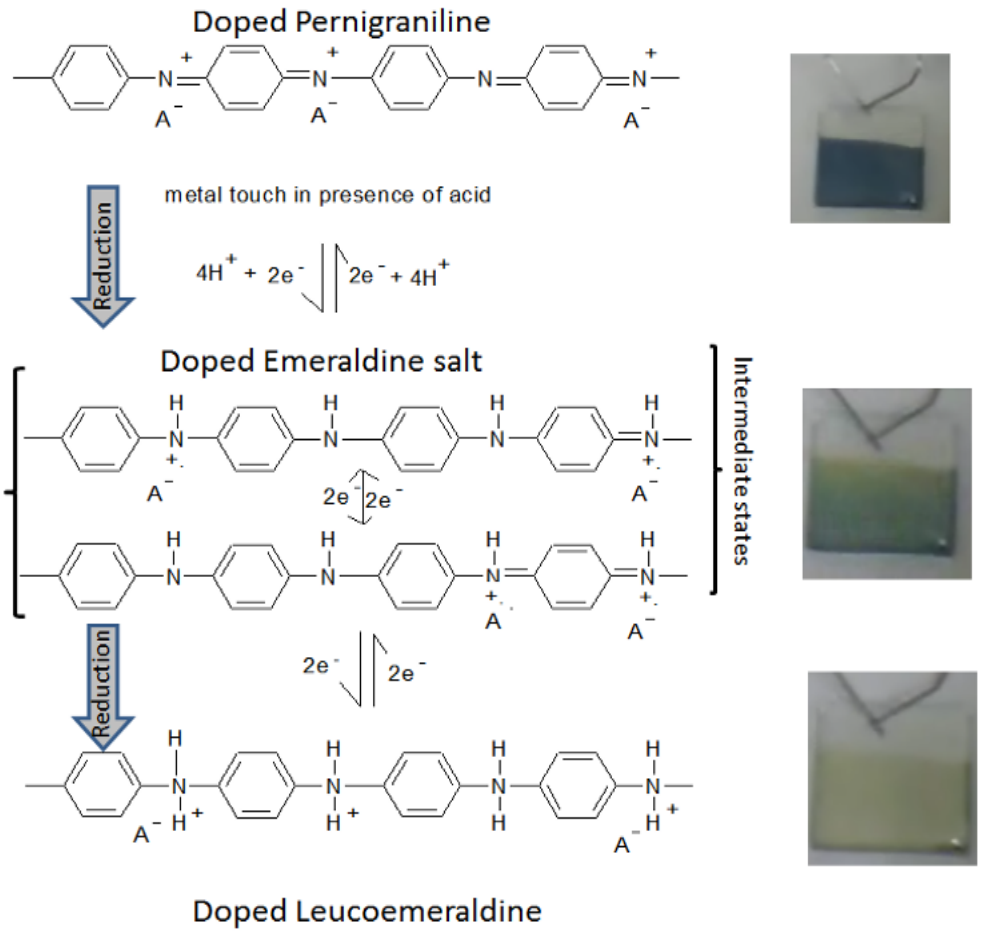

Figure 2-5 The Mechanism of Color Change in the PANI System while in Contact with a Metal in the Presence of an Electrolyte [21]. By M. K. ram et al. © (2016) Elsevier.

are shown in figure 2-6. based on the energy levels of PANI at different oxidation states. The coated polymer on the FTO substrate was emeraldine salt with a green color (bandgap = ~1.5 eV). The standard electrochemical potential of the oxidizer is (E0 = ~ 6.5 eV below vacuum), which is much lower than the Fermi level in PANI. Since polyaniline (emeraldine salt) is a p-type semiconductor and ITO is a high work function material (4.7 eV), the contact between ITO and the polymer is expected to be Ohmic with an upward band bending. There is also a higher Fermi level in PANI than the E0 in the liquid electrolyte, which shows the electron transfer from polymer to the liquid electrolyte. The transfer of an electron from polymer to the electrolyte brings the

Fermi level closer to the valance band, as shown in figure 2-6 b at the polymer-electrolyte interface. The electron transfer takes place from PANI to $S_2O_8^{2-}$, increases the concentration level of reduced ions (SO_4^{2-}), and the electrolyte Fermi level, E, adjusts to the equilibrium Fermi level.

A new equilibrium is achieved when the Fermi level of the contact metal is higher than that of the metal-polymer-electrolyte fermi level [27] as shown in figure 2-6 b, transfer of electrons to the electrolyte and subsequently to the conducting polymer takes place. The hydrogen ions together with the electrons from the electrolyte reduce the PANI and increase its energy band. The film structure changes from emeraldine to the leucoemeraldine form, a faded transparent yellow color. The flow of electrons and the diffusion of ions in the electrolyte bring about this change, as shown in figure 2-6 c. Conversely, removing the metal contact reverses the process and makes the polymer darker, as shown earlier in figure 2-5.

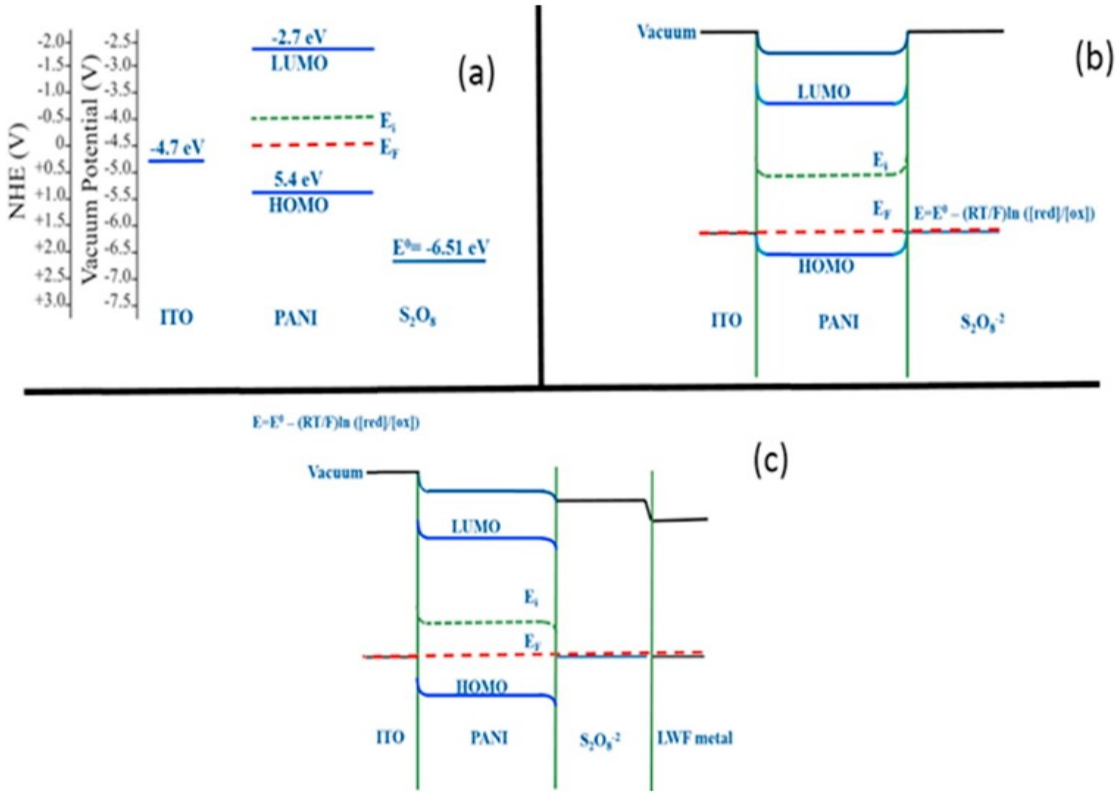

Figure 2-6 Band Diagrams of Individual Layers and Composite Smart Material Film [21]. By M. K. ram et al. © (2016) Elsevier.

2.1.3 Electrochromism

Electrochromism is the phenomenon where the color change occurs in the material due to the application of an electric field. This color change occurs due to the oxidation or reduction of the electrochromic material [28]. Materials that exhibit several redox states possess a unique ability to switch between different color states. Electrochromic materials find their applications in smart windows, optical display technology, antiglare mirrors, electrochromic sunglasses, etc [8,11,28]. Electrochromic materials are incorporated into electrochromic devices as thin films, to allow close contact with the electrodes and ensure the flow of electric current. Commercial inorganic EC devices (figure 2-7) contain a multi-layer structure that can be used to configure the properties by changing the applied voltage [29]. An excellent electrical conductivity among the layers is required for the stable and good performance of the EC device.

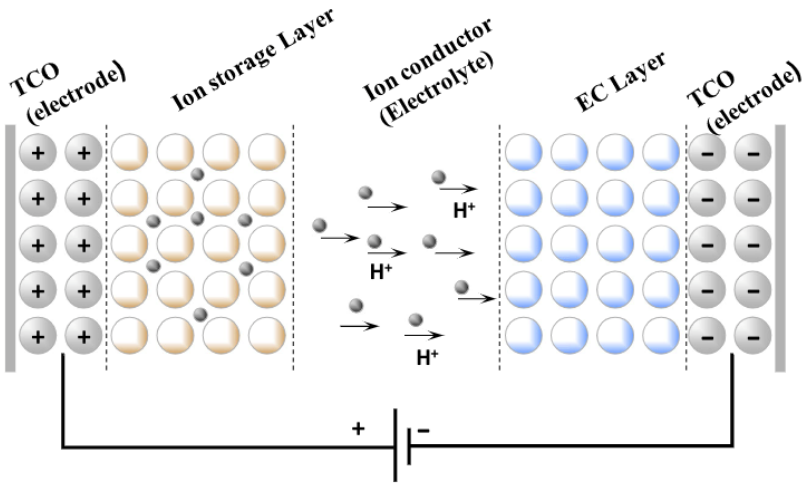

Figure 2-7 Schematic of EC Device [30]. By K. J. Patel et al. © (2016) SpringerLink.

2.1.4 Multi-Layer Organic EC Devices

Figure 2-8 shows an all-polymeric five-layer device configuration. The PEDOT layer is used as an electroactive layer, a poly (ethylene oxide-lithium triflate) electrolyte is deposited onto a commercial foil. When a voltage of 3 V is applied across the electroactive layers, the device

changes color from transparent blue to dark blue. The color change is due to reducing one of the electroactive layers with the other layer being oxidized. When the potential is switched again to 0 V, the device recovers its original state, i.e., transparent blue state. The coloration, decoloration, and color contrast depend on the applied voltages.

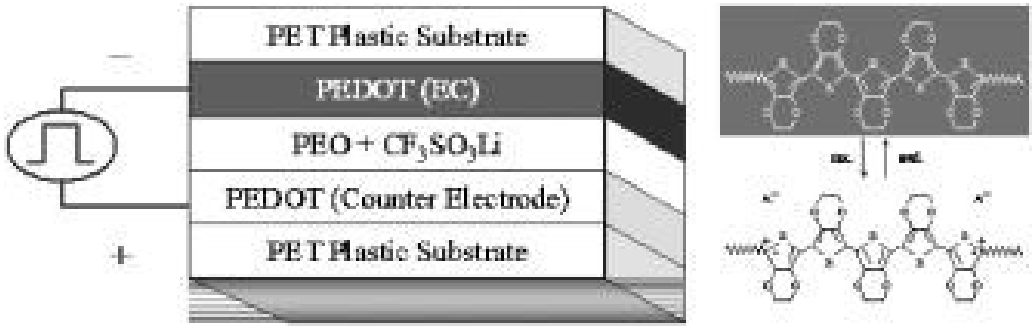

Figure 2-8 Multi-Layer Configuration of an Electrochromic Device [31]. By Ricardo Vergaz et al. © (2006) Society of Photo-Optical Instrumentation Engineers (SPIE).

2.2 Conjugated Polymers

For several decades, polymers have been insulators. It was found that a redox reaction known as doping could impart conductive properties to these polymers. The delocalization of π electrons along their backbone assists in enhancing the conductive properties and hence the name conjugated polymers [32]. The process of conversion from an insulating to a conducting material is known as the doping process [33]. Doping can be P-type and N-type. Doping can be achieved by the addition of an oxidizer/reducer or by an electrochemical synthesis route. Conjugated polymers have gained broad interest due to their thermal stability, electrical conductivity, and ease of preparation. Conjugated polymers have attracted attention in various applications such as supercapacitors, batteries, biosensors, electrochromic devices, light-emitting-diodes, etc (figure 2-10) [4,34]. Some commonly used conjugated polymers are polyaniline, polypyrrole, polythiophene, as shown in figure 2-9.

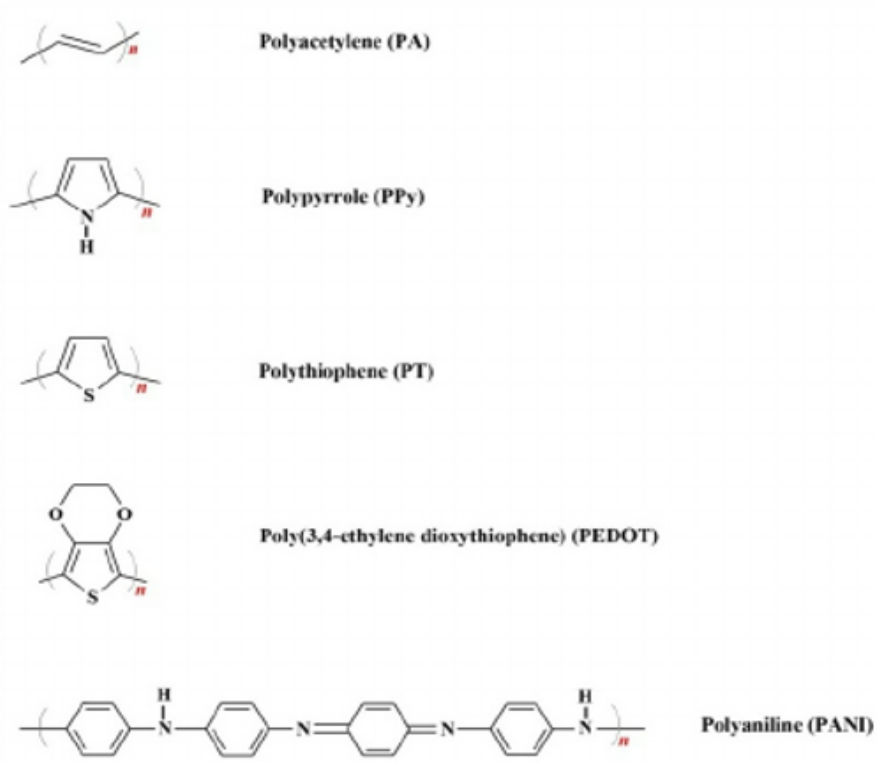

Figure 2-9 Chemical Structures of Various Conducting Polymers [35]. By M. Mozafari et al. © (2012) Licensee IntechOpen.

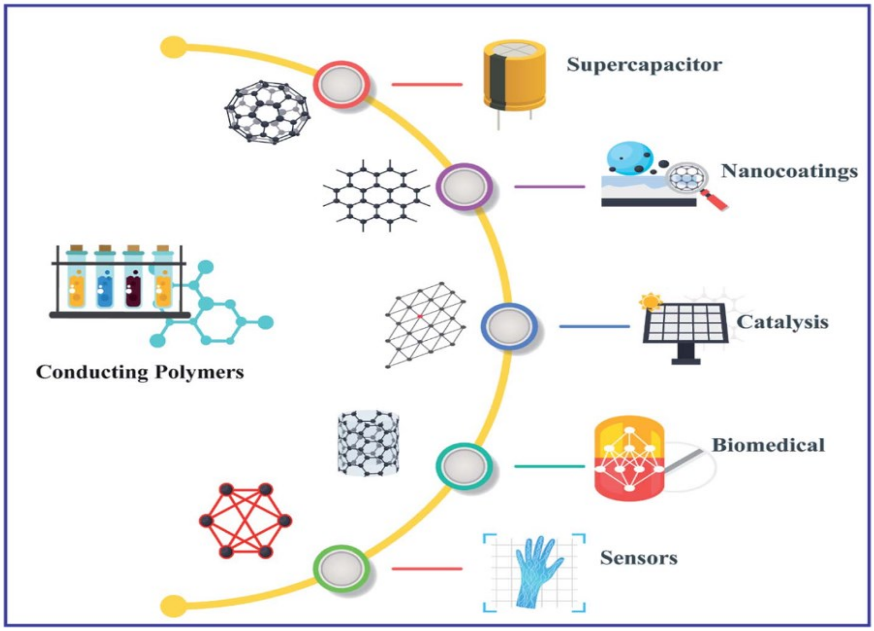

Figure 2-10 Schematic Illustration of Applications of Conducting Polymers and their Composites [36]. By Namsheer K. et al. © (2021) RSC Advances.

2.3 Polypyrrole

Polypyrrole (PPy) is a conducting polymer that has attracted various commercial applications due to its ease of synthesis, good environmental and thermal stability, and excellent electrical conductivity [37]. These conducting polymers are usually polyconjugated. That has good electrical properties while retaining the mechanical properties and ease of processing of conventional polymers (figure 2-11). The electrical conductivity in these polymers is due to the existence of conjugated electrons. PPy has found many potential commercial applications sensors, electronic devices, batteries, biomedical sensors and equipment, micro actuators, etc[38]. PPy possesses a positive charge in its oxidized form and loses its charge and conductivity by overoxidation. In its neutral state, PPy is insulating and mechanically weak. It possesses a suitable stimulus-response property that makes it an excellent smart biomaterial that allows active control of properties in the electrical field.

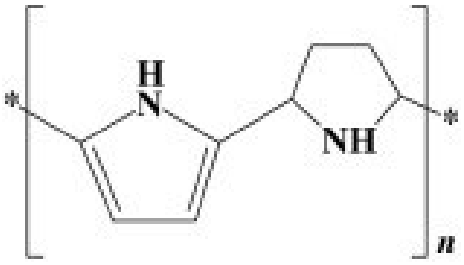

Figure 2-11 Structure of Polypyrrole [39]. Source by Wikipedia.

Recently, PPy has been used in various applications such as fuel cells, optical displays, corrosion protection, surgical tools, biosensors, and drug delivery systems. This is due to the ease of synthesis in bulk quantities using a range of solvents. PPy can be synthesized with varying porosities and surface areas such that it can be modified by integrating bioactive molecules that make it a promising biomaterial. It has been used in neural probes and prosthetics as a substrate to improve the connection between neurons and microelectrodes [37]. Efforts are being made to

improve the processability, conductivity, and thermal stability of this conducting polymer. Many researchers have reported various oxidants for synthesizing PPy. $FeCl_3$ has been a widely used oxidant to synthesize PPy films to study ammonia gas detection, while it has also been used for preparing PPy-graphene nanocomposites. There have been many reports of PPy composites and their enhanced properties such as biosensing, enhanced conductivity, and so on.

2.4 Polythiophene

Polythiophene is a conducting polymer that has attracted research and commercial areas due to its environmental and thermal stability and lower bandgap energy. The ability to form a better contact with the electrodes and room temperature stability makes them an ideal material for solar cells. Polythiophene composites have attracted special attention due to their interesting properties such as electronic, optical conductivity, semiconducting properties paired with a good mechanical properties and ease of processing[40]. It shows remarkable optical properties due to its transparent nature. Polythiophene has a network of conjugated double bonds in the backbone that imparts the conducting nature to the polymer (figure 2-12). Doping of polythiophene, which has a good hole transport with n-type semiconducting particles, has significantly improved the electrical properties. Like in other conducting polymers, oxidation or reduction can change the

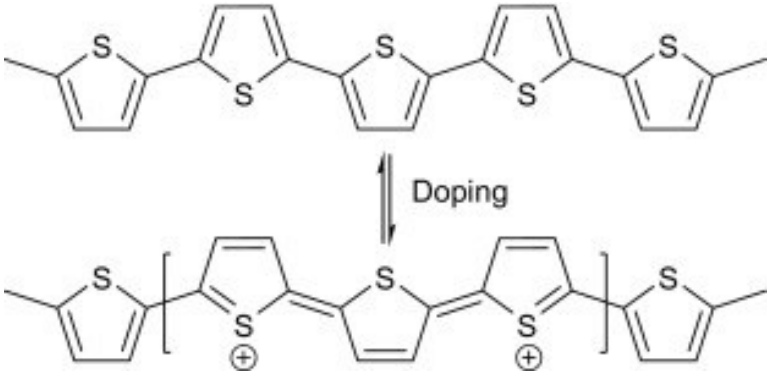

Figure 2-12 Structure of Polythiophene [41]. From Micro and Nano Fibrillar Composites (MFCs and NFCs) from Polymer Blends by M.T. Ramesan et al. © (2017) Elsevier.

polythiophene matrix to be more conductive by generating more polarons and bipolarons in the backbone. Utilizing these properties and characteristics of thiophene, it is used in electrochromic devices, batteries, solar cells, etc.

2.5 Polyaniline

2.5.1 Introduction

Polyaniline has been chosen for conducting this research. Polyaniline (PANI) is a conducting polymer, among many others, that has attracted attention for its reactivity, temperature resistance, excellent electrical conductivity, easy preparation, cost-effectiveness, and good environmental stability. Its phenylene ring has nitrogen and hydrogen bonds on either side [42]. It exists in various forms depending on the oxidation state. It has three majorly known oxide states, fully oxidized pernigraniline; semi-oxidized emeraldine which is the most stable and conductive, and fully reduced leucoemaraldine base.

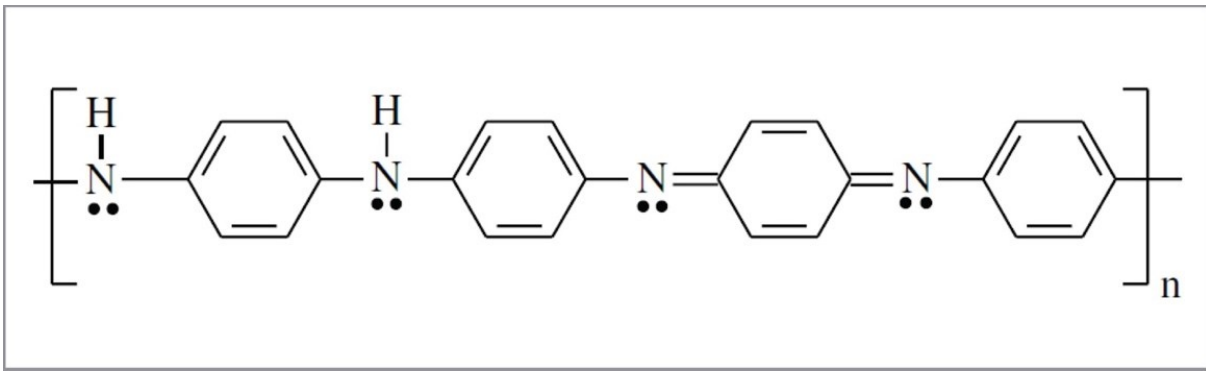

Figure 2-13 Structure of Polyaniline [44]. By M.A.C. Mazzeu et al. © Journal of Aerospace Technology and Management.

The emeraldine base of PANI is not readily soluble and requires specific solvents to process it. This is due to a rigid polymer backbone and the neighboring chain interaction by hydrogen bonding [43]. PANI has a wide range of visual displays, sensors, batteries, electrochromic devices, neural probes, biosensors, etc. [42]. One way of improving the properties

of PANI is the preparation of PANI-based composites comprising inorganic fillers. The inorganic nanoparticles and PANI act complementarily, providing a combination of properties such as conductivity, optical, and electrochemical properties. Such composites are widely used in electrochromic devices, light-emitting diodes, batteries, biosensors, etc.

Conducting PANI has an ordered chain structure with an alternating phenyl ring with a nitrogen group spaced regularly, as shown in figure 2-13. This arrangement helps in the process of polyconjugation, wherein the zig-zag polymer chain lies in one plane, and the electron clouds overlap this plane. A lone pair of electrons in a nitrogen atom acts the same as π-electron and helps in the process of polyconjugation, whose primary purpose is to provide mobility of charge carriers. In the chain of conducting PANI, the aniline units are associated with head-to-toe positioning [44]. Any irregularities or defects in this chain structure occurring during the copolymerization process or introduction of other configurations (ortho- or meta-) may lead to a reduction in conductivity.

2.5.2 Polymerization Mechanism

Figure 2-14 shows that the polymerization process starts with the transfer of electrons of the aniline nitrogen atom, forming a radical cation in polyaniline polymer. This radical cation further reacts with its resonant, which leads to the formation of an oxidized radical cation dimer. The formed radical reacts again with the radical monomer or dimer to form a trimer, and the pattern keeps on repeating until a long chain of PANI is formed.

2.5.3 Morphology of Polyaniline

The granular morphology of PANI powders is most common in PANI prepared by precipitation polymerization when using strong oxidants and high aniline concentrations under strongly acidic conditions, at pH < 2.5.

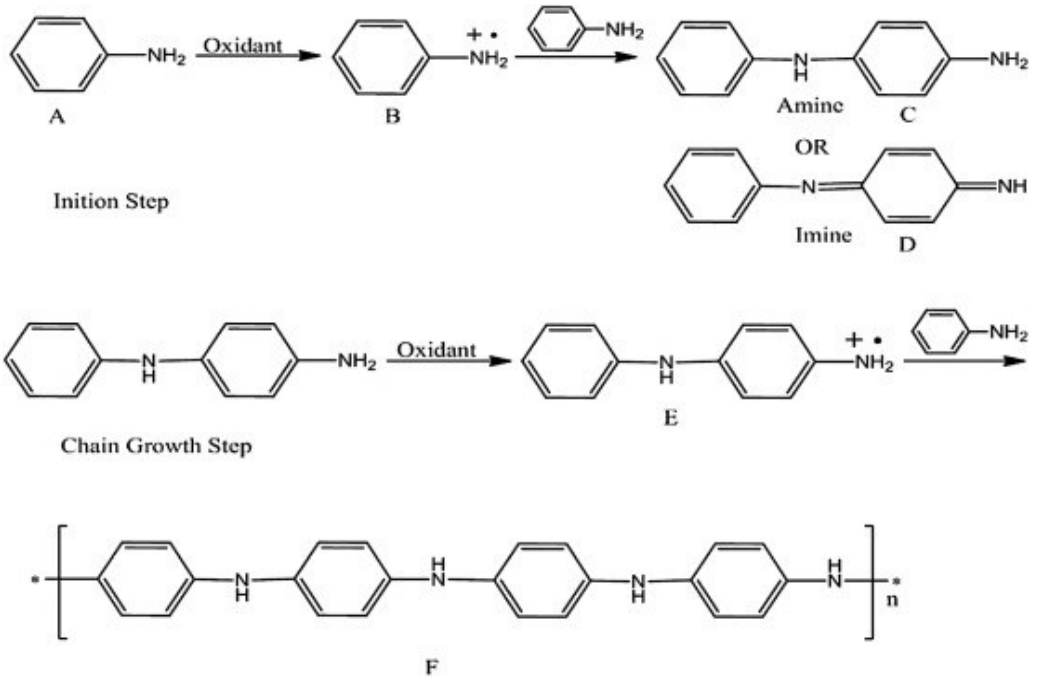

Figure 2-14 Aniline Polymerization Mechanism [45]. By T. David et al. © (2014) Elsevier.

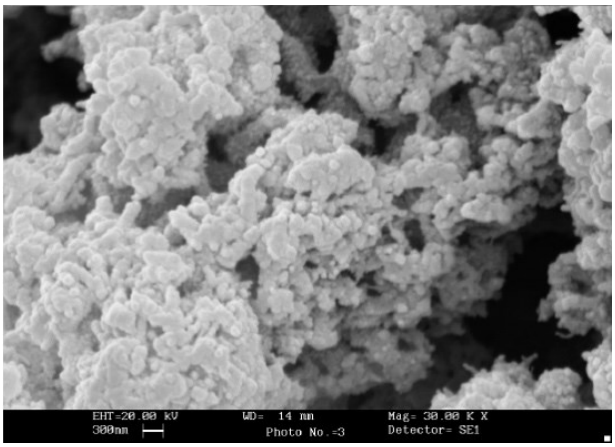

Figure 2-15 SEM Micrograph of PANI [46]. By A. Olad et al. © (2012) SpringerLink.

2.5.4 Applications of Polyaniline

Polyaniline (PANI) is an intrinsically conductive polymer used in various applications (figure 2-14), due to its following properties:

- High conductivity, lightweight and mechanical flexibility.
- Low cost, distinct oxidation states with different colors, and a response to acid/base doping.

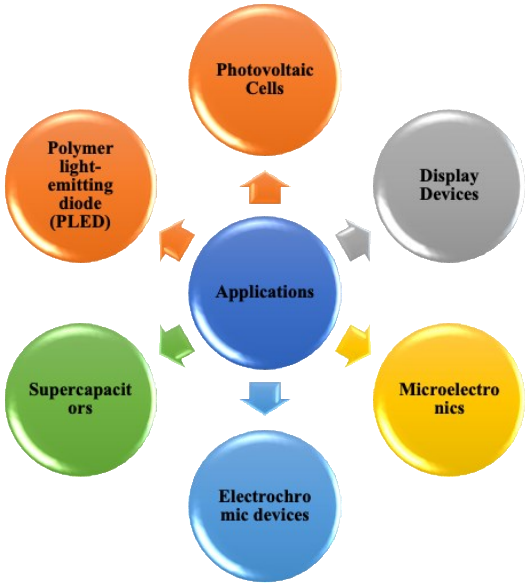

Figure 2-16 Applications of PANI

Chapter 3: Electrochemical Materials and Methods Used for Fabrication and Characterization of Devices

3.1 Introduction

In the previous chapter, chromism, different types of chromogenic materials, electrochromism and touchchromism were described. The nanocomposite gel used in the electrochromic device fabrication has been evaluated using specific electrochemical methods, materials, and characterization tools.

Therefore, this chapter exhibits basic electrochemical characterization methods used in the research activities, including cyclic voltammetry (CV), electrochemical impedance spectroscopy (EIS), chronoamperometry is discussed in this chapter. Also, some advanced spectroscopy characterization techniques used for studying the surface morphologies, structure, and physical properties of the nanocomposite gel are addressed herein. It should be noted that the materials and methods of device fabrication included as an experimental part of the published manuscripts in each of the following chapters.

All the listed chemical materials that were used in the experiments in this dissertation were purchased from Sigma-Aldrich and were used without any further purification. The materials are classified as salt (i.e., sodium chloride, magnesium chloride, iron chloride, and potassium chloride. Acid solution (i.e., hydrochloric acid, HCl with 95%), polymer materials (i.e., polyvinyl alcohol, PVA $(C_2H_4O)_x$), conducting polymer materials (i.e., aniline ($C_6H_5NH_2$)), synthetic dyes materials (i.e., methylene blue, MB ($C_{16}H_{18}ClN_3S_xH_2O$), methyl orange, MO ($C_{14}H_{14}N_3NaO_3S$), methyl Orange, methyl viologen, eosin dye, congo red and rhodamine blue), and oxidizing agents (i.e.,

ammonium persulfate, APS $(NH_4)_2S_2O_8$). The binder clip used for fabricating the device was from Office Depot (8.5 in. × 11 in.). Fluorine doped tin oxide conductive substrate (FTO) was purchased from Sigma-Aldrich with 1.66 mm and 12 Ω cm^{-2} sheet resistance.

3.2 Fabrication of Electrochromic Devices

Steps involved in device fabrication are:

1. Firstly, the FTO coated glass substrates were washed with DI water later cleaned with sonication in acetone and ethanol successively for 5 minutes before fabricating the devices.
2. Then a parafilm of 136-micron thickness in size is cut into a square shape and placed onto the conductive side of the FTO glass substrate.
3. After that, 0.5 ml of nanocomposite gel taken with the help of a syringe and applied onto the FTO glass substrate.
4. Then take a second substrate, sandwich them together such that there are aligned with the parafilm and the conducting surface facing each other to make the device.
5. Later, glue them with the superglue in all the directions and dry under a fan for 8 hours.

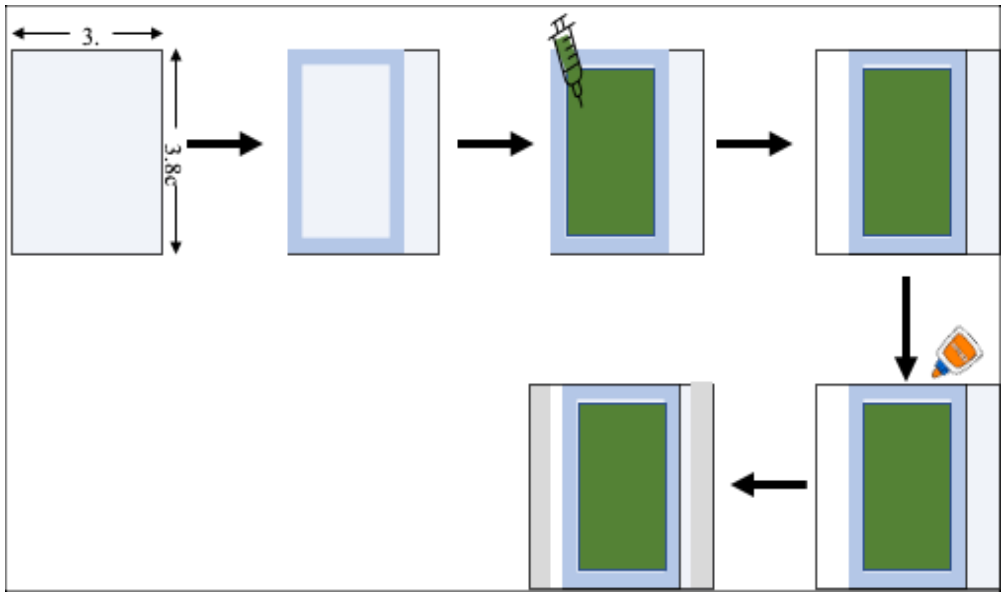

Figure 3-1 Fabrication of Electrochromic Device

3.3 Synthesis of PANI Film

The PANI film was deposited by the In-situ self-assembly technique, which provided a uniform PANI layer. FTO coated glass substrate were dipped in Poly (styrene sulfonate) PSS for 24 hours before depositing the PANI film. Poly (styrene sulfonate) PSS enhances the polymerization of PANI because of its negative charges [47]. To oxidize the polymer, A mixture of 5 ml aniline with 0.1 M APS in 1M HCL [48] is dissolved in 100 ml of DI water at room temperature. • Figure 3-2 shows the formation of emeraldine salt after the oxidation process in the aniline medium containing HCl and APS. Later, all the components are dissolved, FTO coated glass substrate with 3.8 cm in length, and breath is inserted into the mixture. The non-conductive side of the FTO coated glass substrate was taped to the glass breaker allowing the formation of the film on the conductive side. There is a slow stage of chemical reaction where the solution is colorless. The reaction accelerates when oligoaniline radicals are created, and the solution turns into a dark blue color [49]. These oligomers start adsorbing themselves on the surface of the

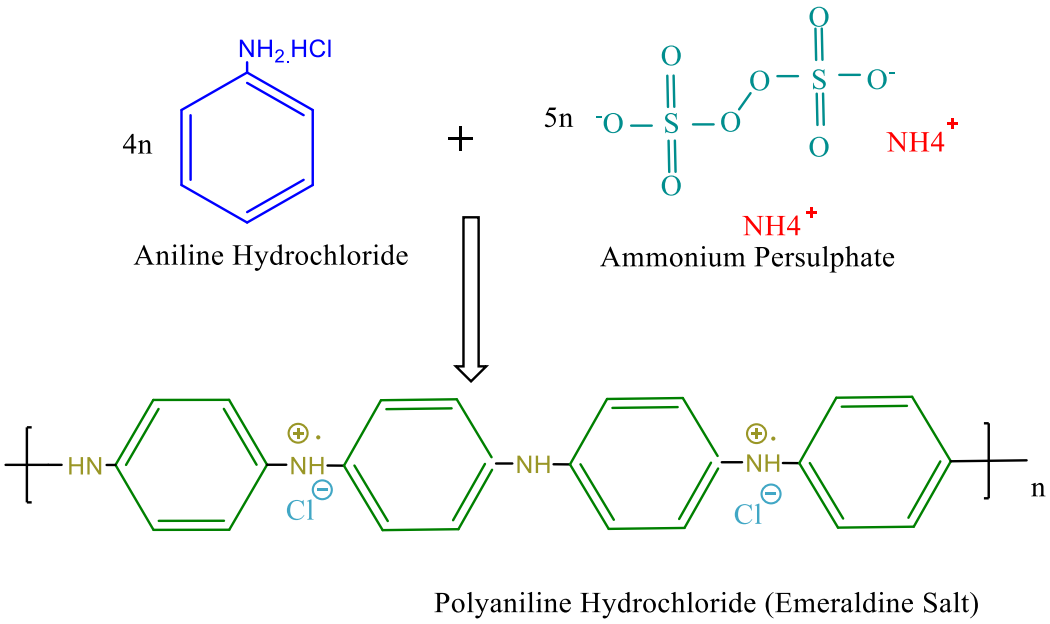

Figure 3-2 Oxidation of Aniline in a Medium Containing Ammonium Persulfate and HCl

conductive side of FTO coated glass substrates. Then, polymerization of aniline takes place, initiating the formation of the PANI chain. The film is spread on the substrate to form an emeraldine form of PANI; as shown in figure 3-3, the PANI thin film is deposited on the FTO coated glass substrate. After the polymerization, the FTO glass substrates are removed from the solution, rinsed with 1M HCl, and dried at room temperature.

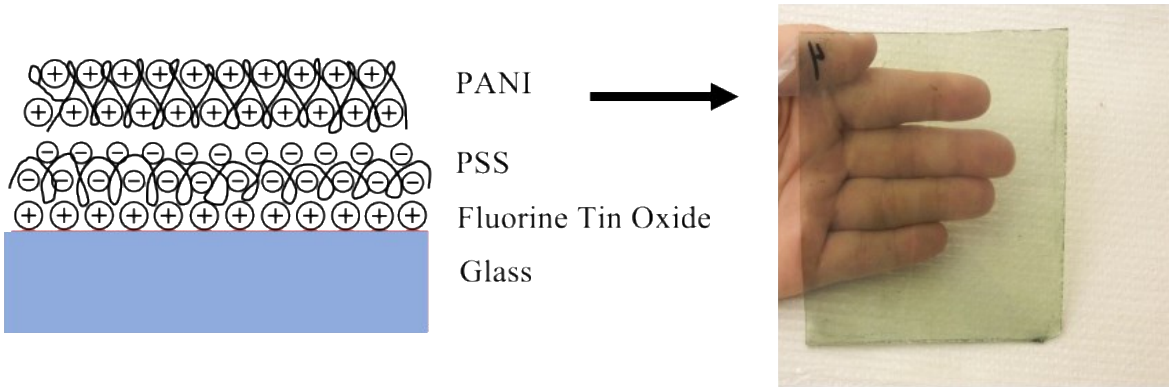

Figure 3-3 In-Situ Self-Assembly of Polyaniline Film

3.4 Synthesis of Polyaniline and Dye solution

In other to expand the color spectrum of the PANI thin film, Methylene Blue (MB) was incorporated: Methylene Blue dye is also known as methylthionium chloride, is a bluish fluorescent dye that is soluble in water. It is commonly used as a staining reagent and pharmaceutical agent.

The synthesis of polyaniline and dye solution is carried out in a four-step process.

1. The monomers of aniline 5ml are mixed with 1M HCl under continuous stirring for 1 hour.
2. After 1 hour, 0.01 M MB dye was slowly added to the mixture solution for 30 minutes, as shown in figure 3-4 [50].
3. Oxidizer 0.1 M APS was mixed with the same concentration of 1M HCl in another breaker.

4. Finally, the second and third mixtures were mixed in other to initiate the polymerization process.

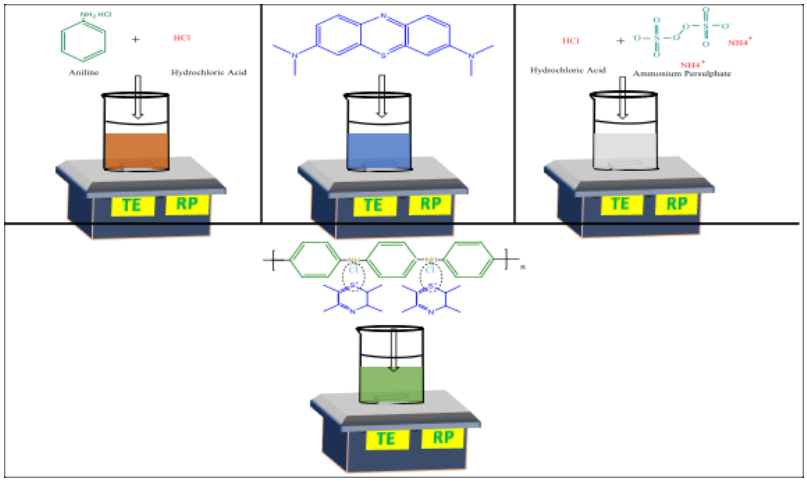

Figure 3-4 Chemical Preparation Process of PANI Films

3.5 Electrochemical Deposition of Conducting Polymer Composite

The Electrochemical deposition was used to make a polyaniline thin film with methylene blue dye, and it is another way to oxidize monomer. The electrochemical deposition was carried out at the electrode-electrolyte interface, consisting of an FTO coated glass slide with PANI film

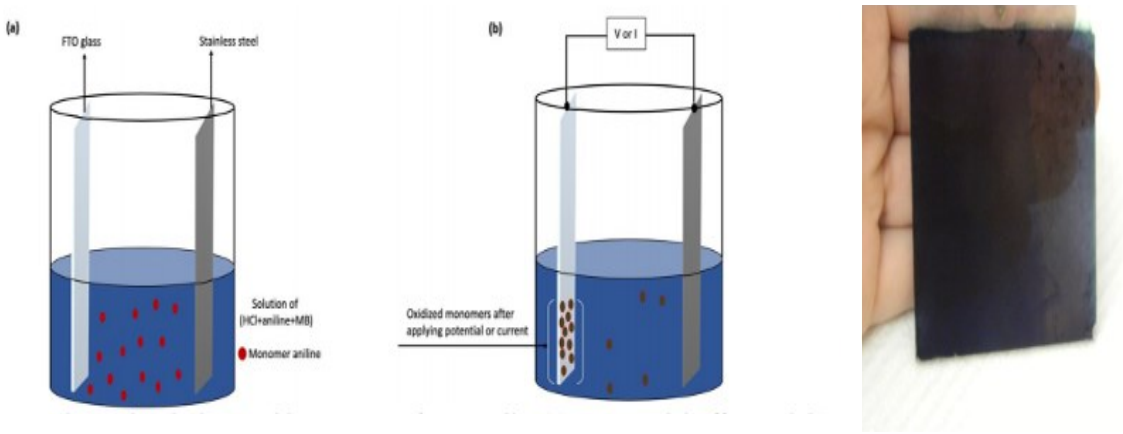

Figure 3-5 Electrochemical Synthesis of PANI Film (a) Under no Applied Voltage, and (b) Under Applied Voltage.

prepared In-situ self-assembly technique as a working electrode. The counter electrode was steel. When a positive potential is applied, the monomers get oxidized, and then again, two oxidized monomers come together to become dimer and then take them oxidized to become oligomer shown in figure 3-5. The oligomer is a combination of monomers that are not oxidized yet because polymerization needs at least 100, 200, or 300 monomers of aniline to form together, which is called the degree of polymerization.

3.6 Preparation of Single Active Composite Gel Electrolyte

The nanocomposite gel electrolyte process is mainly divided into three steps in this dissertation.

3.6.1 Preparation of PVA Gel

The first step for the PVA gel electrolyte preparation is shown in figure 3-6. 1M HCl is dissolved in 500 ml of DI water in a breaker under continuous stirring speed of 500 rpm at 800C for 12 hours till half of the solution evaporated out. The resultant product had a light sunset orange color and became a glue-like gelat room temperature.

3.6.2 Preparation of Liquid Electrolyte

The liquid electrolyte was prepared with HCl with a molarity concentration of 0.1 M dissolved at room temperature by simply mixing the acid solution with DI water under continuous stirring along with the APS oxidizer (concentration of 0.1 M) for 30 minutes (figure 3-6 b).

3.6.3 Preparation of (PVA+HCl+APS+PANI) Gel

The composite gel electrolyte is made by taking 10 ml of liquid electrolyte i.e., (1M HCl+0.1 M APS). Then, 40 ml of PVA gel (PVA-HCl solution) is added to the liquid electrolyte at room temperature and stirred for one hour at 600 rpm. Finally, the composite gel was produced

by adding 3ml of aniline to PVA+HCl+APS and stirred for 12 hours as shown in the figure 3-6 c. The nanocomposite gel is indicated as (PVA+HCl+APS+PANI) in this dissertation.

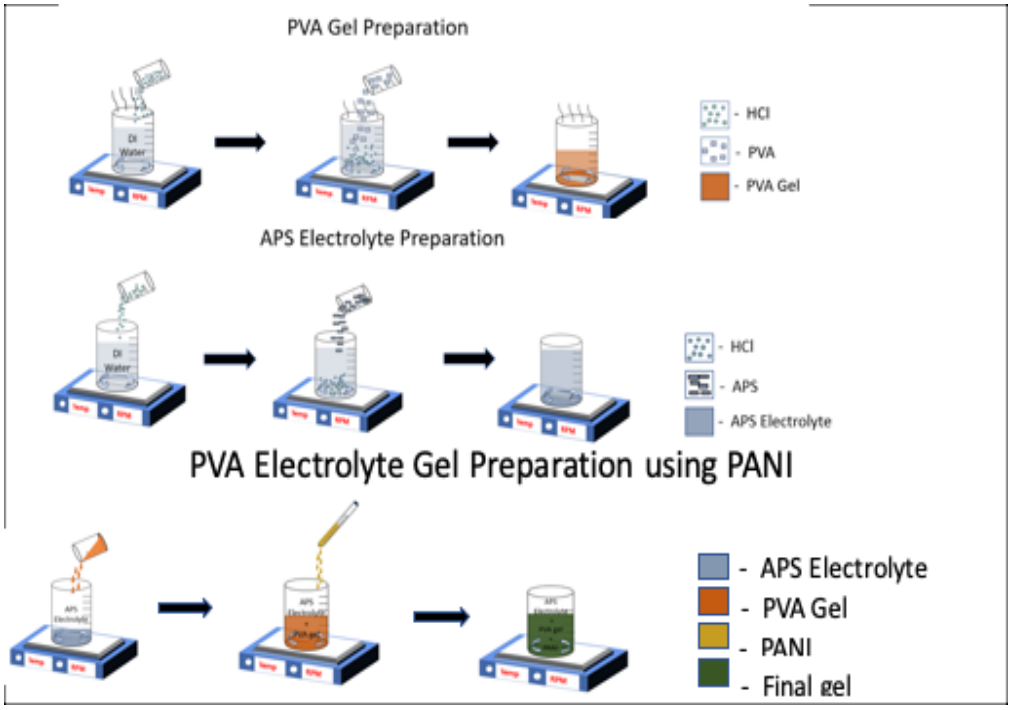

Figure 3-6 Preparation of Single Active Layer Composite Gel Electrolyte

3.7 Characterization

3.7.1 Cyclic Voltammetry

Cyclic voltammetry (CV) is an electrochemical technique used to study redox reactions, i.e., reduction and oxidation of a chemical. Using the CV, we can also analyze the electron transfer in a chemical reaction. The current is measured by taking as many cycles as possible by applying a potential to an electrode. CV analysis was used to investigate the oxidation and reduction peaks of the Polyaniline. There are three primary oxidation states in Polyaniline, Leucoemeraldine (Reduced state), Emeraldine (Half oxidized state), pernigraniline (fully oxidized state), and many other oxidized states in between them.

The structure of PANI is depicted in figure 3-7. The x value ranges between 0 and 1 and, based on the x value, the oxidation state is determined. So, at x equal to 0, 0.5, or 1 the Leucoemeraldine, Emeraldine, or Emeraldine Salt structures, respectively, are obtained. The reduced state, Leucoemeraldine, contains the amine nitrogen functional group, and the oxidized state, Emeraldine Salt, contains the imine nitrogen, functional group. Due to the double bond between nitrogen and carbon (imine function) of the Emeraldine Salt, the protonation happens in an acidic environment. Therefore, this can be used for studying the redox potentials of PANI in different acids.

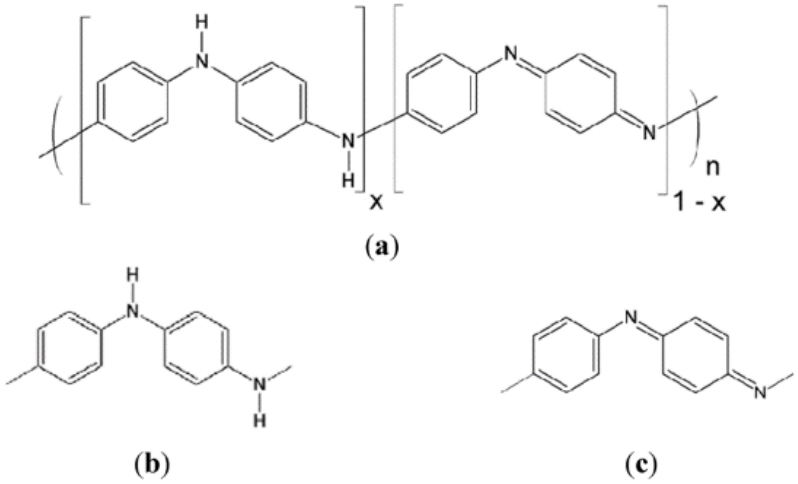

Figure 3-7 Structure of Polyaniline in (a) General Form, (b) Reduced Form, (c) oxidized Form [51]. By Edward Song et al. © (2013) MDPI.

The behavior of PANI can be studied by varying the applied voltage. From the figure 3-8, we can see two sets of peaks, Oxidation and Reduction Peaks. The first peak, oxidation, starting from 0.1 to 0.4 V, is where Leucoemeraldine is changing into Emeraldine. In the second peak of the Reduction, the Emeraldine salt starts changing to Emeraldine state at 1 to 0.4 V. The first peak of the Reduction between -0.25 to -0.8 V, the Emeraldine is getting reduced to Leucoemeraldine, i.e., it is changed to a fully reduced state.

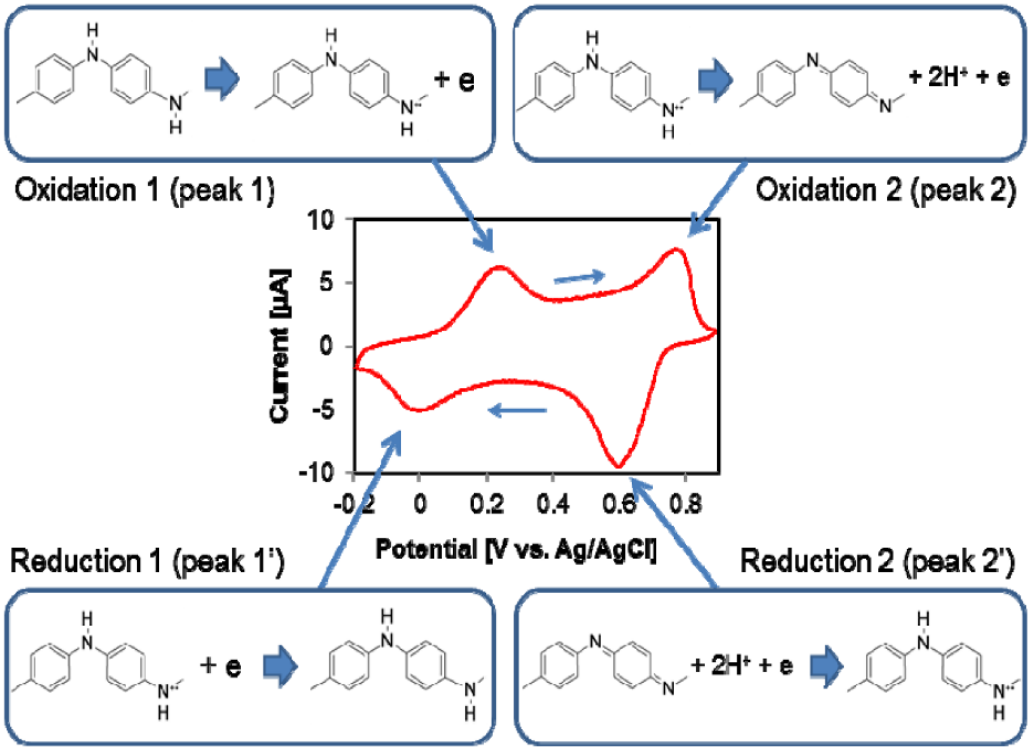

Figure 3-8 Typical Cyclic Voltammetry Curve of Polyaniline [51]. By Edward Song et al. © (2013) MDPI.

3.7.2 Chronoamperometry

Chronoampremetry is an electrochemical technique where a square wave voltage is applied to a working electrode, and it is time dependent. It is used to measure the current as a function of time. The current vs. time results are referenced as chronoamperometry [52].

3.7.3 Electrochemical Impedance Spectroscopy (EIS)

Electrochemical impedance spectroscopy (EIS) is an electrochemical tool used to measure the corrosion current density by calculating the polarization resistance. The impedance spectra can be determined by a potentiostat at a selected band of frequencies [53].

3.7.4 Scanning Electron Microscopy

Scanning Electron Microscope (SEM) is a high-resolution imaging tool useful for evaluating various materials for surface morphologies, flaws, or composition heterogeneities. A

focused beam of electrons emitted from a filament interacts with atoms in the sample that generates signals with information about surface topography and compositional variations in the sample. The imaging can be done to a resolution down to nanometer scale [54]. SEM images were taken using Ultra-high-resolution SEM SU-70 Hitachi to study the surface morphologies and compositional heterogeneities.

Figure 3-9 Scanning Electron Microscopy

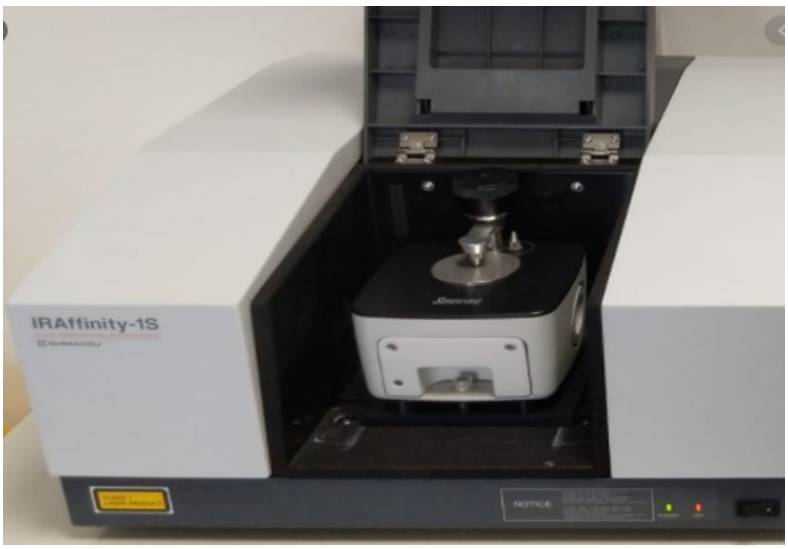

Figure 3-10 Fourier Transform Infrared Spectroscopy

3.7.5 Fourier-Transform Infrared Spectroscopy

This technique is used to obtain an infrared spectrum of absorption or emission of a solid, liquid, or gas. An FTIR spectrometer simultaneously collects high-resolution spectral data over a wide spectral range. It confers a significant advantage over a dispersive spectrometer, which measures intensity over a narrow range of wavelengths at a time [55].

3.7.6 UV-Visible Spectroscopy

UV Visible uses absorption spectroscopy, and this is affected by the color of the chemicals involved. It deals with electronic transitions from the ground state to the excited state by absorbing the light and measuring absorption from the ground to the excited state [56]. The main principle involves the increase in the energy of atoms and molecules when a chemical solution absorbs light.

It follows Beer lamberts law used in analytical chemistry to identify and quantify the materials, and it is also used as a detector in HPLC. Every chemical has a different wavelength, concentration, and molar absorptivity. Hence the response to every chemical solution is different, and the chromatogram obtained has various response factors.

Figure 3-11 UV-Visible Spectroscopy

Chapter 4: Touchchromic Device Based on Nanocomposite Polymer-Dye Film

4.1 Background

This chapter describes the preparation of a nanocomposite-based thin-film layer that reversibly changes color from dark to transparent in the presence of a salt-based electrolyte, without any other external excitation, such as voltage light, and temperature [1, 2]. The building structure of the touchchromic device consists of a coated nanocomposite layer on a conducting surface, a liquid electrolyte on the translucent conductive substrate, and a metal touch for color change. The coloration and decoloration depend upon various attributes like the composition of the electrolyte, film thickness, and the nature of the composite film.

Under this work, we have developed the polymer composite-dye thin film on a conducting substrate using an electrochemical technique. The composite film was characterized using UV-vis, FTIR, SEM, X-ray diffraction techniques. The coloration and decoloration of the composite film were studied with two different metals (iron and nickel). The coloration and decoloration depend on the properties of metal and type of electrolyte. The touch chromic device could find applications in windows and displays.

4.2 Results and Discussion

Figure. 4-1 shows the UV-visible spectra (curves 1-5) of polyaniline-dye active layers on FTO glass plates covered with different electrolyte films. Curve 1 shows the spectra for a chromatic device having NaCl+APS electrolyte, curve 2 shows the spectra for a chromatic device having KCl+APS electrolyte, curve 3 shows the spectra for a chromatic device having

MgCl2+APS electrolyte, curve 4 shows the spectra for a chromatic device having LiCl+APS electrolyte, and curve 5 shows the spectra for a chromatic device having CoCl2+APS electrolyte.

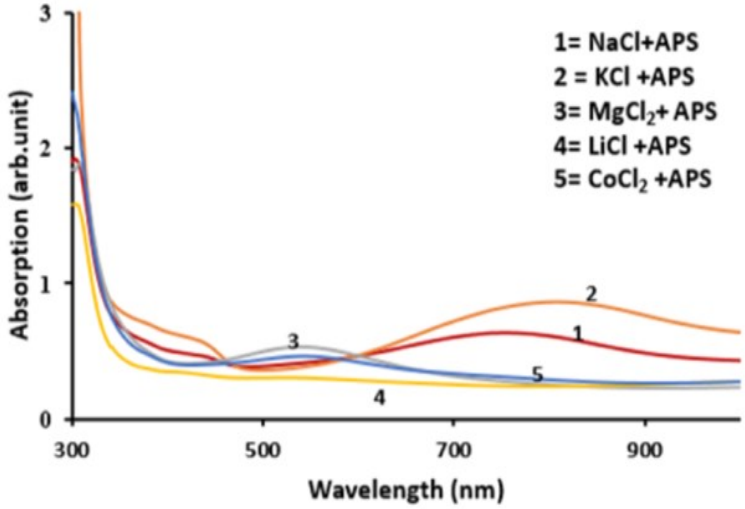

Figure. 4-1 UV-Visible Spectra of Chromatic Devices having a Polyaniline-Dye Active Layer treated with Various Electrolyte Films

Curve 1 shows UV-visible absorption peaks at 750, 437, 375, and 311 nm for the NaCl+APS-based device. Interestingly, a peak at 750 nm is the salt of the electrolyte dopant in the polyaniline structure. In contrast, the peak at 475 nm is due to polaron and bipolaron in the nanocomposite structure. The peaks at 311 to 375 nm are due to the p- p* of the polyaniline structure. Curve 2 shows UV-visible absorption peaks at 813, 437, 386, and 301 nm for the KCl+APS based device. The KCl+APS doping results in a shift of the UV-visible absorption peak from 750 nm to 813 nm. Curve 3 shows UV-visible absorption peaks at 539 and 311 nm for the $MgCl_2$+APS based device. Curve 4 shows UV-visible absorption peaks at 414 and 306 nm for the LiCl+APS-based device. Curve 5 shows UV-visible absorption peaks at 443 and 302 nm for the $CoCl_2$+APS based device. Notably, as peaks were not observed in the range of 700 to 900 nm for the LiCl+APS and $CoCl_2$+APS based devices, those devices do not quickly change color.

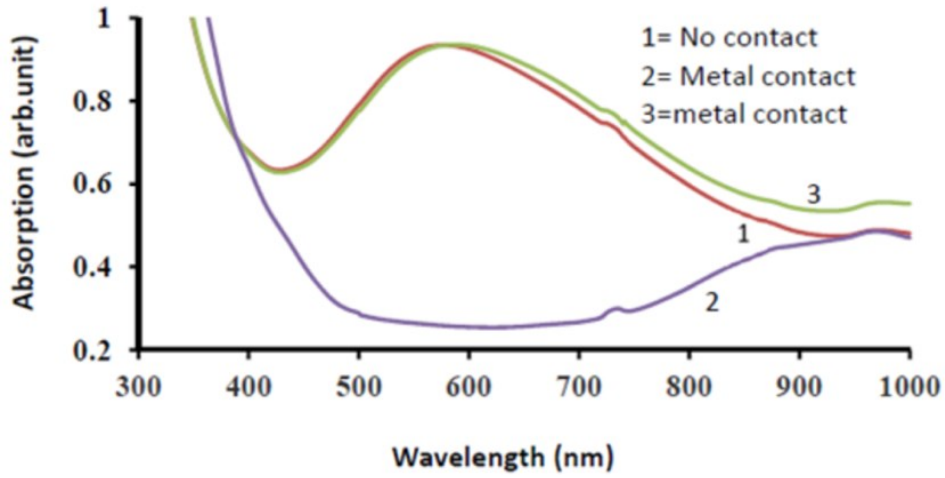

Figure. 4-2 UV-Visible Spectra of a Chromatic Device having a Polyaniline-Dye Active Layer treated with Magnesium Chloride ($MgCl_2$) + Ammonium Persulphate (APS) Electrolyte, both with and without Contact with a Metal

Figure. 4-2 is a graph that shows UV-visible spectra of a chromatic device having a polyaniline-MB dye active layer and a $MgCl_2$+APS electrolyte layer, both with and without contact with a metal. Curve 1 shows UV-visible absorption peaks at 579, 886, and 972 nm for the device before contacting metal. Curve 2 shows UV-visible absorption peaks at 881 and 972 nm after the polyaniline-dye active layer was placed in electrical contact with a metal element. Curve 3 shows UV-visible absorption peaks at 578, 876, and 974 nm immediately after removing the metal element. As can be appreciated from comparing curves 1 and 2, there is a 65% change in absorption between when the metal is and is not in contact with the active layer.

Figure. 4-3 is a graph that shows the UV-visible spectra for a chromatic device having a polyaniline-dye active layer and KCl+APS electrolyte, both with and without contact with metal. Curve 1 shows UV-visible absorption peaks at 560, 870, and 964 nm when there is no contact with metal. Curve 2 shows UV-visible absorption peaks at 569, 883, and 963 nm after the polyaniline-dye active layer was placed in electrical contact with a metal element. Curve 3 shows UV-visible absorption peaks at 371, 885, and 971 nm immediately after removing the metal element. As can

be appreciated from a comparison of curves 1 and 2, there is a 65-68% change in absorption at 550 nm between when metal is and is not in contact with the active layer.

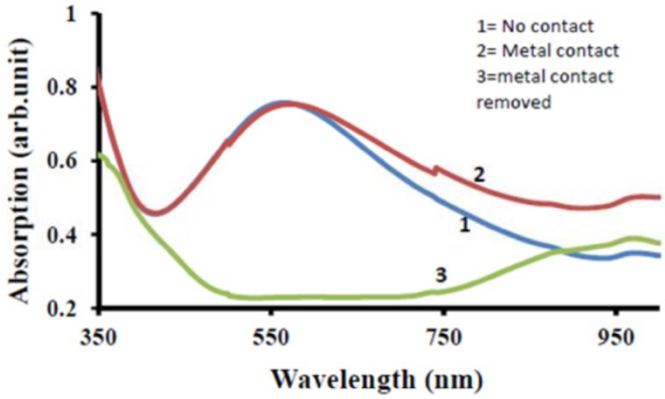

Figure. 4-3 UV-Visible Spectra for a Chromatic Device having a Polyaniline-Dye Active Layer and treated with Potassium Chloride (KCl)+APS Electrolyte, both with and without Contact with a Metal

Figure. 4-4 is a graph that shows the UV-visible spectra for a chromatic device having a polyaniline-dye active layer and NaCl+APS electrolyte, both with and without contact with metal. Curve 1 shows UV-visible absorption peaks at 556, 882, and 976 nm when there is no contact with metal. Curve 2 shows UV-visible absorption peaks at 372, 422, 885, and 968 nm after the

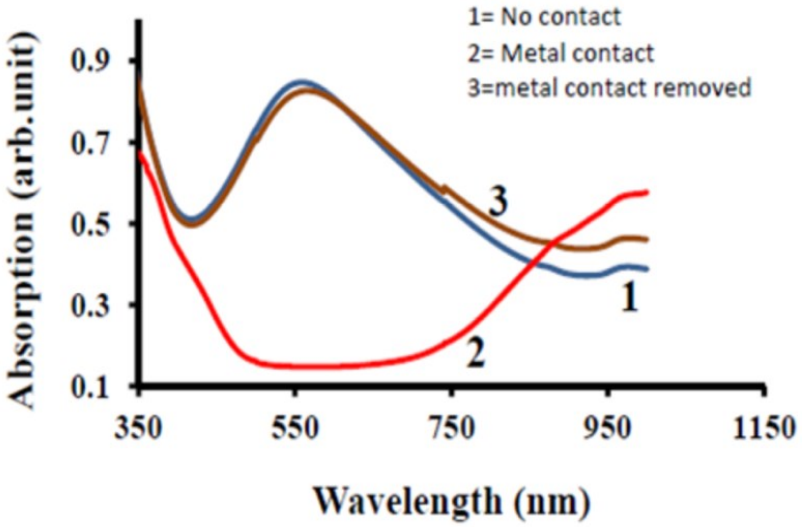

Figure. 4-4 UV-Visible Spectra for a Chromatic Device having a Polyaniline-Dye Active Layer treated with Sodium Chloride (NaCl)+APS Electrolyte, both with and without Contact with a Metal

polyaniline-dye active layer was placed in electrical contact with a metal element. Curve 3 shows UV-visible absorption peaks at 562, 879, and 969 nm immediately after removing the metal element. As can be appreciated from comparing curves 1 and 2, there is a 65% change in absorption at 550 nm between when metal is and is not in contact with the active layer.

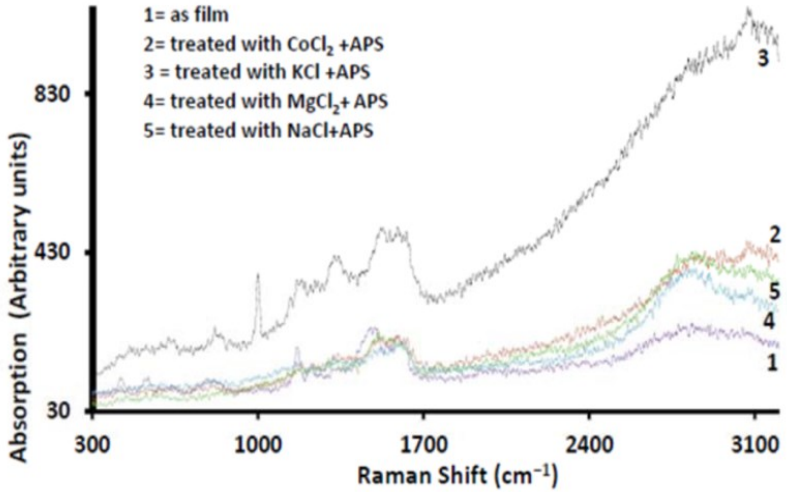

Figure. 4-5 Raman Spectra of a Chromatic Device having a Polyaniline-Dye Active Layer Deposited on a Silicon Substrate treated with Various Electrolytes

Raman spectroscopy was also performed to evaluate the chromatic devices. Figure. 4-5 is a graph that shows the Raman spectra of a polyaniline-dye active layer deposited on a silicon substrate and treated with various electrolytes. Curve 1 shows Raman absorption peaks for the active layer without any electrolyte at 2825, 1621, 1597, 1488, 1332, 1231, 1170, 1018, 826, 543, and 433 cm^{-1}. Curve 2 shows Raman absorption peaks at 3003, 1636, 1531, 1344, 824, 666, 460 cm-1 for the polyaniline-dye active layer when treated with $CoCl_2$+APS electrolyte. Curve 3 shows Raman absorption peaks at 3084, 1594, 1524, 1334, 1188, 1001, 819, 629, 474 cm-1 for the polyaniline-dye active layer when treated with KCl+APS electrolyte. Curve 4 shows Raman absorption peaks at 2855, 1630, 1530, 1331, 1188, 822, and 671 cm-1 for the polyaniline-dye active layer when treated with $MgCl_2$+APS electrolyte. Finally, curve 5 shows Raman absorption

peaks at 2845, 1614, 1525, 1341, 1247, 855, and 600 cm-1 for the polyaniline-dye active layer when treated with NaCl+APS electrolyte.

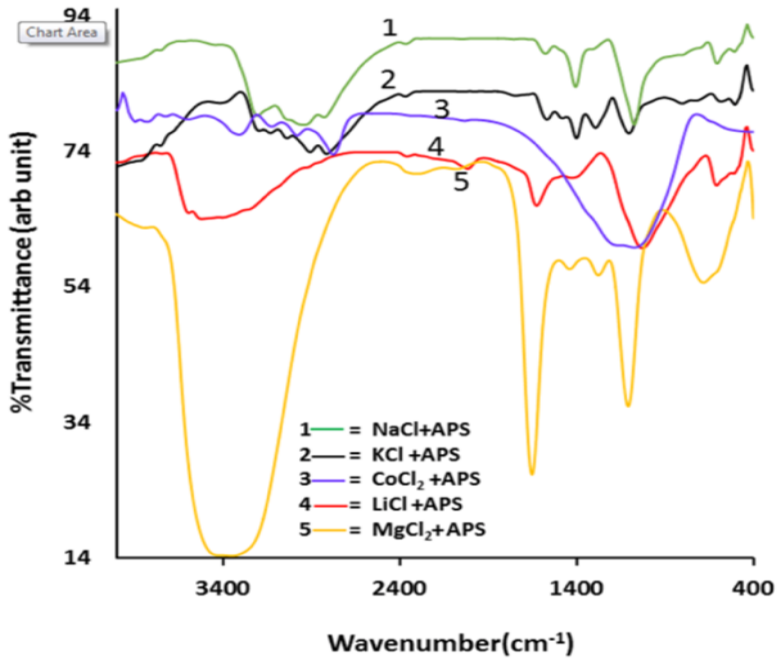

Figure. 4-6 Fourier Transform Infrared (FTIR) Spectra of a Chromatic Device having a Polyaniline-Dye Active Layer Deposited on a Silicon Substrate treated with Various Electrolytes

The Raman shifts are well pronounced compared with the infrared peak (discussed below in relation to Figure. 4-6). However, a Raman peak can be seen at 1636 to 1614 cm-1 due to doping of the polyaniline-dye active layer. The treated polyaniline-dye active layer shows C=N stretching due to the quinoid structure of the pernigraniline form of polyaniline. The Raman peak from 1630 to 1614 cm-1 is due to the quinoid ring, whereas the peak from 1539 to 1534 cm-1 is due to the benzenoid ring. The peak at 1344 to 1332 cm-1 is due to protonated oxazine units and the stretching vibration of C-C in the quinoid ring. However, the Raman spectra are pronounced and different in doped polyaniline-dye active layers. The bands that appeared at 1188 cm-1 and 1001 cm-1 are due to C–H bending vibrations of semi-quinonoid rings, and C–H in-plane bending vibrations in the benzenoid ring are due to KCl+APS electrolyte.

Fourier transform infrared spectroscopy (FTIR) was also performed to evaluate chromatic devices. Figure. 4-6 is a graph that shows the FTIR spectra of a polyaniline-dye active layer deposited on a silicon substrate and treated with various electrolytes. Curve 1 shows FTIR bands at 3202, 3043, 2927, 2816, 2360, 1517, 1483, 1403, 1295, 970, 802, 693, 599, 500 and 469 cm-1 for the polyaniline-dye active layer when treated with NaCl+APS electrolyte. The band at 3200 cm-1 is due to N-H vibration, and the peak at 1517 cm-1 is due to the C-C stretching of the quinoid and benzenoid rings. The band at 1295 cm-1 is due to the (quinoid) emeraldine structure of polyaniline and the "out-of-plane" C-H at 1870 cm-1 for polyaniline. The band at 3043 cm-1 is due to the C=H stretching of polyaniline. However, the doped form of polyaniline is shifted to 1295 cm-1, which is generally found at 1246 cm-1.

Curve 2 shows FTIR bands at 3854, 3746, 3673, 3391, 3195, 3123, 3036, 2905, 2818, 2355, 1761, 1565, 1478, 1398, 1283, 1101, 790, 725, 580, 500 cm-1 for the polyaniline-dye active layer when treated with KCl+APS electrolyte. The peaks shown at 1565, 1478, 1398, 1283, and 1101 cm-1 are due to chlorate or chloride ions in the conducting polymer.

Curve 3 shows FTIR bands at 3869, 3753, 3318,3202, 3043, 2355, 2036, 1630, 1420, 1275, 1072, 804, 681, 580, 500 cm-1 for the polyaniline-dye active layer when treated with CoCl2+APS electrolyte. Curve 4 shows FTIR bands at 3847, 3600, 3500, 3376, 3246, 2920, 2847, 2355, 2022, 1630, 1406,1029, 609, 500 cm-1 for the polyaniline-dye active layer when treated with LiCl+APS electrolyte.

Curve 5 shows FTIR bands at 3833, 3340, 2333, 2072, 1849, 1652, 1427, 1275, 1101, 674, 601, 500 cm-1 for the polyaniline-dye active layer when treated with $MgCl_2$+APS electrolyte. The band from 3340 to 3202 cm-1 is due to N-H bonding in polyaniline. The peak at 2818 cm-1 is due to methylene and methyl interaction due to the group present in the dye. The band at 1565 to 1630

cm-1 is due to C=N stretching due to the quinoid ring, and 1503 cm-1 is due to C-N stretching of the benzenoid ring. The peak at 1101 cm-1 is due to chlorine bonding with the polyaniline-dye active layer. The band at 804 cm-1 is due to C-H vibration out-of-plane bonding in the benzenoid ring of polyaniline. The band at 580 cm-1 is due to C-N-C bonding in the polyaniline. The band 3500 to 3854 cm-1 is due to the vibration band of -OH in the structure of the polyaniline-dye active layer.

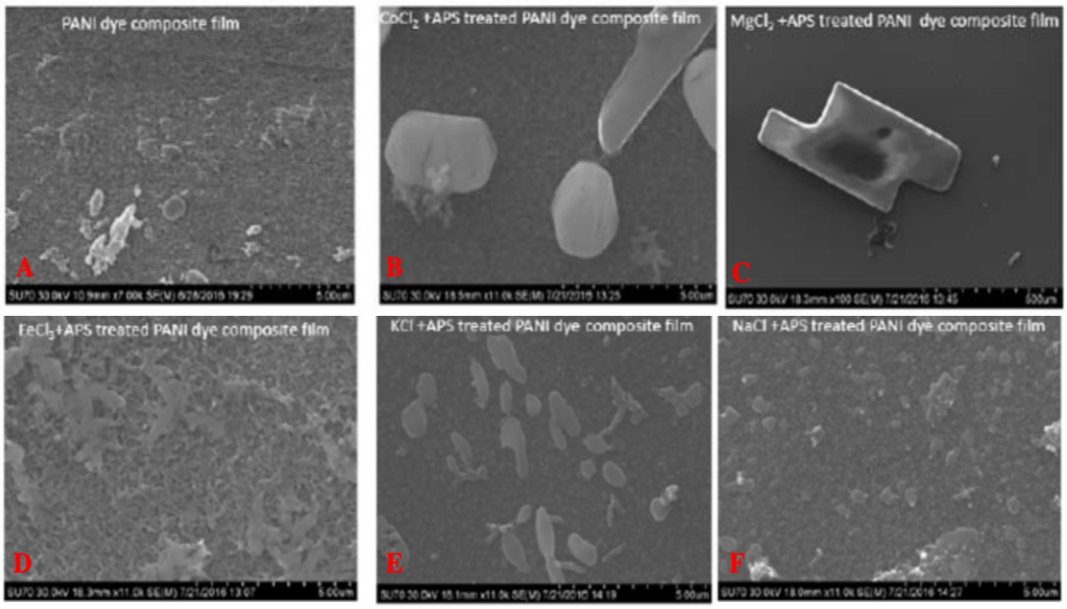

Figs. 4-7(A-F) are Scanning Electron Microscope (SEM) images of Chromatic Devices having Polyaniline-Dye Active Layers with and without treatment with an Electrolyte

Figs. 4-7(A-F) are scanning electron microscope (SEM) images of a polyaniline-dye active layer with and without treatment with an electrolyte. More particularly, Figure. 4-7A shows an untreated polyaniline-dye active layer, Figure. 4-7B shows a polyaniline-dye active layer treated with $CoCl_2$+APS electrolyte, Figure. 4-7C shows a polyaniline-dye active layer treated with MgCl2+APS electrolyte, Figure. 4-7D shows a polyaniline-dye active layer treated with $FeCl_3$+APS electrolyte, Figure. 4-7E shows a polyaniline-dye active layer treated with KCl+APS electrolyte. Figure. 4-7F shows a polyaniline-dye active layer treated with NaCl+APS electrolyte.

The active layers were not washed after the treatment with the various electrolytes. The SEM images show the effect of the electrolyte dopant on the surface of the active layer. The KCl- and NaCl-treated active layers had small grain boundaries in the polymer structure, whereas the $CoCl_2$- and $MgCl_2$-treated active layers had a crystalline salt structure across the layer.

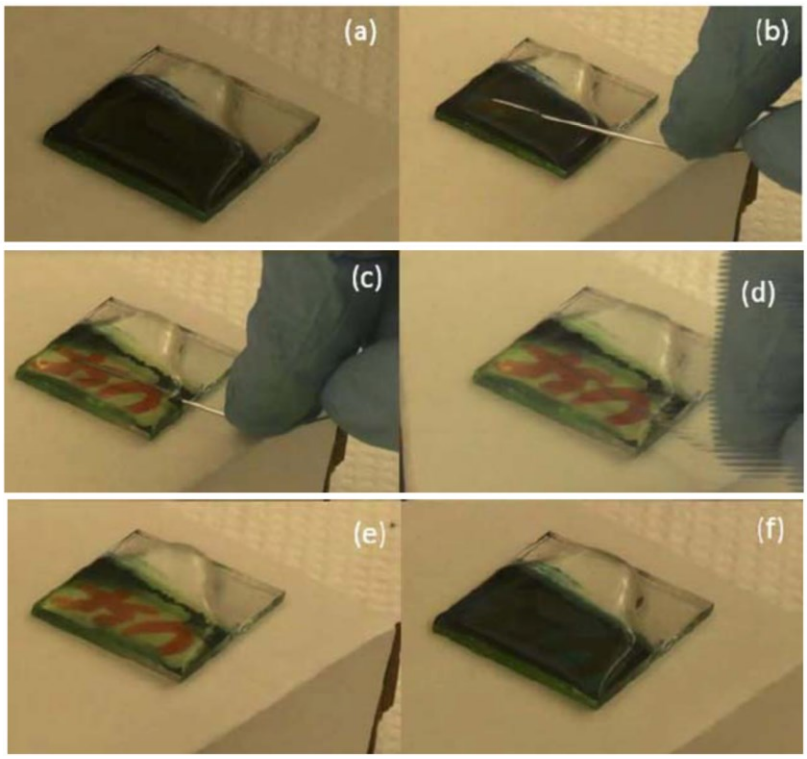

Figs. 4-8(A-F) are Photographs Showing the Color Change of a Chromatic Device with a Polyaniline-Dye Active Layer treated with KCl+APS Electrolyte

The touchchromism of the disclosed chromatic devices was also tested. The color change was observed for polyaniline-dye active layers treated with KCl+APS, LiCl+APS, $MgCl_2$+APS, and NaCl+APS electrolytes. Figs. 4-8(A-F) are photographs showing the color change for the polyaniline-dye active layer treated with KCl+APS electrolyte. Figure. 4.8AA shows the polyaniline-dye active layer before contact with a metal element. Figs. 4-8(B-D) are time-sequential images of the polyaniline-dye active layer after contact with a metal element. Figs. 4-8E and 4-8F are time-sequential images of the polyaniline-dye active layer after the contact with

the metal element is removed. As can be appreciated from these photographs, the letters “USF” written on the substrate of the chromatic device are only visible when the polyaniline-dye active layer has been in contact with the metal element.

The rate at which a color change occurs within the chromatic device depends on the electrolyte used. Table 4-1 identifies the time for a color change for polyaniline-dye active layers treated with various electrolytes. This table highlights the active layer treated with the KCl+APS electrolyte, showing a quick color change of 5 seconds.

Table 4-1 Types of Electrolytes and Time of Color Change.

S. No	Type of salts	Conc. Of oxidant APS	Time of decoloration (sec)
1	NaCl	0.1M	10
2	$MgCl_2$	0.1M	12
3	KCl	0.1M	5
4	LiCl	0.1M	19
5	$CoCl_2$	0.1M	Only at point of contact
6	$FeCl_3$	0.1M	No change

It is noted that the electrolyte concentration can have a significant effect on the reversibility of the color change. As the salt concentration increases, the reversibility of the color change decreases. It is also noted that the electrolyte concentration affects the speed with which the color change occurs as shown in Table 4-2. A gel electrolyte is prepared by dissolving 0.5 g of gelatin in 40 ml of deionized water and heated to 60^{o}C. The gel is cooled, and various salt concentrations are mixed and stirred with a 0.1M APS oxidant. The gel was applied to a polyaniline-dye active layer, and a touchchromic study was performed.

Table 4-2 Rate of Color Change for Different Concentrations of KCl+APS Electrolyte.

S. No	Conc. Of KCl	Conc. Of oxidant APS	Time of decoloration (sec)
1	0.1M	0.1M	At point of contact
2	0.25M	0.1M	14 Sec
3	0.5M	0.1M	12 Sec
4	0.75M	0.1M	3 Sec
5	1M	0.1M	5Sec
6	2M	0.1M	Only at contact

4.3 Conclusions

We have shown a new phenomenon of the color change of a conducting nanocomposite thin film with a liquid electrolyte. When a metal touches the liquid electrolyte, it changes the color of the composite thin film. The smart film changes color without any other external excitation. The color change occurs by transferring electrons from the metal contact to the electrolyte and finally to the nanocomposite thin film. The color contrast of the touchchromic device depends on the ratio of the conducting polymer composite with dyes, APS, and metal. As appealing as this touch chromic device may be, it is difficult to use it in commercial applications.

Chapter 5: Single Active Layer Electrochromic Devices

5.1 Background

Electrochromic (EC) windows have played a pivotal role in privacy protection and, to a smaller extent, energy savings in buildings. Commercial EC windows are expensive, with the active part containing several layers with complicated structures and slow switching ability. In this work, we present a new relatively simple and potentially inexpensive electrochromic (EC) device consisting of a single composite gel active layer placed between two transparent conducting fluorine doped tin oxide glass plates. The active EC layer is a mixture of the conducting polymer polyaniline, poly vinyl alcohol (PVA), hydrochloric acid, oxidant, and methylene blue (MB) dye. The EC device color changes from dark blue to transparent when an electric potential is applied in the range of +1.5 to -0.5 V. The color change in the EC active layer at various gel mole fractions of polyaniline and methylene blue dye have been studied using cyclic voltammetry, Fourier transform infrared spectroscopy (FTIR), UV-vis and electrochemical impedance measurements at various biasing voltages. The coloration and decoloration of the active layer at different voltages is driven by the oxidation and reduction of methylene blue and polyaniline. These effects are explained in terms of changes in the chemical structures of polyaniline and methylene blue at different bias voltages.

In this work, we have demonstrated EC devices with a single active gel layer composed of variations of (PVA+ ammonium persulfate (APS)+ methylene blue (MB), (PVA+APS+PANI) or (PVA+APS+MB+PANI) sandwiched between two conducting fluorine doped tin oxide (FTO) coated glass plates. These gel single active layer devices are produced by the polymerization of

PANI in PVA gel consisting of APS with a monomer ‘aniline’. A dark green-blue gel has been obtained depending on the ratio of APS to aniline as well as the presence of MB in the active layer.

5.2 Methods

5.2.1 Preparation

The single layer EC gel was prepared by the following four steps:

1. Preparation of PVA electrolyte: Initially, 50 g of PVA was dissolved in 500 ml of 1 M HCl in a flask. The solution was stirred continuously and heated at 80^{o}C for 12 hours. The PVA gel in HCl was formed due to condensation reaction [57]. The solution was allowed to cool to room temperature. Later, the gelling has been performed for several days. Such solution was used for preparation of active layer. However, the presence of oxidant “APS” created loss of electrons or oxidized the PVA molecule.
2. Preparation of PANI based electrolyte: Initially, 100 ml solution of 0.1 M APS in 1M HCl was prepared. The 10 ml solution of 1M HCl and 0.1 APS was added in 40 ml of PVA-HCl gel (named PVA gel). The addition of APS and HCl solution in PVA gel was performed slowly and lastly, 5 ml of aniline was added. The aniline was polymerized to PANI and formed blend with PVA-gel. In a conventional aniline polymerization to polyaniline, the oligomers which are formed are separated using the filtration process. So, the formation of any oligomer which has formed is also wrapped in the PVA gel.
3. Preparation of MB based electrolyte: 0.16 g of MB was dissolved in 10 ml of solution prepared in 1 M HCl and 0.1 M APS. The MB solution was added slowly using 40 ml of PVA gel and stirred for 12 hours to obtain the PVA+APS+MB gel. The solution was kept for a week to gel before use in the EC device.

4. Preparation of the MB+PANI electrolyte: Initially, 2.5 ml of aniline were added to the MB based electrolyte (the preparation is explained in the previous section). The aniline was polymerized over the PVA+APS+MB gel under constant stirring for 12 hours. The 1 mg to 2.5 to 3.0 ml ratio of methylene blue to aniline (1:2.5 and 1:3), before the polymerization of aniline to PANI, is presented in the text. Attempts were made to separately add 3ml, 3.5ml, 3.75ml, 5ml, 7.5ml and 10ml of aniline to the MB gel. Better results were obtained using 3 ml of aniline containing 0.16 g in MB gel in the fabrication of the (PVA+APS+MB+PANI) gel. The (PVA+APS+MB+PANI) gel was also aged before fabrication of the EC device.

5.2.2 Device Preparation and Measurements

The composite gel was characterized using UV-vis, Fourier transform infrared spectroscopy (FTIR) and scanning electron microscopy (SEM). The single layer (PVA+APS +MB), (PVA +APS+PANI) or (PVA +APS+MB+PANI) electrochromic devices were made by coating the entire surface of one of the electrodes with a composite gel, using a 130 μm thick boundary layer of parafilm as separator, and covering it with the second electrode. Then, the two electrodes and gel thin film were pressed together with binder clips and glued together. The effective area of the electrochromic device was 2.0 cm×2.0 cm and was used for all the measurements.

5.3 Results and Discussion

5.3.1 Physical Characterization

Figure 5-1a shows schematics and real pictures of the single layer electrochromic device in two states, opaque and transparent, when 1.5 V and -0.5 V were applied, respectively. Curve 1 in figure 5-1b reveals UV-vis optical absorption at 381, 673 and 764 nm of the PVA+APS gel

coated on a glass plate and dried at room temperature. Curve 2 in figure 5-1b shows the UV-vis absorption at 405, 623, 679, 739 and 753 nm of the (PVA+HCl+APS+MB) gel deposited on a glass substrate. Curve 3 shows UV-vis absorption peaks at 386, 427 and 820 nm for (PVA+APS+PANI+MB).

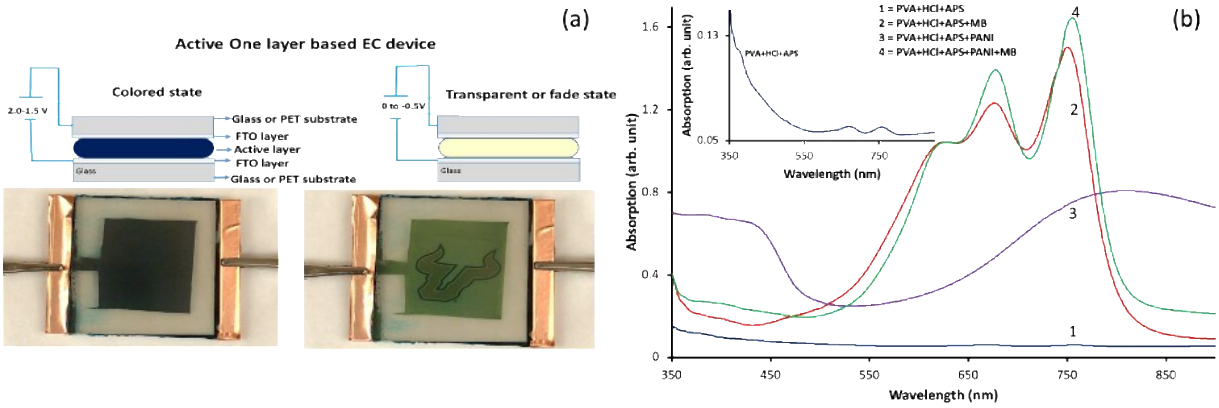

Figure 5-1 (a) Schematic and Real Pictures of a Device with an All in One Active Layer (PVA+APS+MB+PANI) biased at 1.5 -2.0 V for the Colored State and at 0 - -0.5 V for the Transparent State; (b) UV-Vis Spectra of (1) PVA+APS, (2) PVA+APS+MB, (3) PVA+APS+PANI and (4) PVA+APS+PANI+MB (the inset in figure (b) shows the UV-Vis Spectra of the PVA+APS Film on Glass Plate)

However, absorption peaks at 405, 626, 680, 739 and 757 nm are observed for the (PVA+APS+PANI+MB) electrolyte on a glass plate. The presence of a peak at 820 nm in curve 3 and 757 nm in curve 4 of Figure 5-1b are indicative of the doped state of PANI regardless of the presence of APS oxidant.

Figure 5-2 shows SEM pictures of just the gels i.e., (PVA+APS+MB), (PVA+APS+PANI) or (PVA+APS+MB+PANI) on an FTO coated glass plate dried at room temperature. Figures 5-2 (left and right) show typical compact symmetric structures with a packed pebble structure regardless of the type of sample. A 0.1M MB in the (PVA+APS+MB+PANI) sample produced a fibrillar structure (Figure 5-2 right).

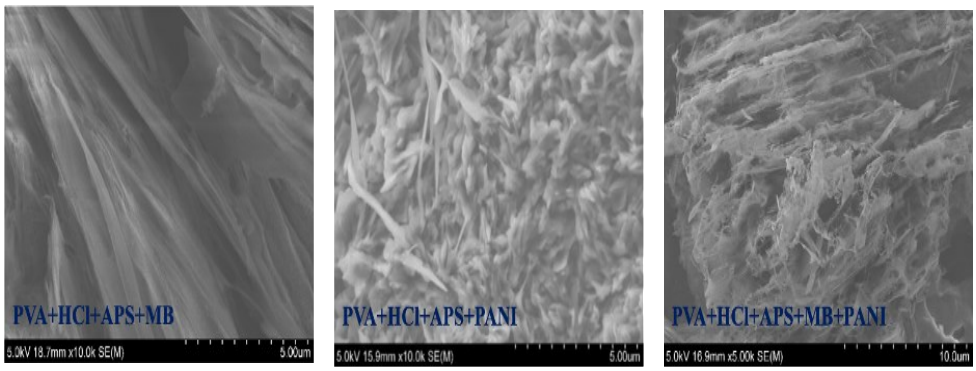

Figure 5-2 SEM pictures of the PVA +APS+MB, PVA+APS+PANI or PVA +APS+PANI+MB on FTO Coated Glass Plates Dried at Room Temperature

Figure 5-3 shows FTIR transmission peaks at 3416 (stretching vibration O-H with strong hydrogen bonding intermolecular and intramolecular types), 2953 (to C-H alkyl group) [58][59], 2345, 2099,1737 (C=O),1650 (C=O stretching) ,1409 (C-H2), 1206 (C–N stretching of amine)

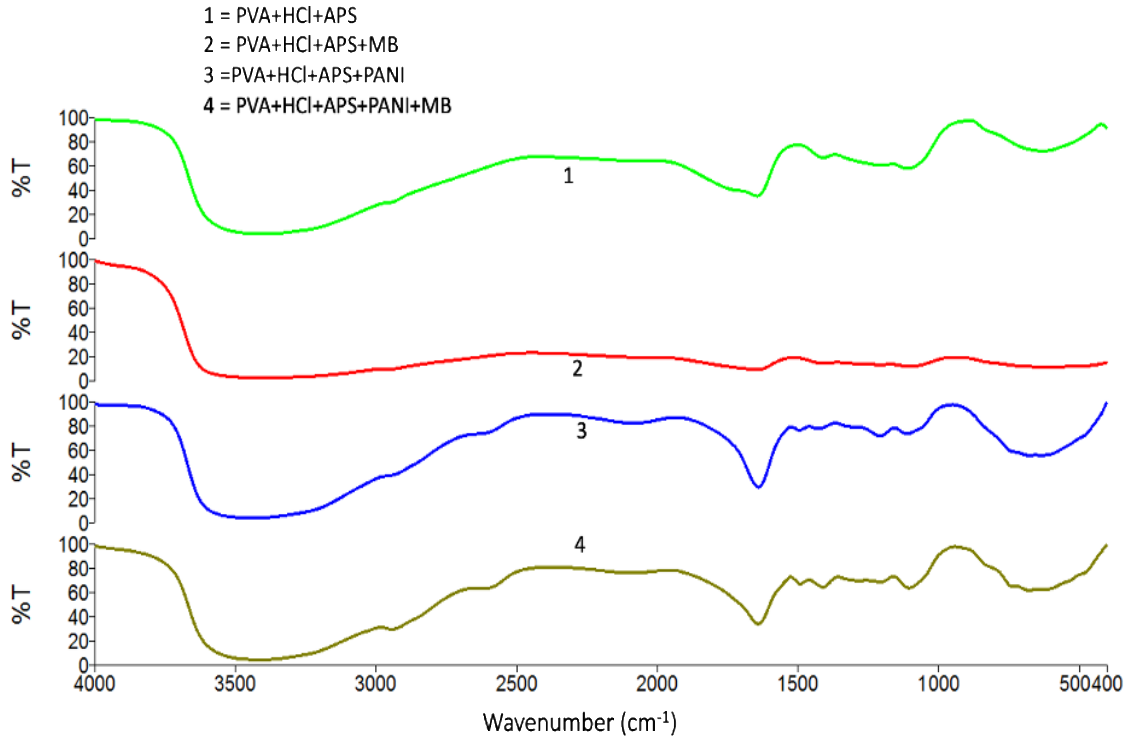

Figure 5-3 FTIR Spectra of (1) PVA+APS, (2) PVA+APS+MB, (3) PVA+APS+PANI and (4) PVA+APS+PANI+MB

[58][60], 1105 (is due to S=O) and 820 cm-1 (C-S bond) for PVA+APS gel based electrolyte. The characteristic peaks of PVA+APS gel at 3420, 2927, 2156, 1645, 1418, 1221, 1090, 839, 593 cm-1 with little shift are observed due to the presence of MB in curve 2 figure 5-3. The peak 1409 has been shifted to 1418 cm-1 due to the presence of MB.

The characteristic peaks of methylene blue at 1595, 1487, 1390 as well as 816 cm-1 are not observed rather the characteristic peaks have shifted due to the presence of MB in the (PVA+APS+MB) gel, as shown in curve 2 figure 5-3 [61]. The presence of PANI in (PVA+APS+PANI+MB) shows transmission peaks at 3445 (ν(N–H) (stretching vibrations), 3222 (H-bonded ν(N–H), 2948, 2601, 1645 (1486 benzenoid ring stretching), 1418 (phenyl ring stretching), 1312 (ν(C-N.+), 1211 (ν(C-N), 1109 (B-NH-B/δ(C-H), 728(c(C–H) (monosubstituted or 1,2-disubstituted ring), 685(Out-of-plane ring bending (monosubstituted ring)), 598(Cl –) and 482 cm-1, curve 3 figure 5-3. The 1109 cm-1 is associated with the charged polymer units quinoid (Q)=NH+− benzene B or (B)−NH+•−B [62]. The PVA+APS+PANI+MB shows FTIR transmission peaks at 3416, 3213, 2943, 2601, 2108, 1640, 1491, 1408, 1283, 1201, 1098, 820, 733, 675, 612, 521 and 477 cm-1, curve 4 figure 5-3. The peaks are due to the presence of PVA, MB, and PANI in doped states [62].

The UV-vis, FTIR and SEM properties of fabricated films are indicative of the emeraldine salt (ES) form of the PANI active layer.

5.3.2 Cyclic Voltametric and Spectroscopic Studies

To study the electrochromic response of the gels, devices were made by applying a thin gel layer between two FTO coated glass plates. The fabricated devices were then tested by applying a potential across the conductive glass plates. Figure 5-4a shows the cyclic voltammetry (CV) results of a (PVA+APS+MB) device at different scan rates. The CVs show the oxidation peak varying

from 1.39 to 1.32V, and reduction peaks at -0.73 V, and -0.13 V. A dark blue color was observed at a potential of about 1.35 V, depending on the scan rate. On the other hand, the transparent color was observed at a potential around -0.2 V. Figure 5-4b shows the CVs of the (PVA+APS+PANI) gel electrolyte EC device. It shows a broad oxidation peak from +1.30 to +1.69 V as well as a small oxidation peak between 1.37 V and 1.67 V, and a reduction peak in the range of 0.47 V to 0.8 V as a function of scan rate. Figure 5-4c, for the (PVA+APS+PANI+MB) single active EC layer, indicates that the redox potential changes as a function of scan rate. In figure 5-4d (2) a faster color change was obtained for a gel containing 1 mg of methylene blue and 3.0 ml aniline. The redox potential for the gel containing (PVA+APS+PANI+MB) shows a sharp oxidation peak

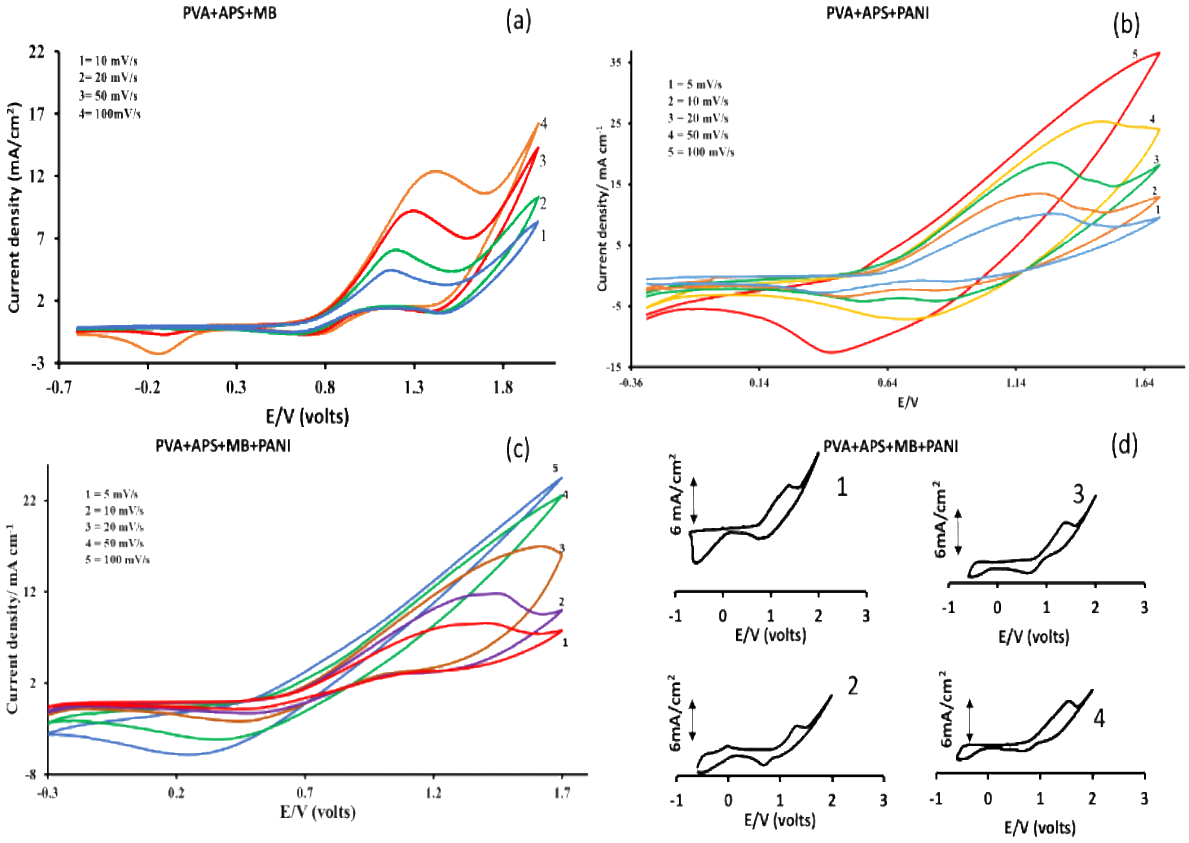

Figure 5-4 CVs of EC Devices Containing EC gels as a Function of Scan Rate. Figure (a) for PVA+APS+MB; Figure (b) for PVA+APS+PANI and Figure (c) for PVA+APS+MB +PANI

at ~1.42 V and a reduction peak at around -0.5 V. There is no appreciable change in the characteristics of the CV curves when varying the ratio of aniline to MB for the preparation of the active (PVA+APS+PANI+MB) layer. However, better transparency has been observed for the 1:3 ratio of aniline to MB.

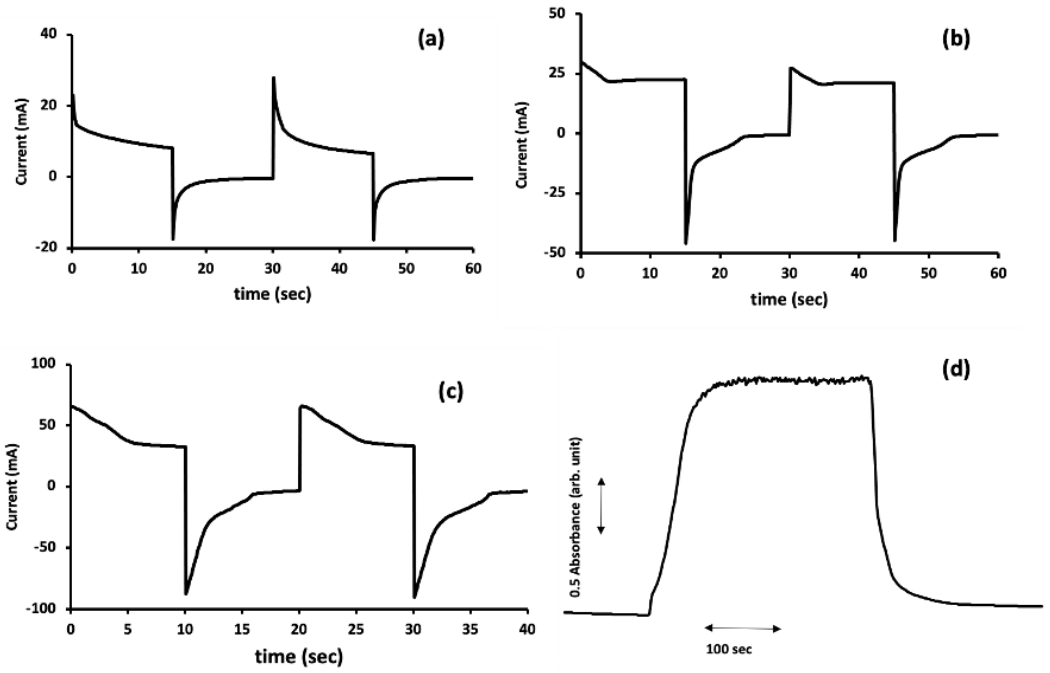

Figure 5-5 Chronoamperometric Plots of (a) PVA+APS+MB, (b) PVA+APS+ PANI, and (c) PVA+APS+PANI+MB in the Single Active Layer Device; and (d) Absorption Change by the PVA+APS+PANI+MB Active Layer at an Excitation Wavelength of 550 nm is Changed for -0.2V and 1.5 V for between two FTO Coated Glass Plates

Figure 5-5a shows the chronoamperometric results of (PVA+APS+MB), (PVA+PANI+APS) and (PVA+APS+PANI+MB) for a single active layer between two FTO coated glass plates. Figure 5-5a shows the chronoamperometric results for the (PVA+APS+MB) single layer, indicating that the reduction current is larger than the oxidation of the electrolyte. This chronoamperometric study was carried out by applying a voltage from 1.5 to -0.5 V. The colored state of the active layer was maintained at 1.5 V whereas -0.5 V showed a transparent state. When the applied potential of 1.5V was switched on, the dark blue color remained and,

similarly, the potential -0.5V switched off showed the transparent color. Figure 5-5b shows the redox states of (PVA+APS+PANI) for a single layer electrochromic device. Also, the redox states for (PVA+APS+PANI+MB) are asymmetric, like (PVA+APS+PANI), as shown in figure 5-5c. The presence of PANI and MB in (PVA+APS+PANI+MB) contributes to faster coloration and decoloration as compared to use of just MB or PANI.

In figure 5-5d, the EC device shows a higher color contrast at the voltage window from 1.5 to -0.5 V in the wavelength range of 580 to 875 nm. The experimental results show that color contrast can also be obtained in the wavelength range of 500 to 900 nm. Figure 5-6 shows Spectro-electrochemical studies on the (PVA+APS+MB+PANI) EC device at 1.7 V (curve 1) and -0.7 V (curve 2). The absorption magnitude at 1.7V saturates the absorption from 600 to 870 nm whereas, the characteristic color (light color) is observed at -0.7 V [62].

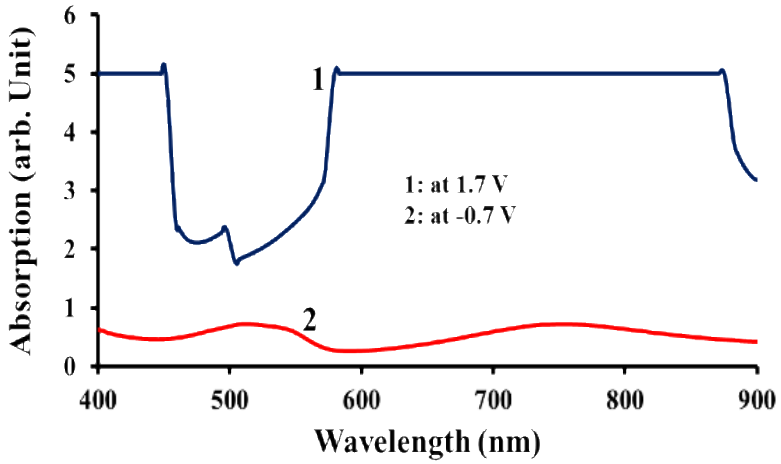

Figure 5-6 The Spectro-Electrochemical Study of PVA+APS+MB+PANI Gel base EC device at potential (1) 1.7 V and (2) -0.7 V

5.3.3 Electrochemical Impedance Spectroscopy

To study the electrical properties of the (PVA+APS+PANI+MB) gel, the impedance of the device was measured at 0.0 V (transparent mode) and 2.0 V (dark mode). Figure 5-7a shows the

impedance magnitude and phase versus frequency. The results reveal an astonishing difference in the electrical behavior of the (PVA+APS+MB+PANI) gel at the two different states. At a high biasing voltage, when the film is dark, the device is showing almost a pure resistive behavior ($\angle Z < 6$ degrees) with a low resistance of ~65 Ω for a wide range of frequency from 0.1 Hz to 10 kHz. The (PVA+APS+MB+PANI) EC device has shown a complex impedance behavior at the transparent state (0.0 V).

To analyze the complex impedance at the transparent state, the imaginary part of the impedance is plotted versus the real part, as shown in figure 5-7b. The presence of two semicircles in the Nyquist plot suggests having at least two-time constants in the gel-based EC device. This supports the transition current in the pulse data (figure 5-5c). To analyze the impedance data, an equivalent circuit model is proposed (inset Figure 5-7b). An EIS Spectrum Analyzer 1.0 software was used to find the value of each component in the model for the best fit to the data.

The results of the simulated circuit are presented in figure 5-7b. The component values extracted from the simulation are also shown in the same figure (different inset). The series resistance (Rs=58.68 Ω) in the device is slightly lower than the measured 65 Ω resistance in the opaque state. The combination of Cdl, Rct, CPE, and RP is very similar to an electrochemical interface between a conductive electrode and an electrolyte with a double layer capacitor (Cdl), a charge transfer resistor (Rct), a constant phase element (CPE) and a parallel resistor (RP). Considering the planar structure of the electrodes, the magnitude of the double layer capacitance is in good agreement with the dimensions of the electrodes. It should be noted that due to the symmetrical structure of the device, Cdl is equivalent to two series double layer capacitances formed at each electrode-gel interface. Similarly, Rct, CPE, and RP cover the corresponding effects on both electrodes. In addition to the interface, the equivalent circuit model suggests the

presence of charge storage in the bulk of the gel material [63]. The bulk capacitance, Cbk=79.68 mF, is much larger than the double layer capacitance.

A typical electrochemical cell does not have any charge storage capability in the electrolyte of the cell. However, the (PVA+APS+MB+PANI) gel electrolyte contains PANI which can store charge through changing the oxidation state of the polymer. Due to a relatively large amount of polymer used in the electrolyte, in fact, it is reasonable to assume the presence of a bulk capacitance larger than Cdl. Although the proposed equivalent circuit model explains the impedance of the device at 0.0 V biasing, the significant change in both the magnitude and complexity of the impedance at 2.0 V is arguable. The combination of the color change, current-voltage characteristics and impedance results can be used to explain the device behavior.

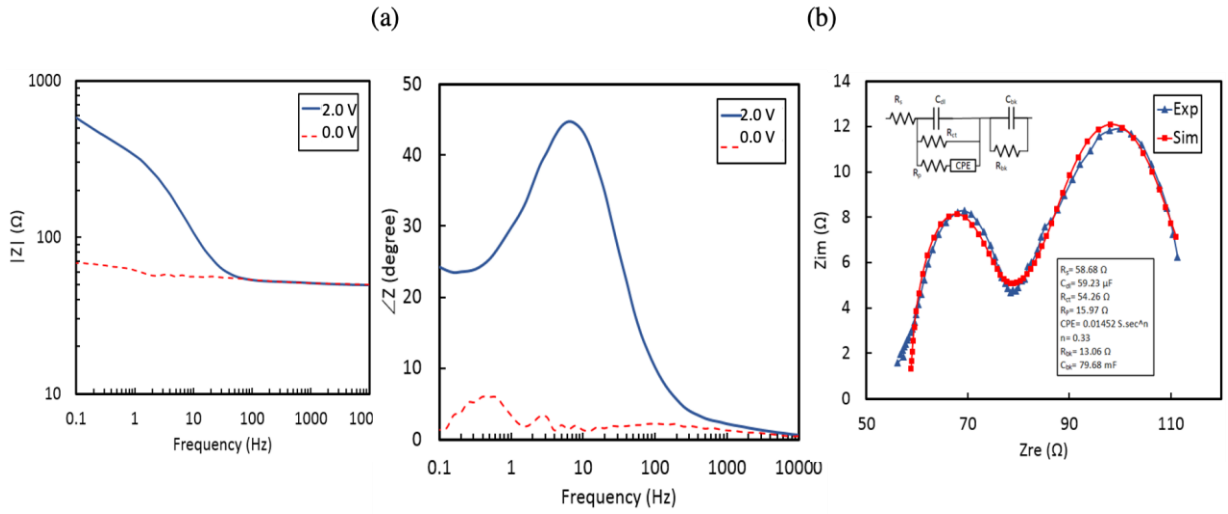

Figure 5-7 (a) Magnitude and Phase of the PVA+APS+PANI+MB Device Impedance vs Frequency at a Biasing Voltage of 0.0 V (Transparent Color) and 2.0 V (Dark Color). (b) Experimental and Simulation Results for the Complex Impedance of the Device at 0.0 V

5.4 Mechanism of Single Layer based Electrochromism

Both the color change and the current peak around 1.5 V indicate that the redox state of the polymer changes from leucoemeraldine (LEU) to emeraldine to pernigraniline (PG) at higher voltages. The emeraldine state (ES) has a smaller bandgap (Eg=2.2 eV) with a dark blue color.

Since the gel electrolyte is a composite material that includes the PANI polymer, the variation in the conductivity is expected to be less than that of just the polymer film. The change in the magnitude of the impedance at 0.1 Hz supports the existence of the emeraldine structure of polyaniline in the gel at 2.0 V biasing.

The conversion of LEU to emeraldine as well as PG is due to an oxidation process through which the polymer loses electrons. In contrast to the emeraldine and pernigraniline (PG) states, the leucoemeraldine state is transparent with a bandgap of Eg=3.9 eV. The lower conductivity of the LEU and its capacity to store positive charges (by losing electrons in the oxidation process) are the likely reasons for having such complex impedance values at 0.0 V. One possible explanation is that the application of a step voltage of 2.0 V pumps a significant amount of positive charge into the gel, thus leading to larger impedance at the LEU state. The injected charge into the gel would be used to complete the polymer charge balance at the oxidation state (i.e., charging the bulk capacitor). This forms a space charge limiting situation in the gel. Once the polymer is converted to the ES state, the gel would be more conductive with a lower resistance. The presence of APS in the gel would convert the PG to EM and then to LEU at 0.0 V (short circuit condition) or -0.5 V, resulting in a transparent state.

5.5 Mechanism of Gelling the Single Layer EC device

The PVA gelling depends on the condensation reaction and temperature applied to the PVA in the HCl solution. The water molecules are released and chlorine ions (from the dissociation of HCL) are attached to the PVA in the gelling process. Figure 5-8a shows the gelling process of PVA in the HCl solution. Further, the oxidant “APS’ addition to the PVA gel causes a loss of electrons from the polymer structure. Such process produces the lone pair effect in the carbon

structure as shown in figure 5-8b. The aniline addition in PVA+APS causes oxidative polymerization and forms the emeraldine salt (ES) form of PANI.

The possible interaction of ES with the (PVA+APS) gel yields the (PVA+APS+PANI) structure. One can assume that the ES state interacts with chlorine ions in the (PVA+APS) gel because of the lone pair effect of the ES state of PANI (figure 5-8c). However, the presence of APS causes the oxidation of the ES polymer and forms pernigraniline (purple or dark blue in color) of polyaniline (based on UV-vis measurements and optical observation). Figure 5-8d shows

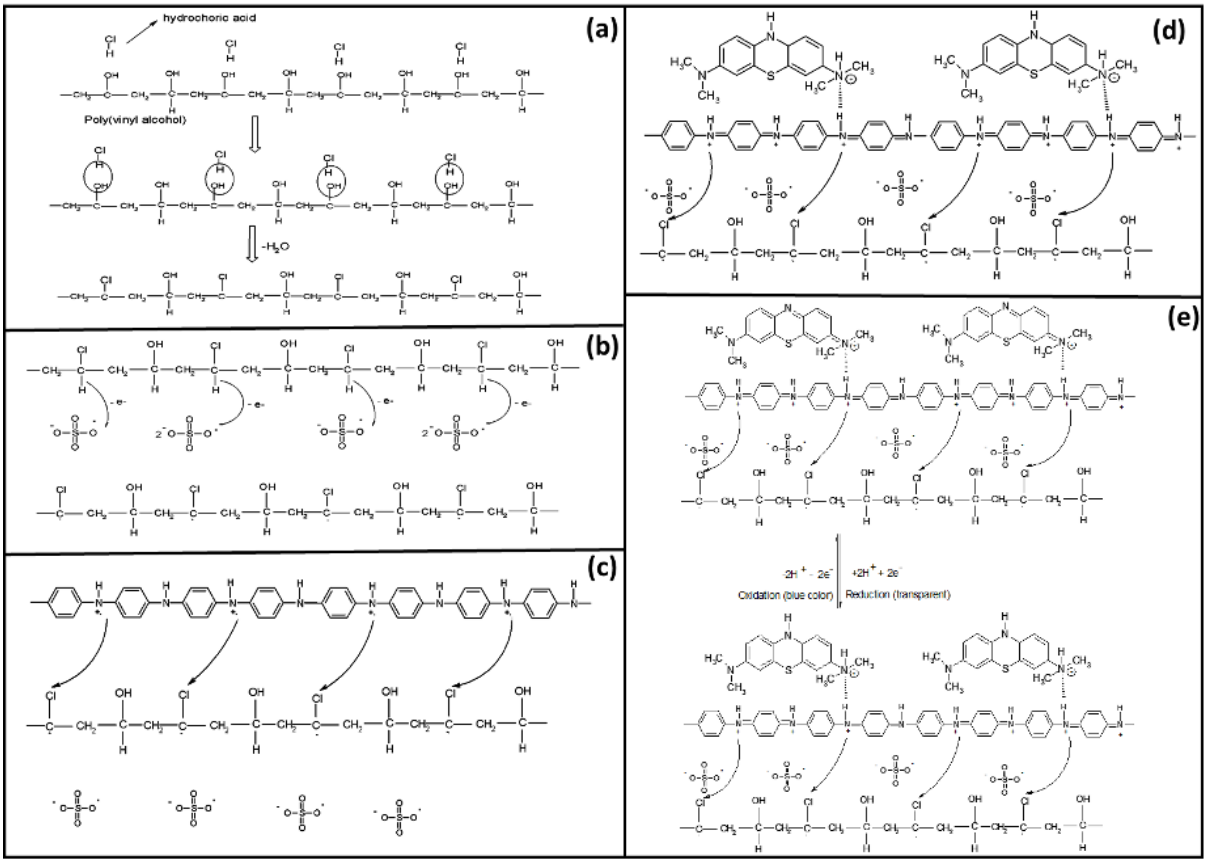

Figure 5-8 (a) The Gelling Process of PVA in HCl; (b) The PVA-gel in HCl with Ammonium Persulfate (APS) Oxidant Process; (c) Emeraldine Salt Forms in the Presence of HCl and APS after Polymerization of Aniline to Emeraldine salt; (d) Emeraldine Salt Changes to Pernigraniline due to the Presence of APS and Oxidized PVA in APS; (e) Coloration and Decoloration due to the Application of a Voltage across the Single PVA+HCl +APS+MB+PANI Layer

possible interaction of MB with the (PVA+APS +PANI) structure. There is a weak bond which is established between the nitrogen of MB to hydrogen–bonded with nitrogen present in the PANI structure. The application of a voltage to the single (PVA+APS+MB+PANI) device produces a color change from blue to transparent or light yellow in color. The oxidation of MB and PANI produces a dark blue color in (PVA+APS+MB+PANI) EC device as shown in figure 4-8e. The color changes from dark blue to transparent when the applied voltage changes from -0.7 to 2.0 V. To produce the electrochromic effect both electron donors and electron acceptors must be present in the gel. The color contrast, potential window, stability of gel and reversibility of the EC device depends on the type of gel.

5.6 Conclusions

This work presents a promising new EC device that can be used for the development of low- cost EC windows. The device is simple to make, and the use of a single active layer greatly simplifies the manufacturing process. The single (all-in-one) gel active layer consists of (PVA + oxidant + conducting polymer; or PVA + oxidant +dye + conducting polymer) placed between

two transparent conducting fluorine doped tin oxide glass plates. The single active layer EC device can be easily used in large size applications such as windows, without involving complicated vacuum deposition processes. However, because the active layer contains a water-based electrolyte and organic components, the device has some drawbacks, such as, bubble formation resulting from the electrolysis of the water-based electrolyte (for applied voltages above 1.23 volts) and photodegradation when the window is exposed to sunlight (from UV and other wavelengths in the solar spectrum). The elimination of these drawbacks is presently under investigation.

Chapter 6: Single Active Layer Electrochromic Devices with Different Colors

6.1 Background

This chapter presents the research results on stable nanocomposite single active gel layers of different colors that can be used in auto-dimming rear-view mirrors, windows, camouflage applications, partitions in buildings, etc. The single gel active layer contains a water-soluble polymer, poly (vinyl alcohol) (PVA), an oxidant, ammonium perdisulphate (APS), and a water-soluble dye, such as methylene blue, methyl orange, methyl viologen, eosin, rhodamine b, and congo red, at various compositions. The active gel layer (polyaniline+dye+PVA+APS) was characterized using SEM, UV-visible, cyclic voltammetry and chronoamperometric techniques. The coloration and decoloration of the EC device, with the gel active layer sandwiched between two conducting fluorine doped tin oxide transparent glass plates, was achieved in the applied voltage range of +2.0 V to –2.0 V. The oxidation-reduction potentials of the gel layer were identified by using cyclic voltammetry, chronoamperometry and in-situ opto-electrochemical techniques. The coloration and decoloration of the EC all-in-one layers were deduced from the expected chemical structures of the active layers containing different ratios of polyaniline and dye. The results show that the redox characteristics of the dye greatly influence the overall oxidation and reduction potentials of the EC device active gel layer.

In this work, the physical properties of the (PVA + APS + dye (methyl orange ‘MO’, methyl viologen ‘MV’, eosin ‘EO’, congo red ‘CR’, rhodamine b ‘RB’, methylene Blue ‘MB’) + PANI) active layers have been characterized using SEM, UV-visible, cyclic voltammetry and chronoamperometry techniques. We investigated the coloration and de-coloration of the active

layer by measuring the UV-vis absorption from 350 nm to 900 nm at 2 V and -0.7 V and used cyclic voltammetry at various scan rates to understand the reversibility and oxidation-reduction process in various dyes in the single (all-in-one) active layer EC device.

6.2 Materials and Methods

- Preparation of PVA gel: Initially, a PVA gel was prepared by dissolving 50 g of PVA in a solution of 500 ml of 1 M HCl in a round bottom flask. The solution was heated for 12 hrs. at 80^{o}C and then cooled at ambient temperature and was kept gelling for several days (more than a week before use).
- (PVA+APS+PANI) gel: The PVA gel was used to prepare the (PVA+APS) gel electrolyte. Separately, 0.1 M of APS solution was mixed in 1M HCl and 10 ml of the resultant solution was added to 40 ml of PVA gel and stirred for one hour. The reaction with APS in PVA created an oxidized (PVA+APS) gel. The 50 ml gel containing PVA+APS was added to a 5 ml aniline solution over an interval of 3 minutes. The aniline was polymerized in PVA gel in the presence of the APS "oxidizer". The final gel is referred to as (PVA+APS+PANI).
- (PVA+APS+dye+PANI) gel: The final active layer was prepared by using 0.01M of each dye (MO, MV, EO, CR, RB, and MB) in a solution of 0.1 APS oxidant in 1M HCl. The resulting solution of 10 ml was added 3 ml at a time, under continuous stirring, to obtain a 40 ml PVA+APS gel. Later, 5 ml of aniline were added to the solution of (PVA+APS+dye (MO, MV, EO, CR, RB and MB)), and stirred for 12 hours at room temperature. Table 6-1 presents information about the amount of each dye used in the preparation of the (PVA+APS+Dye (MO, MV, EO, CR, RB or MB) + PANI) active electrochromic gels.

Table 6-1 Experimental Conditions and Dye, Aniline, PVA Gel Required to Obtain Active One-Layer Electrochromic Material

S.No	Active layer gel	Dye added in 10 ml of (0.1M APS+1M HCl (0.01M))	40 ml of PVA gel with HCl	Aniline	Reaction of aniline with PVA+APS+dye
1	PVA+APS+ MO+PANI	0.1636g	40 ml	5 ml	12 hrs
2	PVA+APS+ MV+PANI	0.1285g	40 ml	5ml	12 hrs
3	PVA+APS+ EO+PANI	0.3239g	40 ml	5 ml	12 hrs
4	PVA+APS+ CR+PANI	0.3483g	40 ml	5 ml	12 hrs
5	PVA+APS+ RB+PANI	0.2395g	40 ml	5 ml	12 hrs
6	PVA+APS+ MB+PANI	0.1599g	40 ml	5 ml	12 hrs

Table 6-2 Chemical Structure of the Dyes and Pictures of their Reduced and Oxidized States, taken from Videos of EC devices Operating in the Voltage Range of -0.7 to 2 Volts

Type of dye	Chemical Structure	Oxidized state	Reduced state
Methyl Orange	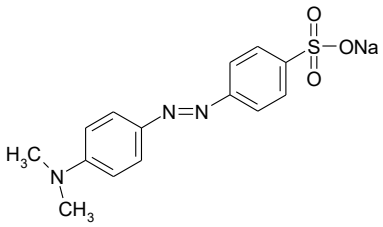	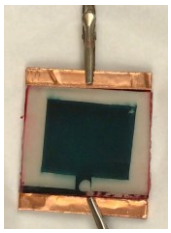	
Methyl viologen	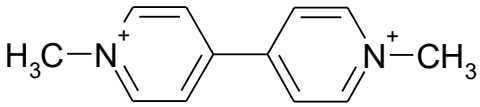	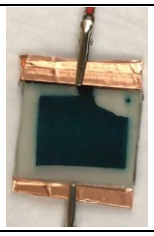	
Eosin	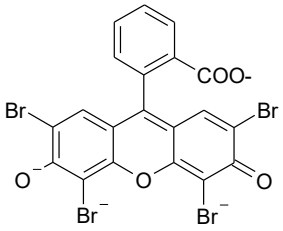	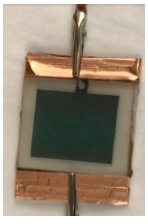	

Table 6-2 (Continued)

Type of dye	Chemical Structure	Oxidized state	Reduced state
Congo Red	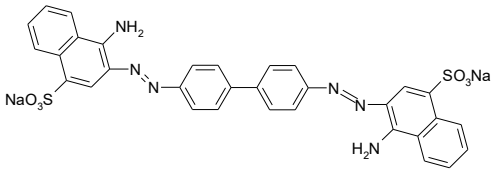	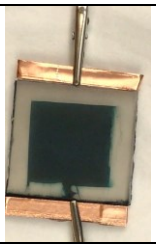	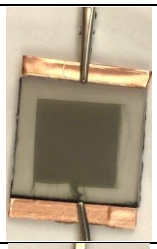
Rhodamine B	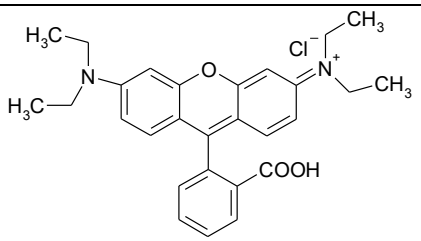	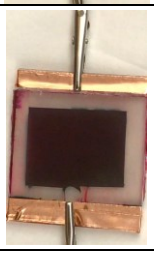	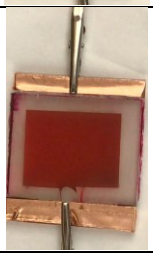
Methylene blue	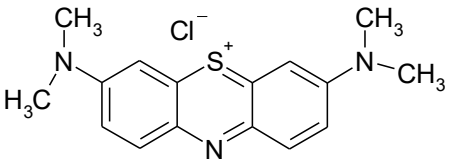		

6.3 Results and Discussion

6.3.1 SEM Studies

Figure 6-1 shows SEM pictures of the composites (PVA+APS+ PANI) and (PVA+APS+ dye (MO, MV, EO, CR, RB, or MB) +PANI) used as active layers between two FTO coated glass plates. A solution of each dye containing the active layer material was applied on the FTO coated glass plate and allowed to dry for 24 hrs. The samples were then heated at ~40-50 ºC to remove any remaining water. The presence of the dye in each of the composite (PVA+APS+DYE+PANI) mixtures greatly affects the dried gel morphology. Figure 6-1(a) shows the PVA gel containing PANI. The film shows both flat and rough surfaces after the drying process. Figure 6-1(b) shows

axe like structures on the dried composite (PVA+APS+MO+PANI) layer. More flake-like structures are visible on the entire surface of the composite (PVA+APS+ MV+PANI) film, figure 6-1(c). Figure 6-1(d) displays a rougher and charged surface in the SEM image due to its insulating nature and consequent charge by the SEM electron beam. Nearly equally distributed flakes are present on the composite (PVA+APS+CR+PANI) single layer surface (figure 6-1(e)). The surface of the composite (PVA+APS+ RB+PANI) layer shows mountain and valley type structures in addition to sharp needle like structures (figure 6-1(f)). Figure 6-1(g) shows a layered and smooth surface of the composite (PVA+APS+MB+PANI) layer due to the presence of the MB dye.

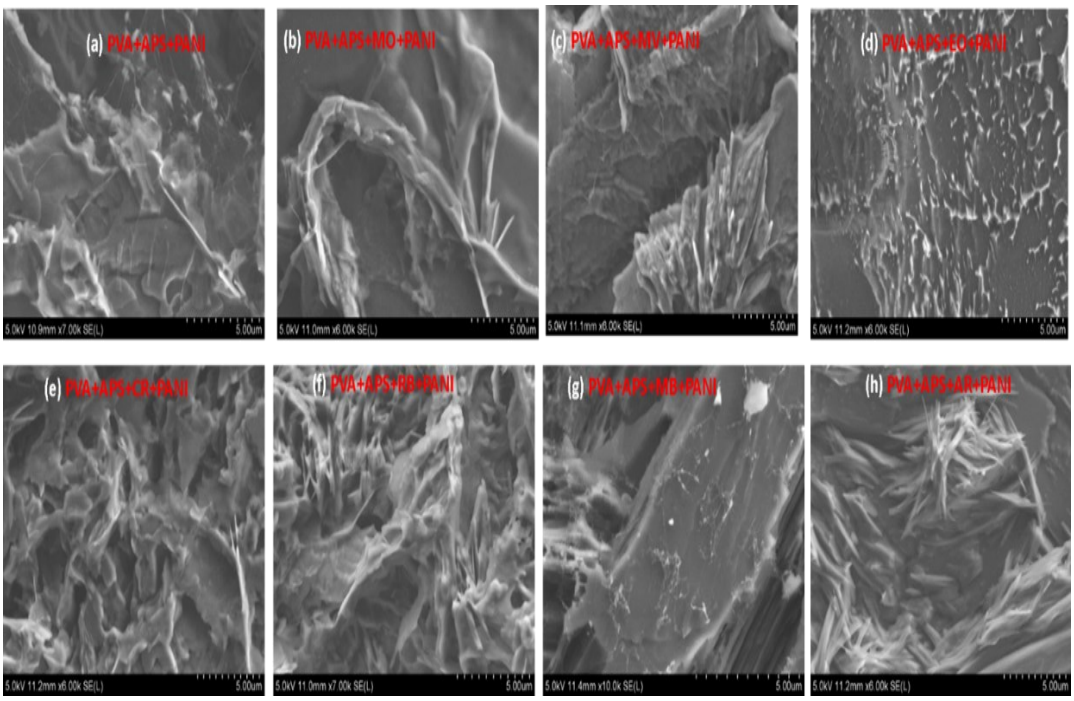

Figure 6-1 SEM Pictures of Single Layer Gels for Different Dyes: (a) No Dye; (b) Methyl Orange (MO); (c) Methyl Viologen (MV); (d) Eosin (EO); (e) Congo Red (CR); (f) Rhodamine Blue (RB); and (g) Methylene Blue (MB)

6.3.2 UV-Vis Studies

Figure 6-2, curve 1, shows the UV-vis absorption spectrum of the (PVA+APS+PANI) active layer film coated on a glass plate. It shows absorption peaks at 807, 498, 390 nm. The peaks

at 390 and 498 nm are due to polaron and bipolaron sites; however, the layer also shows a wide peak at 807 nm [64]. Figure 6-2, curve 2, shows absorption peaks for the composite (PVA+APS+MO+PANI) layer at 538 and 516 nm. It has the characteristics of MO peaks, which is an anionic dye. Figure 6-2, curve 3, shows absorption peaks for the composite (PVA+APS+MV+PANI) layer at 858, 663 and 428 nm. The MV dye has characteristic peaks at 428 nm due to the cationic radical which could possibly be due to the oxidizer [65]. It also shows the characteristic absorption peaks of MV at 663 and 858 nm.

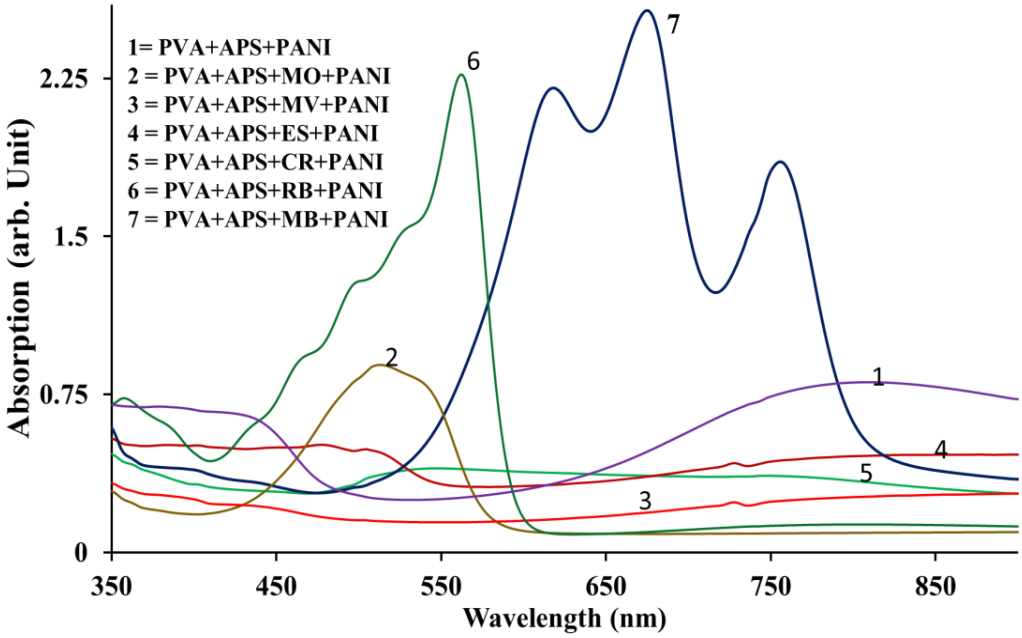

Figure 6-2 UV-Visible Absorption Spectra of Active Gel Layers Containing Different Dyes

The UV-vis absorption peaks for the composite (PVA+APS+EO+PANI) layer are present in Figure 6-2, curve 4, shows local minima peaks at 506, 482, 447 and 364 nm. Curve 5 shows UV-vis local minima peaks at 506, 482 and 381 nm due to the presence of CR in the composite (PVA+APS+CR+PANI)[66]. The peak observed at 482 nm is due to the CR red dye and is blue shifted due to the concentration of acid in the gel. The characteristic peaks of RB are shown in figure 6-2, curve 6, at 561, 530, 468, 387 nm, and the characteristic peaks of MB+ PANI peaks are

shown in figure 6-2, curve 7, at 758, 738, 676, 619, 362 nm. The absorption peaks at around 758 and 738 nm are due to the presence of dopant in PANI. The presence of peaks at 676 and 619 nm are due to the n to π* transition indicating the presence of emeraldine base.

6.3.3 UV-Visible Absorption of Composite Gel

Figure 6-3 (a) shows the UV-visible absorption of the composite (PVA+APS+MO+PANI) at 1.7 V (curve 1) and -0.7 V (curve 2). Interestingly, the absorption magnitude at 1.7 V extends from 600 to 870 nm, on the other hand, the characteristic color (light red –pinkish color) is observed at -0.7 V [62]. The purple pinkish color is also observed for the single layer composite (PVA+APS+CR+PANI) gel electrolyte (figure 6-3 (b), curve1) at a potential of -0.7 V. The presence of CR gives a dark color and a color contrast different than that of the MO dye (figure 6-3 (b), curve 3). Figure 6-3 (c) shows changes in color from dark to red in the applied voltage range of -0.7 V to 1.7 V. The sharp characteristic peak at 561 nm is present at the oxidized potential (curve 1) and the reduced potential of -0.7 V in curve 2 in figure 6-3 (c).

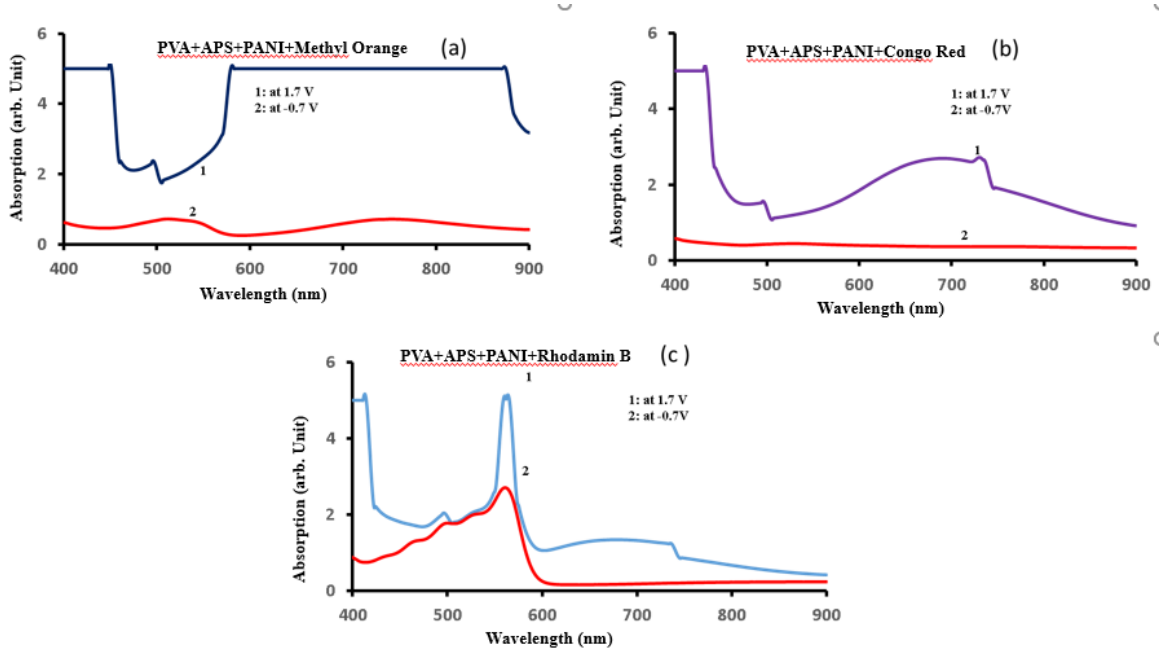

Figure 6-3 UV-Vis Absorption Spectra for Single Gel Electrolyte Layers with Different Dyes at Applied Voltages of 1.7 and -0.7 Volts

6.3.4 Cyclic Voltammetry Studies

The CV graphs of the composite (PVA+APS+ dye (MO, MV, EO, CR, RB or MB) +PANI) active layers, each sandwiched between two conducting FTO coated glass plates, are shown in Figure. 5-4. Figure 6-4 (a) shows the CV graphs of the composite (PVA+APS+MO+PANI) layer at various scan rates. The complete CV curves are repeatable, however, there is a change in the CV pattern at different scan rates due to the change in the diffusion properties of the active layer, an oxidation peak is seen around 1.55 V and reduction peaks at 0.81 V and -0.58 V. The oxidation peak is related to the oxidized pernigraniline state and the oxidized state of the MO, whereas the two reduction peaks are due to the emeraldine and leucoemeraldine forms of PANI. The pinkish color is reduced for the MO dye case, as shown at the potential of -0.7 V. The CV of the composite (PVA+APS+MV+PANI) active layer shows an oxidation peak at 1.55 V and two reduction peaks at 0.95 V and -0.59 V (PANI reduced to leucoemeraldine). The CV of the composite (PVA+APS+EO+PANI) active layer shows oxidation peaks at 1.2 V and 1.75 V and reduction peaks at 0-0.6, 0.46 and 0.76 V (figure 6-4 (c)) like those of the composite (PVA+APS+MV+PANI) active layer (figure 6-4 (b)). The viologen dye exhibits two reduction states in the -0.4 to -1.1 V voltage range [65], while, previously, we were able to observe only one reduction state as we scanned to -0.7 V.

However, the presence of the CR dye in the composite (PVA+APS+CR+PANI) active layer shows a pinkish color at the reduced state. It has an oxidation peak at 1.657 V and reduction peaks at 0.45 V and -0.63 V (figure 6-4 (d)). This interesting color feature was previously observed with the RB dye in the composite (PVA+APS+RB+PANI) active layer (figure 6-4 (e)). However, the complete leucoemeraldine peak is missing because the RB has a very high reduction potential. The presence of the MB dye has given similar results, with oxidation peaks at 1.32 and 1.8 V and

reduction peaks at 0.89, 0.29 and -0.58 V. The complete leucoemeraldine state is achieved with the MB in the (PVA+APS+MB+PANI) active layer (figure 6-4 (f)).

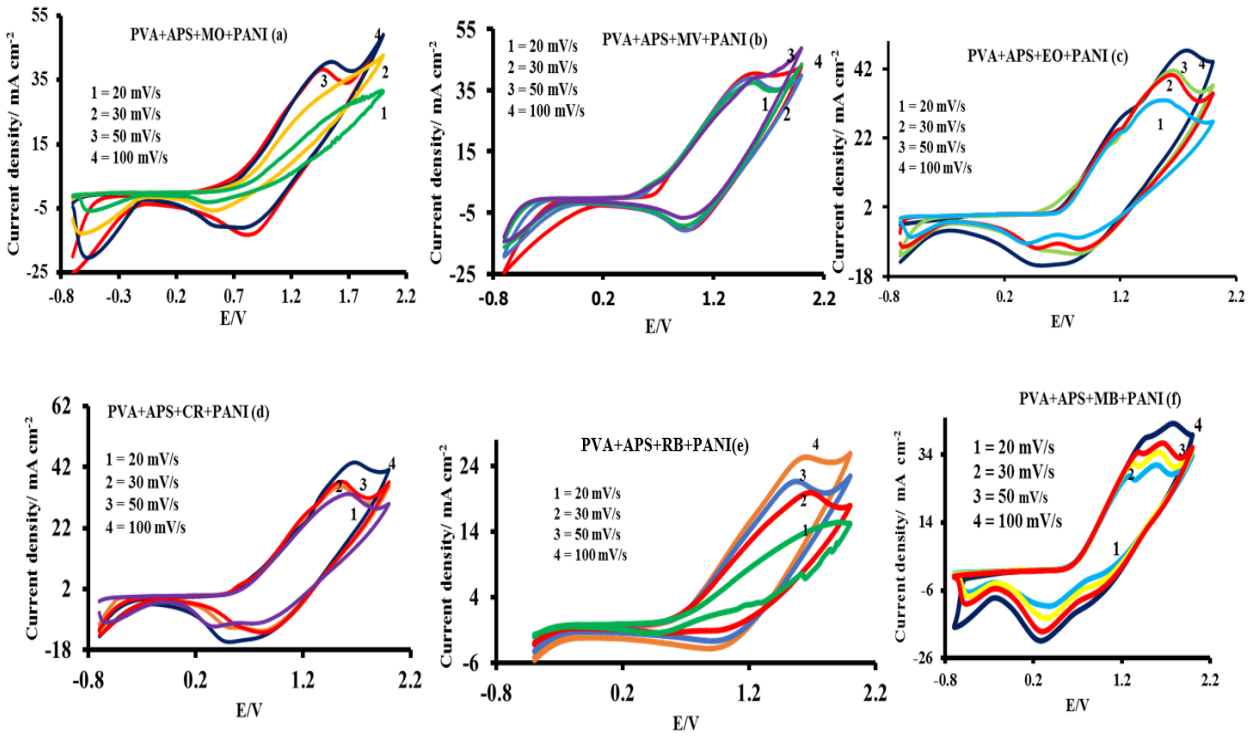

Figure 6-4 Cyclic Voltammetry Results of Various Dyes in the (PVA +APS+PANI) Active Gel Layer

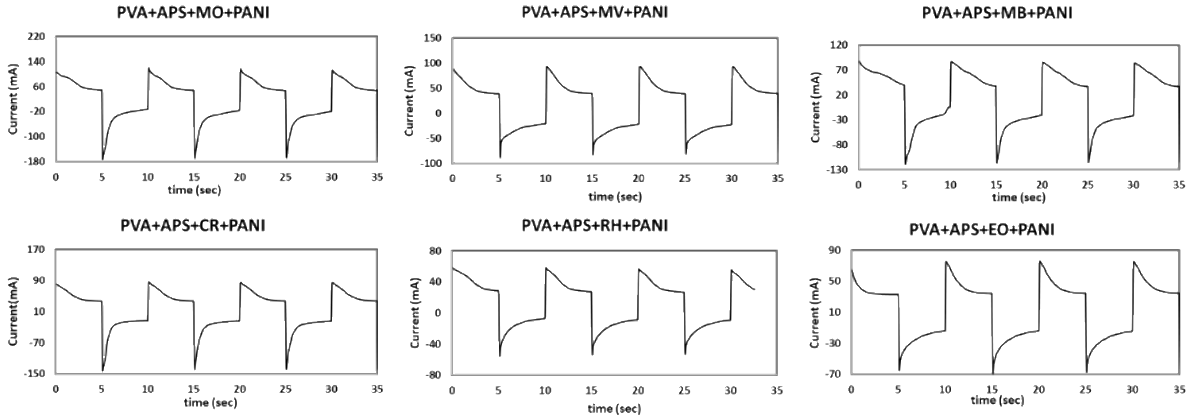

Figure 6-5 Chrono-Amperometry Results of Active Layers in EC Devices

Figure 6-5 shows the chrono-amperometry results for the composite (PVA+APS+PANI) and the composite (PVA+APS+ dye (MO, MV, EO, CR, RB, MB) +PANI) active layers deposited on FTO coated glass plates. The oxidation and reduction processes are not symmetric in each single active layer EC device. There is a marked difference between the oxidation and reduction potentials of the active layers containing CR and RB compared to the rest of the studied dyes. The decrease in the reduction as well as oxidation potentials (peaks) have been identified for different dye active layers.

6.4 Observations

An attempt is made to understand the coloration and decoloration resulting from the incorporation of various dyes contained in the single active layer of each ECD. The oxidation of each dye yields a dark color regardless of the nature of the dye. The PANI together with the dye produce a dark color (oxidized, pernigraniline) in the electric potential range of 1.5 to 1.8 V. The oxidation of the single (PANI+MB) layer has been presented in a patent by Ram et al [67] (the combined colors being even darker in the oxidized states). However, the contrast between the two-color states (oxidized and reduced) can be seen even more clearly when the reduction of the dye exceeds -0.7 V.

Figure 6-6 shows the chemical structure of the oxidized and reduced states of the composite (PVA+APS+ MO +PANI) active layer in the EC device. It is interesting to note that the oxidation state is related to the oxidized state of nitrogen in the MO dye as well as in the PANI structure. The reduction returns the MO to its original state when the reduction potential is about -0.7 V.

Similarly, the presence of the CR dye facilitates the removal of electrons from the nitrogen side of the polymer structure, as shown in figure 6-7, the oxidation and reduction are similar to the MO dye. The reduction shows a purple color which is an intermediate state.

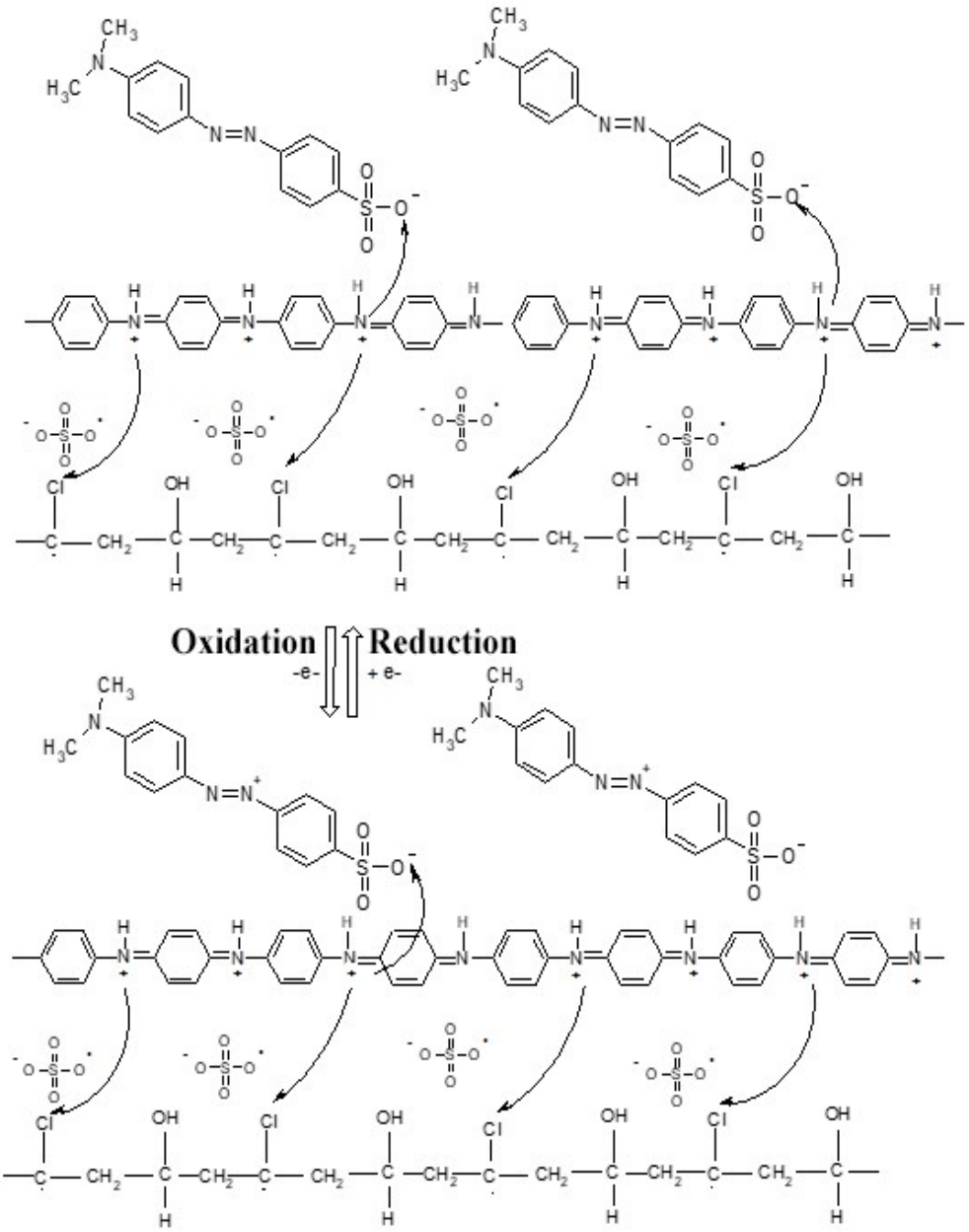

Figure 6-6 Color Coloration and Decoloration of the (PVA+APS+ MO +PANI) Active Layer EC Device

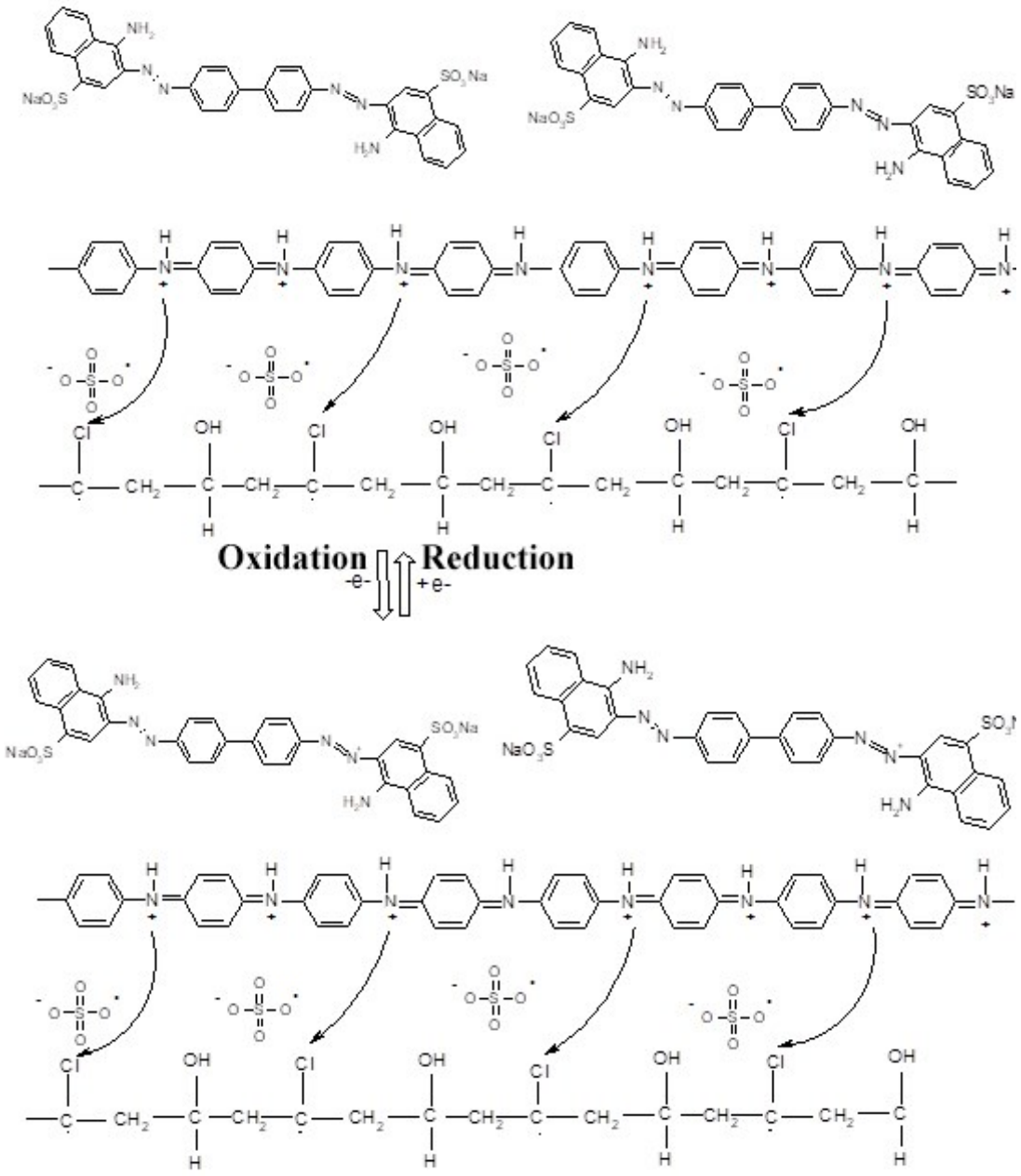

Figure 6-7 Coloration and Decoloration of the Composite (PVA+APS+ CR +PANI) Active Layer EC Device

The most striking color change was observed in the (RB + PANI) active layer, the nitrogen group being partially oxidized thus producing a red color (figure 6-8). Even though the oxidation of PANI takes place in the voltage range of 2.0 to -0.7 volts, the dominance of the RB dye produces a red color.

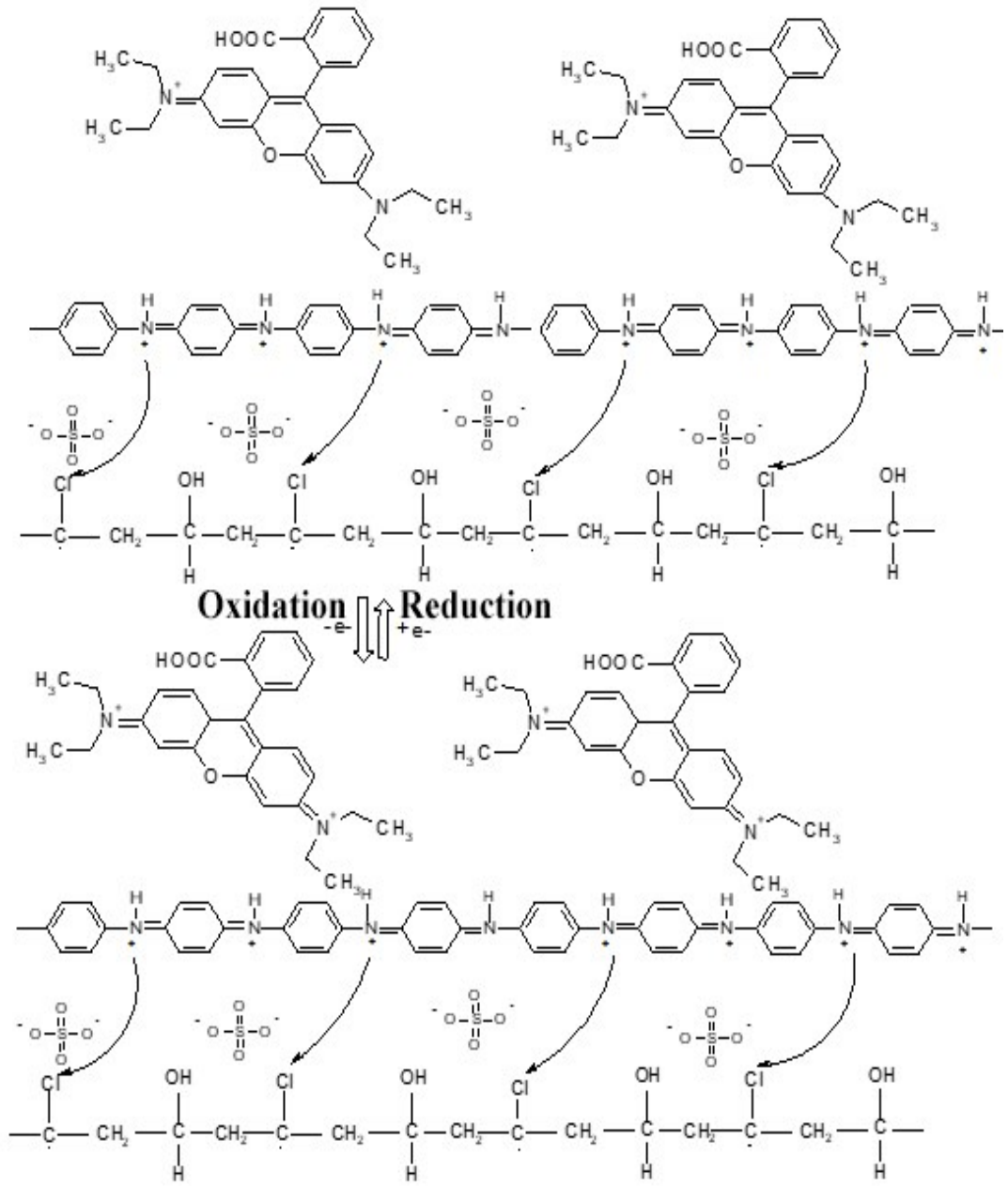

Figure 6-8 Chemical Structures explaining the Coloration and Decoloration of a Composite PVA+APS+ RB +PANI All in One Layer EC Device

6.5 Conclusions

This work was pursued to achieve various color transitions (red to black, red to blue, purple to black, etc.) and identify the required oxidation and reduction potentials for single (all in one) gel active layer EC devices. A PVA gel, containing PANI and APS, was used with various dyes

(methyl orange, methyl viologen, eosin, congo red, rhodamine b, mono-azo dyes, etc.) to produce these gel active layers. The results indicate that the redox characteristics of each dye greatly affect the overall oxidation and reduction potentials at which color change takes place. The results also show that, often, relatively high (in the order of -0.7 V) reduction potentials may be needed to achieve the transparent states. The different color states have been explained by means of the chemical structures of the [PVA + APS + DYE +PANI] single gel layer composites. All these different color ECDs exhibit short lifetimes due to the high oxidation potential, to achieve the dark color, and corresponding water electrolysis (bubble formation).

Chapter 7: Lower Power and Longer Lifetime Asymmetric Electrode Single Active Layer Electrochromic Devices

7.1 Background

In this chapter we present a recently developed single active layer technology that prevents bubble formation and reduces the power consumption of ECDs. The electrochromic device structure consists of a composite gel made by mixing polyvinyl alcohol (PVA), hydrochloric acid (HCl), an oxidant (ammonium persulphate-APS), a conducting polymer (polyaniline, PANI), sandwiched between two different conducting electrodes, having different surface work functions. The two conducting electrodes chosen for this study are FTO on glass and FTO on glass coated with a thin gold film. Experimental and theoretical results are presented to explain the color change mechanism in terms of changes in the chemical structure of the composite gel.

7.2 Materials and Methods

7.2.1 Materials

The single active layer composite layer gel electrolyte was made by following the procedure outlined in previous chapters. The FTO on the glass substrates had a thickness of 1.66mm and a surface resistance of 12 Ω-cm was used as one of the electrodes. For the second electrode gold (Au) on an FTO glass substrate. Figure 7-1 shows a schematic representation of the symmetric (FTO-Gel-FTO) and asymmetric (FTO-gel-Au) ECDs at different bias voltages.

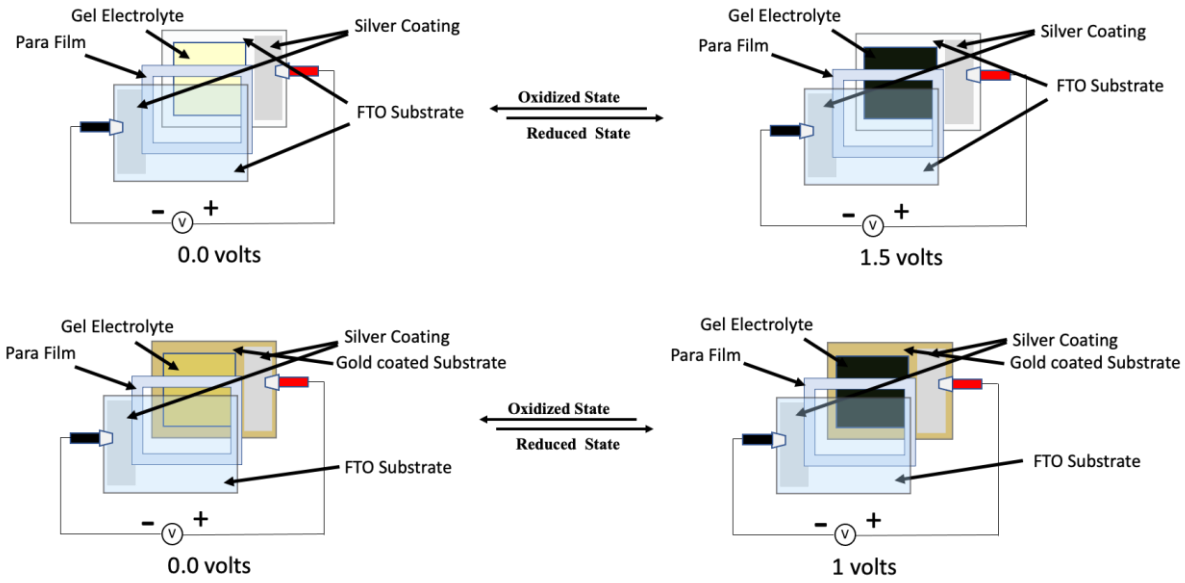

Figure 7-1 Systematic Representation of Symmetric and Asymmetric Electrochromic Device Configuration at Different Bias Voltages

7.2.2 Characterization

The elemental, structural, chemical bonding, and absorption of the composite gel (PVA-HCl-APS-PANI) has already been studied in chapters 5 and 6 for UV-Visible Spectroscopy, Fourier Transform Infrared Spectroscopy, and Scanning Electron Microscopy.

7.3 Results and Discussion

7.3.1 Cyclic Voltammetry Studies

The electrochemical properties of the composite gel (PVA-HCl-APS-PANI) single active layer for the asymmetric (FTO-Gel-Au) and the symmetric (FTO-Gel-FTO) ECDs were investigated by cyclic voltammetry (CV) [68]. The potential window was set between -1.5 V to +1.5 V for the symmetric device and -1.0 V to +1.0 V for the asymmetric device, to prevent over-oxidation of the gel. The resultant CV curves are shown in Figure 7-2.

One can see the oxidation potential of the symmetric ECD showing a broad oxidative peak at 1.39 V and a smaller peak at 1.03 V and a reduction peak at 0.8 V and -0.75 V, corresponding

to the color change of the PANI gel from deep- green to yellow or colorless (transitions from pernigraniline to leucoemeraldine).

In contrast, the asymmetric device in Figure 7-2 b shows a reduction in the oxidation peak from about 1.4 V (symmetric) to about 0.6 V (asymmetric). The reduction peak for the asymmetric device is at about -0.3 V. In addition, the device current was reduced from 25 mA (symmetric) to 12 mA (asymmetric). The reduction of both the current and voltage at the corresponding oxidation peaks of the symmetric and asymmetric devices, implies a significant reduction in the power consumption of the asymmetric device.

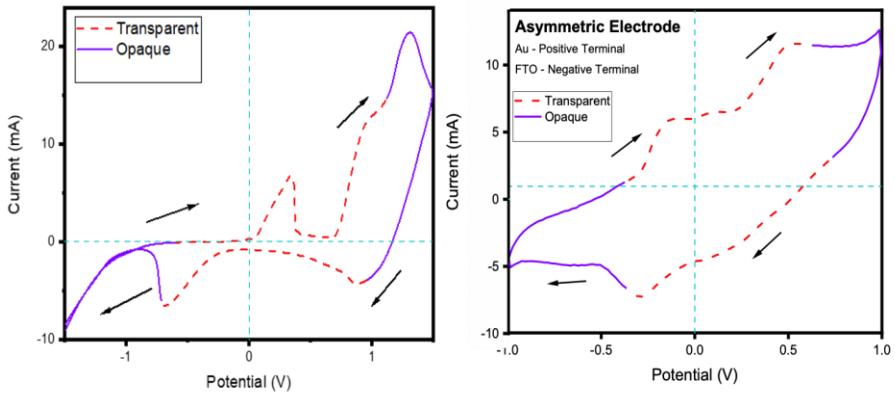

Figure 7-2 Cyclic Voltametric Analysis of Composite Gel PVA-HCl-APS-PANI with Symmetric and Asymmetric Electrode Device Configuration with a Scan Rate of 50 mV/s

7.3.2 Mechanism of Color Change

Figure 7-3 a show the gelling process of PVA in the HCl solution. The condensation of the hydroxyl group of PVA and dissociation of chlorine ions from HCl acid depends upon the chemical interaction and temperature applied to the PVA in the HCl solution. Under high temperatures, the water molecules are released, and chlorine is attached to the PVA in the gelling process. It essential to form a light-yellow transparent gel by keeping the temperature below 90°C; otherwise, the gel becomes dark and brownish. Figure 7-3a shows the formation of free radical carbon atoms in the

PVA gel structure using the initiator APS as an oxidant. An electron is removed from the PVA-HCl gel structure, producing an electron acceptor material due to the oxidant (APS) [22,24]. Figure 7-3b shows that the PVA-HCl structure is having an electron acceptor material. Figure 7-3c reveals the formation of emeraldine salt as the doped form of the PANI structure, which is green in color with the addition of aniline to PVA-HCl-APS. The possible chemical interaction of ES with the (PVA-HCl-APS) gel yield to the structure (PVA-HCl-APS-PANI) structure has the ES state interacts with the chlorine ions in the PVA-HCl-APS because of the lone pair effect of the ES state of PANI. Figure 7-3d shows the transition of PVA-HCl-APS-PANI composite gel between ES and LS states by adding or removing electron-proton (H^+) pairs. However, the oxidation state of PANI can also be changed to an emeraldine base by removing protons (H^+) and de-doping the polymer. Upon applying a voltage to the composite gel, the electrochromic device changes color from dark

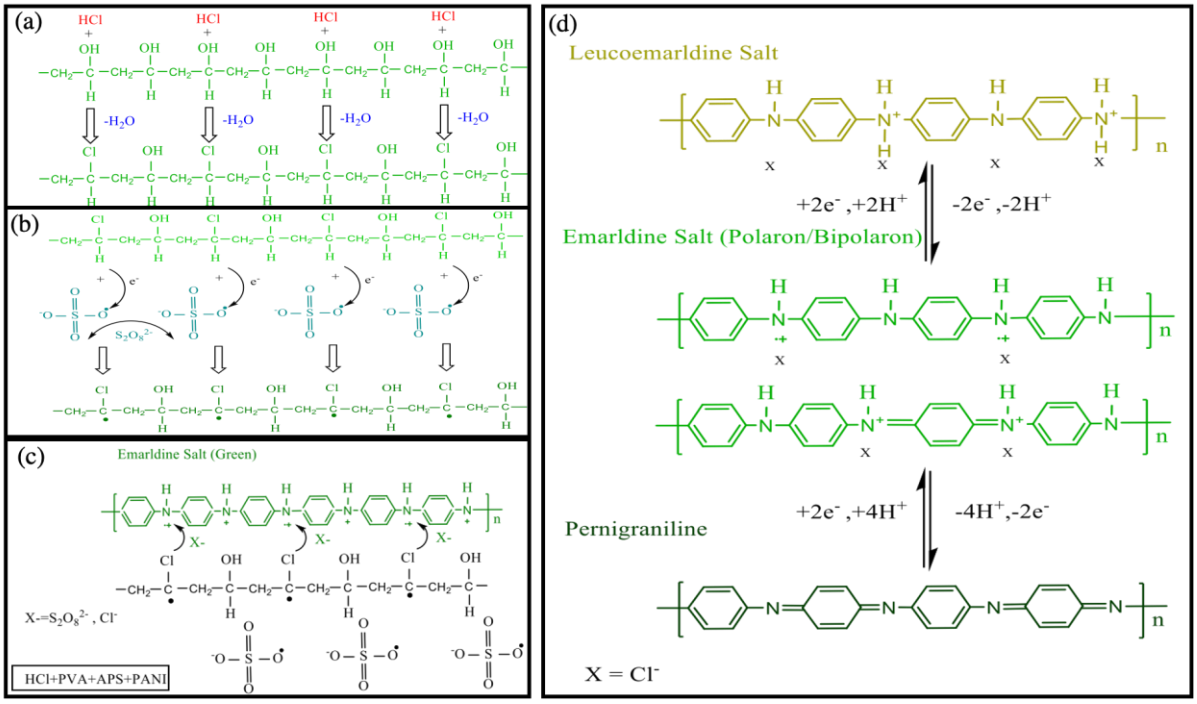

Figure 7-3 Gelling process of the Composite Gel: a) The Gelling Chemical process of PVA in HCl; b) The PVA-HCl gel with Ammonium Persulfate (APS); c) The Interaction of PVA-HCl gel with APS and PANI after Polymerization; and d) Chemical Reactions in three Different Oxidation States of PANI

purple to green- faded yellow [26,69,70]. The coloration and de-coloration from dark blue to transparent depend upon the applied voltage between -1.5 and 1.5V.

7.4 Conclusions

The electrochemical behavior of the asymmetric EC devices was studied using cyclic voltammetry at the potential -1V to +1V for the asymmetric EC devices (FTO-Gel-Au) and -1.5 V to +1.5 V for the symmetric EC device (FTO-Gel-FTO). An explanation of the coloration and decoloration of the asymmetric device has been presented based on the chemical structure of polyaniline and PVA present in the composite gel. The asymmetric ECD has great potential to produce commercial ECDs.

Chapter 8: Conclusions and Recommendations for Future Research

8.1 Conclusions

A great deal of research has been carried out in gel and liquid electrolytes for Electrochromic and Touchchromic devices. Although, initially, the research was focused on touchchromic devices, the difficulties of applying this technology to commercial devices, changed the research direction. The single active layer-based electrochromic devices are easy to fabricate, suitable for flexible-wearable devices and can quickly switch color. Asymmetric electrode ECDs have greater durability and require less power to operate. All of these features represent competitive advantages over other multilayer electrochromic devices. Specific contributions that have been made in the areas of touch chromic and electrochromic devices are:

- A novel touch chromic device with reversible color change from dark to transparent, when the active layer is touched by a specific metal, without any other external excitation such as voltage.
- A new relatively simple and potentially inexpensive electrochromic (EC) device consisting of a single composite gel active layer placed between two transparent conducting glass plates.
- A new asymmetric electrochromic (EC) device that eliminates the problem of bubble formation in the electrolyte, extends the device lifetime and reduces the power consumption.

This knowledge can help in the development of a low cost, abundant and non-toxic ECD that uses an extensively studied polymeric material.

8.2 Recommendations for Future Research

To continue this work, further study is needed to understand the transfer of charges, i.e., ions and electrons in the redox-active composite gel electrolyte, to enhance the total efficiency of the electrochromic device and increase its lifecycle. For this purpose, the following additional research on the composite gel PVA+HCl+APS+PANI could be pursued:

- Doping the composite gel with a metal oxide such as Nickel Oxide, Tungsten oxide, etc., to improve the operation at low voltages and decrease energy consumption.
- Trying different types of acidic solutions in the redox-active gel material to change the oxidation state of PANI.
- Mixing different types of conjugated polymers to optimize the device, particularly in processing techniques.
- Improving the thermal and UV stability of the Electrochromic device through proper anti-reflective coatings.
- Incorporating nanostructures (i.e., mxene) in the thin film to improve switching speed and device stability.

References

[1] Print Resource | Texas Gateway, (n.d.). https://www.texasgateway.org/node/70171/print (accessed June 3, 2021).

[2] S.D. Rezaei et al., "A review of conventional, advanced, and smart glazing technologies and materials for improving indoor environment," Solar Energy Materials and Solar Cells 159 (2017)26-51.

[3] C.C. Mardare, A.W. Hassel, Review on the Versatility of Tungsten Oxide Coatings, Phys. Status Solidi Appl. Mater. Sci. 216 (2019). https://doi.org/10.1002/pssa.201900047.

[4] P. Monk, R. Mortimer, D. Rosseinsky, Introduction to electrochromism, Electrochromism and Electrochromic Devices. (2009) 1–24. https://doi.org/10.1017/cbo9780511550959.003.

[5] S.K. Deb, "Opportunities and challenges of electrochromic phenomena in transition metal oxides," Solar Energy Materials and Solar Cells 25 (1992) 327-338.

[6] S.K. Deb et al., "Stand-alone photovoltaic-powered electrochromic smart window," Electrochimica Acta 46 (2001) 2125-2130.

[7] Y. Ke, J. Chen, G. Lin, S. Wang, Y. Zhou, J. Yin, P.S. Lee, Y. Long, Smart Windows: Electro-, Thermo-, Mechano-, Photochromics, and Beyond, Adv. Energy Mater. 9 (2019). https://doi.org/10.1002/aenm.201902066.

[8] S.S. Kalagi et al., "Limitations of dual and complementary inorganic-organic electrochromic device for smart window application and its colorimetric analysis," Synthetic Metals 161 (2011)1105-1112.

[9] A. Karuppasamy et al., "Studies on electrochromic smart windows based on titanium doped WO3 thin films, "Thin Solid Films 516 (2007) 175-178.

[10] B.P. Jelle et al., "Fenestration of today and tomorrow: A state-of-the-art review and future research opportunities," Solar Energy Materials and Solar Cells 96 (2012) 1-28.

[11] K. S. Ahn et al., "Tandem dye-sensitized solar cell powered electrochromic devices for the photovoltaic-powered smart window," Journal of Power Sources 168 (2007) 533-536.

[12] B.P. Jelle, Accelerated climate ageing of building materials, components and structures in the laboratory, J. Mater. Sci. 47 (2012) 6475–6496. https://doi.org/10.1007/s10853-012-6349-7.

[13] M.S. Wang, G. Xu, Z.J. Zhang, G.C. Guo, Inorganic-organic hybrid photochromic materials, Chem. Commun. 46 (2010) 361–376. https://doi.org/10.1039/b917890b.

[14] A. Seeboth, D. Lötzsch, R. Ruhmann, O. Muehling, Thermochromic polymers - Function by design, Chem. Rev. 114 (2014) 3037–3068. https://doi.org/10.1021/cr400462e.

[15] B. Aljafari, S.K. Indrakar, M.K. Ram, P.K. Biswas, E. Stefanakos, A. Takshi, A Polyaniline-Based Redox-Active Composite Gel Electrolyte with Photo-Electric and Electrochromic Properties, ChemElectroChem. 6 (2019) 5888–5895. https://doi.org/10.1002/celc.201901850.

[16] Marina S. Zavakhina et al., "Halochromic coordination polymers based on a triarylmethane dye for reversible detection of acids," Dalton Trans., 2017, 46, 465-470.

[17] F. Fages, Chapter 23 MAGNETO-SENSITIVE GELS, (2006) 793–794.

[18] X. Song, H. lin Wang, J. Shi, J.W. Park, B.I. Swanson, Conjugated polymers as efficient fluorescence quenchers and their applications for bioassays, Chem. Mater. 14 (2002) 2342–2347. https://doi.org/10.1021/cm011681f.

[19] Y. Yang, K.Z. Wang, D. Yan, Smart Luminescent Coordination Polymers toward Multimode Logic Gates: Time-Resolved, Tribochromic and Excitation-Dependent Fluorescence/Phosphorescence Emission, ACS Appl. Mater. Interfaces. 9 (2017) 17399–17407. https://doi.org/10.1021/acsami.7b00594.

[20] B. Liu, G.C. Bazan, Optimization of the molecular orbital energies of conjugated polymers for optical amplification of fluorescent sensors, J. Am. Chem. Soc. 128 (2006) 1188–1196. https://doi.org/10.1021/ja055382t.

[21] M.K. Ram et al.,"A new chromic (TouchChromic) thin film," Acta Materialia 121 (2016) 325-330.

[22] R. Djara, Y. Holade, A. Merzouki, N. Masquelez, D. Cot, B. Rebiere, E. Petit, P. Huguet, C. Canaff, S. Morisset, T.W. Napporn, D. Cornu, S. Tingry, Insights from the Physicochemical and Electrochemical Screening of the Potentiality of the Chemically Synthesized Polyaniline, J. Electrochem. Soc. 167 (2020) 066503. https://doi.org/10.1149/1945-7111/ab7d40.

[23] United States Patent Application: 0190033625, (n.d.). https://appft.uspto.gov/netacgi/nph-Parser?Sect1=PTO1&Sect2=HITOFF&p=1&u=/netahtml/PTO/srchnum.html&r=1&f=G&l=50&d=PG01&s1=20190033625.PGNR. (accessed June 2, 2021).

[24] A. Kraft, Electrochromism: a fascinating branch of electrochemistry, ChemTexts. 5 (2019) 1–18. https://doi.org/10.1007/s40828-018-0076-x.

[25] Metal Sensitized Color Changing Material, (2015).

[26] S. Elmas, W. Beelders, J. Nash, T.J. Macdonald, M. Jasieniak, H.J. Griesser, T. Nann, Photo-doping of plasma-deposited polyaniline (PAni), RSC Adv. 6 (2016) 70691–70699. https://doi.org/10.1039/c6ra12886f.

[27] Work Functions - an overview | ScienceDirect Topics, (n.d.). https://www.sciencedirect.com/topics/physics-and-astronomy/work-functions (accessed June 2, 2021).

[28] R.J. Mortimer, A.L. Dyer, J.R. Reynolds, Electrochromic organic and polymeric materials for display applications, Displays. 27 (2006) 2–18. https://doi.org/10.1016/j.displa.2005.03.003.

[29] A. V. Shchegolkov, E.N. Tugolukov, A. V. Shchegolkov, Overview of Electrochromic Materials and Devices: Scope and Development Prospects, Adv. Mater. Technol. 2 (2020) 066–073. https://doi.org/10.17277/amt.2020.02.pp.066-073.

[30] K.J. Patel, G.G. Bhatt, J.R. Ray, P. Suryavanshi, C.J. Panchal, All-inorganic solid-state electrochromic devices: a review, J. Solid State Electrochem. 21 (2017) 337–347. https://doi.org/10.1007/s10008-016-3408-z.

[31] R. Vergaz, Electrical analysis of new all-plastic electrochromic devices, Opt. Eng. 45 (2006) 110501. https://doi.org/10.1117/1.2388278.

[32] R. John, Electrochemical studies of heterocyclic conducting polymers, (1992) 98–103. http://ro.uow.edu.au/theses/1142.

[33] A. Streitwieser, A. Harman, A. Butcher, M. Pagni, A. Mayeda, if! if, 24 (1978) 1971–1973.

[34] G.A. Evtyugin, E.E. Stoikova, Electrochemical biosensors based on dendrimers, J. Anal. Chem. 70 (2015) 517–534. https://doi.org/10.1134/S1061934815050044.

[35] M. Mozafari, M. Mehraien, D. Vashaee, L. Tayebi, Electroconductive Nanocomposite Scaffolds: A New Strategy Into Tissue Engineering and Regenerative Medicine, Nanocomposites - New Trends Dev. (2012). https://doi.org/10.5772/51058.

[36] Namsheer K et al., "Conducting polymers: a comprehensive review on recent advances in synthesis, properties and applications," RSC Adv., 2021, 1, 5659.

[37] D.D. Ateh, H.A. Navsaria, P. Vadgama, Polypyrrole-based conducting polymers and interactions with biological tissues, J. R. Soc. Interface. 3 (2006) 741–752. https://doi.org/10.1098/rsif.2006.0141.

[38] J.D. Madden, Polypyrrole actuators: Properties and initial applications, in: Electroact. Polym. Robot. Appl. Artif. Muscles Sensors, Springer London, 2007: pp. 121–152. https://doi.org/10.1007/978-1-84628-372-7_5.

[39] E.H. Yu, K. Sundmacher, Enzyme electrodes for glucose oxidation prepared by electropolymerization of pyrrole, Process Saf. Environ. Prot. 85 (2007) 489–493. https://doi.org/10.1205/psep07031.

[40] M.R. Karim, C.J. Lee, M.S. Lee, Synthesis and characterization of conducting polythiophene/carbon nanotubes composites, J. Polym. Sci. Part A Polym. Chem. 44 (2006) 5283–5290. https://doi.org/10.1002/pola.21640.

[41] M.T. Ramesan, K. Suhailath, Role of nanoparticles on polymer composites, in: Micro Nano Fibrillar Compos. (MFCs NFCs) from Polym. Blends, Elsevier Inc., 2017: pp. 301–326. https://doi.org/10.1016/B978-0-08-101991-7.00013-3.

[42] Z.A. Boeva, V.G. Sergeyev, Polyaniline: Synthesis, properties, and application, Polym. Sci. - Ser. C. 56 (2014) 144–153. https://doi.org/10.1134/S1811238214010032.

[43] T. Hagiwara, T. Demura, K. Iwata, Synthesis and properties of electrically conducting polymers from aromatic amines, Synth. Met. 18 (1987) 317–322. https://doi.org/10.1016/0379-6779(87)90898-8.

[44] M.A.C. Mazzeu, L.K. Faria, A. de M. Cardoso, A.M. Gama, M.R. Baldan, E.S. Gonçalves, Structural and morphological characteristics of polyaniline synthesized in pilot scale, J. Aerosp. Technol. Manag. 9 (2017) 39–47. https://doi.org/10.5028/jatm.v9i1.726.

[45] T. David et al., " Part A: Synthesis of Polyaniline and Carboxylic acid functionalized SWCNT composites for electromagnetic interference sheilding coatings," Polymer 55 (2014) 5665-5672.

[46] A. Olad, M. Khatamian, B. Naseri, Removal of toxic hexavalent chromium by polyaniline modified clinoptilolite nanoparticles, J. Iran. Chem. Soc. 8 (2011). https://doi.org/10.1007/bf03254291.

[47] A. Montes-Rojas, M. Ramírez-Orizaga, J.G. Ávila-Rodríguez, L.M. Torres-Rodríguez, Study of polyaniline/poly(Sodium 4-styrenesulfonate) composite deposits using an electrochemical quartz crystal microbalance for the modification of a commercial anion exchange membrane, Membranes (Basel). 10 (2020) 1–19. https://doi.org/10.3390/membranes10120387.

[48] S. Shahabuddin, N.M. Sarih, M.A. Kamboh, H.R. Nodeh, S. Mohamad, Synthesis of polyaniline-coated graphene oxide@SrTiO3 nanocube nanocomposites for enhanced removal of carcinogenic dyes from aqueous solution, Polymers (Basel). 8 (2016). https://doi.org/10.3390/polym8090305.

[49] S. Rami, Synthesis , Characterization , and Electrochemical Properties of Polyaniline Thin Films, J. Macromol. Sci. Part A - Chem. (2015). http://scholarcommons.usf.edu/etd/5563.

[50] M. Ayad, S. Zaghlol, Nanostructured crosslinked polyaniline with high surface area: Synthesis, characterization and adsorption for organic dye, Chem. Eng. J. 204–205 (2012) 79–86. https://doi.org/10.1016/j.cej.2012.07.102.

[51] E. Song, J.-W. Choi, Conducting Polyaniline Nanowire and Its Applications in Chemiresistive Sensing, Nanomaterials. 3 (2013) 498–523. https://doi.org/10.3390/nano3030498.

[52] Chronoamperometry - an overview | ScienceDirect Topics, (n.d.). https://www.sciencedirect.com/topics/chemistry/chronoamperometry (accessed June 3, 2021).

[53] Electrochemical Impedance Spectroscopy - an overview | ScienceDirect Topics, (n.d.). https://www.sciencedirect.com/topics/engineering/electrochemical-impedance-spectroscopy (accessed June 3, 2021).

[54] Scanning Electron Microscopy - an overview | ScienceDirect Topics, (n.d.). https://www.sciencedirect.com/topics/engineering/scanning-electron-microscopy (accessed June 3, 2021).

[55] I. Amenabar, S. Poly, W. Nuansing, E.H. Hubrich, A.A. Govyadinov, F. Huth, R. Krutokhvostov, L. Zhang, M. Knez, J. Heberle, A.M. Bittner, R. Hillenbrand, Structural analysis and mapping of individual protein complexes by infrared nanospectroscopy, Nat. Commun. 4 (2013) 2890. https://doi.org/10.1038/ncomms3890.

[56] M.N. Berberan-Santos, Beer's law revisited, J. Chem. Educ. 67 (1990) 757–759. https://doi.org/10.1021/ed067p757.

[57] S. Kuwabata, K. Mitsui, H. Yoneyama, Angle of Di ffract:i on, New York. 139 (1992) 1824–1830.

[58] M. Srimathi, R. Rajalakshmi, S. Subhashini, Polyvinyl alcohol-sulphanilic acid water soluble composite as corrosion inhibitor for mild steel in hydrochloric acid medium, Arab. J. Chem. 7 (2014) 647–656. https://doi.org/10.1016/j.arabjc.2010.11.013.

[59] H.S. Mansur, C.M. Sadahira, A.N. Souza, A.A.P. Mansur, FTIR spectroscopy characterization of poly (vinyl alcohol) hydrogel with different hydrolysis degree and chemically crosslinked with glutaraldehyde, Mater. Sci. Eng. C. 28 (2008) 539–548. https://doi.org/10.1016/j.msec.2007.10.088.

[60] T. Bora, P. Sathe, K. Laxman, S. Dobretsov, J. Dutta, Defect engineered visible light active ZnO nanorods for photocatalytic treatment of water, Catal. Today. 284 (2017) 11–18. https://doi.org/10.1016/j.cattod.2016.09.014.

[61] F. Ahmed, R. Dewani, M.K. Pervez, S.J. Mahboob, S.A. Soomro, Non-destructive FT-IR analysis of mono azo dyes, Bulg. Chem. Commun. 48 (2016) 71–77. http://webbook.nist.gov.

[62] A.R. Prasad, A. Joseph, Synthesis, characterization and investigation of methyl orange dye removal from aqueous solutions using waterborne poly vinyl pyrrolidone (PVP) stabilized poly aniline (PANI) core-shell nanoparticles, RSC Adv. 7 (2017) 20960–20968. https://doi.org/10.1039/C7RA01790A.

[63] B. Aljafari et al., Polyvinyl alcohol-acid redox active gel electrolytes for electrical double-layer capacitor devices, J Solid State Electrochem (2019) 23:125-133.

[64] J. Oakes, P. Gratton, Kinetic investigations of the oxidation of Methyl Orange and substituted arylazonaphthol dyes by peracids in aqueous solution, J. Chem. Soc. Perkin Trans. 2. (1998) 2563–2568. https://doi.org/10.1039/a807272h.

[65] K. Moon, J. Grindstaff, D. Sobransingh, A.E. Kaifer, Cucurbit[8]uril-mediated redox-controlled self-assembly of viologen-containing dendrimers, Angew. Chemie - Int. Ed. 43 (2004) 5496–5499. https://doi.org/10.1002/anie.200460179.

[66] T.E. Sladewski et al., The effect of ionic strength on the UV-vis spectrum of congo red in aqueous solution, Spectrochimica Acta Part A 65 (2006) 985-987.

[67] W.I. Property, I.P. Number, I.P. Date, Wo 2018/213411, 10 (2018).

[68] N. Elgrishi, K.J. Rountree, B.D. McCarthy, E.S. Rountree, T.T. Eisenhart, J.L. Dempsey, A Practical Beginner's Guide to Cyclic Voltammetry, J. Chem. Educ. 95 (2018) 197–206. https://doi.org/10.1021/acs.jchemed.7b00361.

[69] W. Lu, A.G. Fadeev, B. Qi, E. Smela, B.R. Mattes, J. Ding, G.M. Spinks, J. Mazurkiewicz, D. Zhou, G.G. Wallace, D.R. MacFarlane, S.A. Forsyth, M. Forsyth, Use of ionic liquids for π-conjugated polymer electrochemical devices, Science (80-.). 297 (2002) 983–987. https://doi.org/10.1126/science.1072651.

[70] S.J. Tang, A.T. Wang, S.Y. Lin, K.Y. Huang, C.C. Yang, J.M. Yeh, K.C. Chiu, Polymerization of aniline under various concentrations of APS and HCl, Polym. J. 43 (2011) 667–675. https://doi.org/10.1038/pj.2011.43.

Appendix A: Copyrights and Permissions

Below is copyright permission for figure 1-2

CCC | RightsLink®

My Orders | My Library | My Profile | Welcome sharankumar@usf.edu Log out | Help

My Orders > Orders > All Orders

License Details

This Agreement between Mr. sharan indrakar ("You") and John Wiley and Sons ("John Wiley and Sons") consists of your license details and the terms and conditions provided by John Wiley and Sons and Copyright Clearance Center.

Print Copy

License Number	5098381304728
License date	Jun 29, 2021
Licensed Content Publisher	John Wiley and Sons
Licensed Content Publication	physica status solidi (a) applications and materials science
Licensed Content Title	Review on the Versatility of Tungsten Oxide Coatings
Licensed Content Author	Cezarina C. Mardare, Achim W. Hassel
Licensed Content Date	Apr 29, 2019
Licensed Content Volume	216
Licensed Content Issue	12
Licensed Content Pages	16
Type of Use	Dissertation/Thesis
Requestor type	University/Academic
Format	Electronic
Portion	Figure/table
Number of figures/tables	1
Will you be translating?	No
Title	Doctoral student
Institution name	university of south florida
Expected presentation date	Jan 2022
Portions	Figuree 9
Requestor Location	Mr. sharan indrakar [redacted] Attn: university of south florida
Publisher Tax ID	EU826007151
Total	**0.00 USD**

Below is copyright permission for Figure 2-2, Figure 2-5, and Figure 2-6

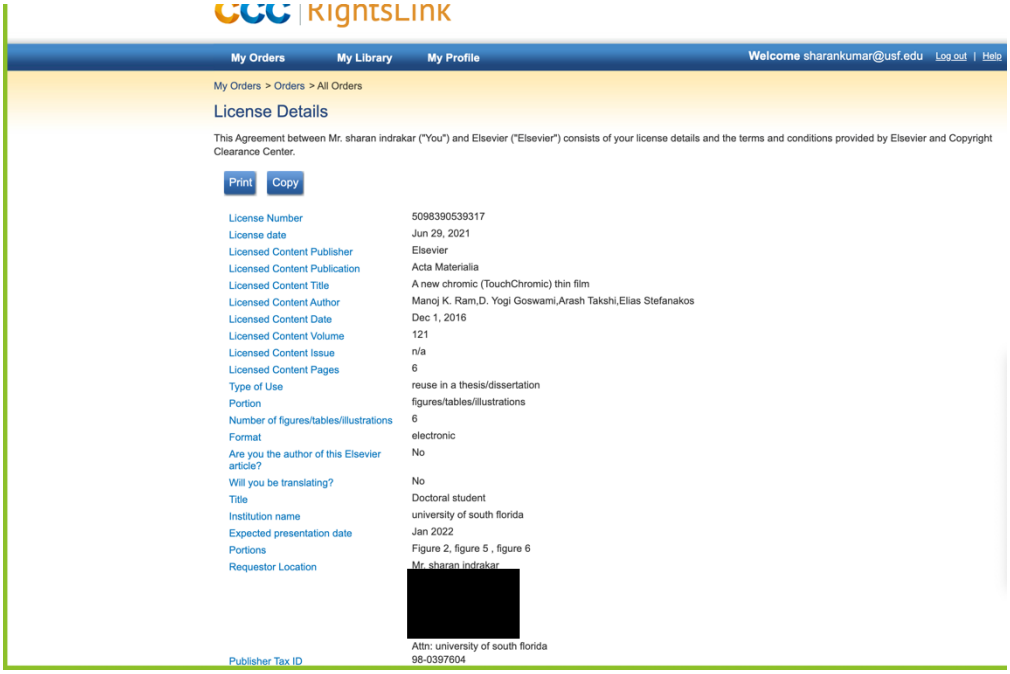

RightsLink

My Orders | My Library | My Profile | Welcome sharankumar@usf.edu Log out | Help

My Orders > Orders > All Orders

License Details

This Agreement between Mr. sharan indrakar ("You") and Elsevier ("Elsevier") consists of your license details and the terms and conditions provided by Elsevier and Copyright Clearance Center.

Print Copy

License Number	5098390539317
License date	Jun 29, 2021
Licensed Content Publisher	Elsevier
Licensed Content Publication	Acta Materialia
Licensed Content Title	A new chromic (TouchChromic) thin film
Licensed Content Author	Manoj K. Ram,D. Yogi Goswami,Arash Takshi,Elias Stefanakos
Licensed Content Date	Dec 1, 2016
Licensed Content Volume	121
Licensed Content Issue	n/a
Licensed Content Pages	6
Type of Use	reuse in a thesis/dissertation
Portion	figures/tables/illustrations
Number of figures/tables/illustrations	6
Format	electronic
Are you the author of this Elsevier article?	No
Will you be translating?	No
Title	Doctoral student
Institution name	university of south florida
Expected presentation date	Jan 2022
Portions	Figure 2, figure 5 , figure 6
Requestor Location	Mr. sharan indrakar [redacted] Attn: university of south florida
Publisher Tax ID	98-0397604

Below is copyright permission for Figure 2-4

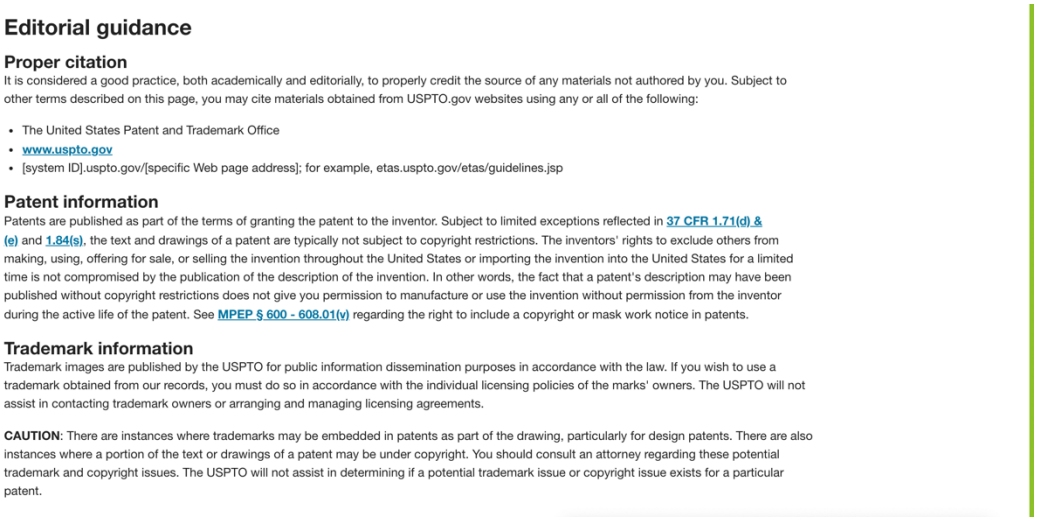

Editorial guidance

Proper citation

It is considered a good practice, both academically and editorially, to properly credit the source of any materials not authored by you. Subject to other terms described on this page, you may cite materials obtained from USPTO.gov websites using any or all of the following:

- The United States Patent and Trademark Office
- www.uspto.gov
- [system ID].uspto.gov/[specific Web page address]; for example, etas.uspto.gov/etas/guidelines.jsp

Patent information

Patents are published as part of the terms of granting the patent to the inventor. Subject to limited exceptions reflected in 37 CFR 1.71(d) & (e) and 1.84(s), the text and drawings of a patent are typically not subject to copyright restrictions. The inventors' rights to exclude others from making, using, offering for sale, or selling the invention throughout the United States or importing the invention into the United States for a limited time is not compromised by the publication of the description of the invention. In other words, the fact that a patent's description may have been published without copyright restrictions does not give you permission to manufacture or use the invention without permission from the inventor during the active life of the patent. See MPEP § 600 - 608.01(v) regarding the right to include a copyright or mask work notice in patents.

Trademark information

Trademark images are published by the USPTO for public information dissemination purposes in accordance with the law. If you wish to use a trademark obtained from our records, you must do so in accordance with the individual licensing policies of the marks' owners. The USPTO will not assist in contacting trademark owners or arranging and managing licensing agreements.

CAUTION: There are instances where trademarks may be embedded in patents as part of the drawing, particularly for design patents. There are also instances where a portion of the text or drawings of a patent may be under copyright. You should consult an attorney regarding these potential trademark and copyright issues. The USPTO will not assist in determining if a potential trademark issue or copyright issue exists for a particular patent.

Below is copyright permission for Figure 2-7

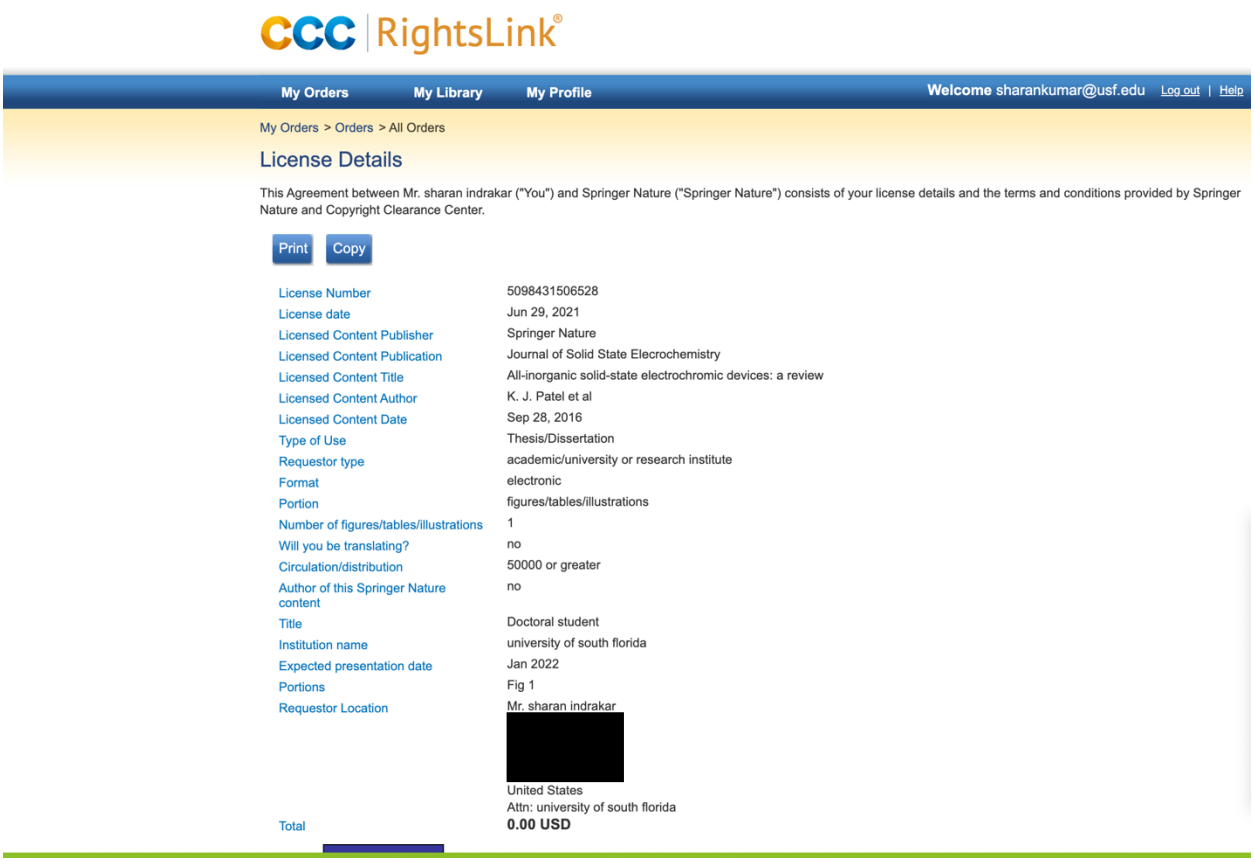

CCC | RightsLink®

My Orders | My Library | My Profile | Welcome sharankumar@usf.edu | Log out | Help

My Orders > Orders > All Orders

License Details

This Agreement between Mr. sharan indrakar ("You") and Springer Nature ("Springer Nature") consists of your license details and the terms and conditions provided by Springer Nature and Copyright Clearance Center.

Print | Copy

License Number	5098431506528
License date	Jun 29, 2021
Licensed Content Publisher	Springer Nature
Licensed Content Publication	Journal of Solid State Elecrochemistry
Licensed Content Title	All-inorganic solid-state electrochromic devices: a review
Licensed Content Author	K. J. Patel et al
Licensed Content Date	Sep 28, 2016
Type of Use	Thesis/Dissertation
Requestor type	academic/university or research institute
Format	electronic
Portion	figures/tables/illustrations
Number of figures/tables/illustrations	1
Will you be translating?	no
Circulation/distribution	50000 or greater
Author of this Springer Nature content	no
Title	Doctoral student
Institution name	university of south florida
Expected presentation date	Jan 2022
Portions	Fig 1
Requestor Location	Mr. sharan indrakar [redacted] United States Attn: university of south florida
Total	**0.00 USD**

Below is copyright permission for Figure 2-8

CCC RightsLink®

My Orders | My Library | My Profile | Welcome sharankumar@usf.edu | Log out | Help

My Orders > Orders > All Orders

License Details

This Agreement between Mr. sharan indrakar ("You") and Elsevier ("Elsevier") consists of your license details and the terms and conditions provided by Elsevier and Copyright Clearance Center.

Print Copy

License Number	5098460084487
License date	Jun 29, 2021
Licensed Content Publisher	Elsevier
Licensed Content Publication	Electrochimica Acta
Licensed Content Title	A simplified all-polymer flexible electrochromic device
Licensed Content Author	David Mecerreyes,Rebeca Marcilla,Estibalitz Ochoteco,Hans Grande,Jose A. Pomposo,Ricardo Vergaz,Jose M. Sánchez Pena
Licensed Content Date	Sep 1, 2004
Licensed Content Volume	49
Licensed Content Issue	21
Licensed Content Pages	5
Type of Use	reuse in a thesis/dissertation
Portion	figures/tables/illustrations
Number of figures/tables/illustrations	1
Format	electronic
Are you the author of this Elsevier article?	No
Will you be translating?	No
Title	Doctoral student
Institution name	university of south florida
Expected presentation date	Jan 2022
Portions	Scheme 2.
Requestor Location	Mr. sharan indrakar [redacted] Attn: university of south florida
Publisher Tax ID	98-0397604

Below is copyright permission for Figure 2-9

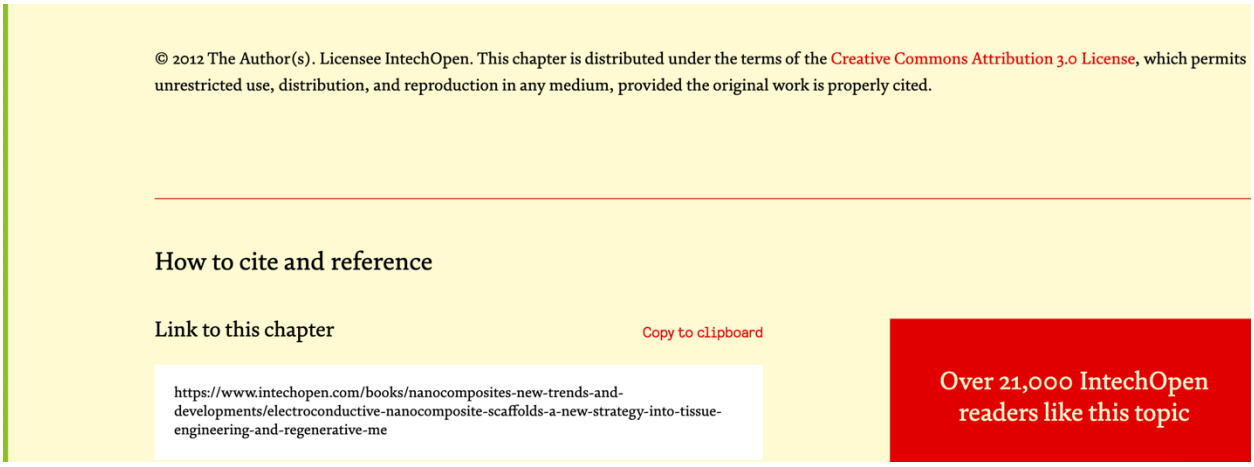

© 2012 The Author(s). Licensee IntechOpen. This chapter is distributed under the terms of the Creative Commons Attribution 3.0 License, which permits unrestricted use, distribution, and reproduction in any medium, provided the original work is properly cited.

How to cite and reference

Link to this chapter

Copy to clipboard

https://www.intechopen.com/books/nanocomposites-new-trends-and-developments/electroconductive-nanocomposite-scaffolds-a-new-strategy-into-tissue-engineering-and-regenerative-me

Over 21,000 IntechOpen readers like this topic

Below is copyright permission for Figure 2-10

Conducting polymers: a comprehensive review on recent advances in synthesis, properties and applications

Check for updates

Namsheer K[a] and Chandra Sekhar Rout [b]*[a]

Author affiliations

Abstract

Conducting polymers are extensively studied due to their outstanding properties, including tunable electrical property, optical and high mechanical properties, easy synthesis and effortless fabrication and high environmental stability over conventional inorganic materials. Although conducting polymers have a lot of limitations in their pristine form, hybridization with other materials overcomes these limitations. The synergetic effects of conducting polymer composites give them wide applications in electrical, electronics and optoelectronic fields. An in-depth analysis of composites of conducting polymers with carbonaceous materials, metal oxides, transition metals and transition metal dichalcogenides *etc.* is used to study them effectively. Here in this review we seek to describe the transport models which help to explain the conduction mechanism, relevant synthesis approaches, and physical

Article HTML

Article information

https://doi.org/10.1039/D0RA07800J

Submitted	11 Sep 2020
Accepted	25 Dec 2020
First published	03 Feb 2021

This article is Open Access

Citation *RSC Adv.*, 2021, **11**, 5659-5697

BibTex Go

Article type Review Article

Permissions Request permissions

Below is copyright permission for Figure 2-11

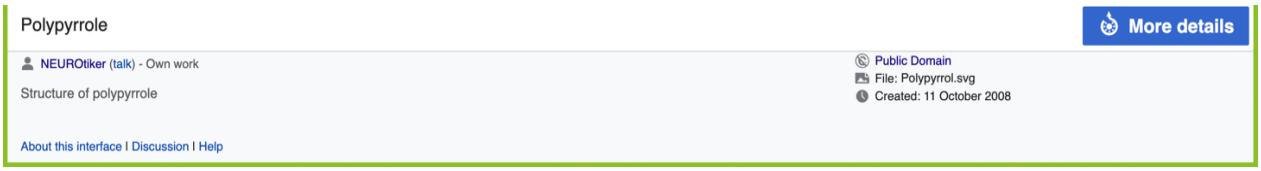

Polypyrrole

More details

NEUROtiker (talk) - Own work

Structure of polypyrrole

Public Domain
File: Polypyrrol.svg
Created: 11 October 2008

About this interface | Discussion | Help

Below is copyright permission for Figure 2-12

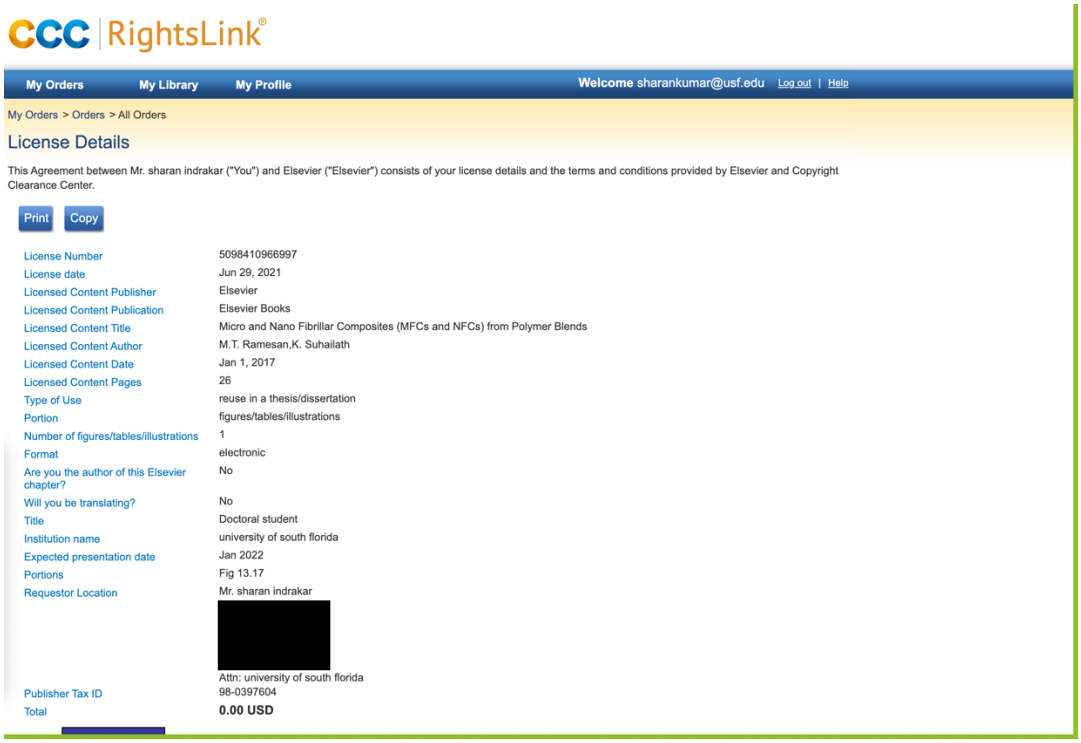

CCC | RightsLink®

My Orders | My Library | My Profile | Welcome sharankumar@usf.edu Log out | Help

My Orders > Orders > All Orders

License Details

This Agreement between Mr. sharan indrakar ("You") and Elsevier ("Elsevier") consists of your license details and the terms and conditions provided by Elsevier and Copyright Clearance Center.

Print Copy

License Number	5098410966997
License date	Jun 29, 2021
Licensed Content Publisher	Elsevier
Licensed Content Publication	Elsevier Books
Licensed Content Title	Micro and Nano Fibrillar Composites (MFCs and NFCs) from Polymer Blends
Licensed Content Author	M.T. Ramesan,K. Suhailath
Licensed Content Date	Jan 1, 2017
Licensed Content Pages	26
Type of Use	reuse in a thesis/dissertation
Portion	figures/tables/illustrations
Number of figures/tables/illustrations	1
Format	electronic
Are you the author of this Elsevier chapter?	No
Will you be translating?	No
Title	Doctoral student
Institution name	university of south florida
Expected presentation date	Jan 2022
Portions	Fig 13.17
Requestor Location	Mr. sharan indrakar [redacted] Attn: university of south florida
Publisher Tax ID	98-0397604
Total	**0.00 USD**

Below is copyright permission for Figure 2-13

ISSN 2175-9146

JATM JOURNAL OF AEROSPACE TECHNOLOGY AND MANAGEMENT

STRUCTURAL AND MORPHOLOGICAL CHARACTERISTICS OF POLYANILINE SYNTHESIZED IN PILOT SCALE

Maria Alice Carvalho Mazzeu, Lohana Komorek Faria, Andreza de Moura Cardoso, Adriana Medeiros Gama, Maurício Ribeiro Baldan, Emerson Sarmento Gonçalves

ABSTRACT

Polyanilines have many applications in Aerospace, especially in their doped form. Studies on their synthesis in a pilot scale can contribute to obtain products with desirable characteristics for such applications. The present study reports the chemical oxidative synthesis of polyaniline in pilot scale and different reaction times in order to determine if there are variations in the polyaniline structure, morphology and conductivity due to these synthesis conditions. It is very common to analyze these data for polymers obtained through bench scale. However, several parameters change the properties of final material in major scales, such as thermal, mechanic and diffusive variables. Therefore, the reaction time is the only variable into the 9 syntheses carried out, and polyaniline is obtained in a doped form, being dedoped with ammonium hydroxide and redoped with dodecylbenzenesulphonic acid. The doped and redoped samples were characterized by their molecular structure, thermal behavior, crystallinity and morphology. The electrical conductivity of redoped samples was determined. Some differences in the structure and morphology of doped and dedoped forms, identifying the doping structures, were reported. This paper aims to present the relationship between changes on structure and morphology of doped and undoped polyaniline obtained by the mentioned experiments. Furthermore, some addicts on conductivity are carried out. It was possible to contribute in order to obtain a more conductive polyaniline in pilot scale.

KEYWORDS

Polyaniline; Crystallinity; Morphology; Raman spectroscopy; Electrical conductivity.

FULL TEXT:

PDF

REFBACKS

There are currently no refbacks.

';

SHARE

This work is licensed under a Creative Commons Attribution 4.0 International License.

Below is copyright permission for Figure 2-14

CCC | RightsLink®

My Orders My Library My Profile Welcome sharankumar@usf.edu Log out | Help

My Orders > Orders > All Orders

License Details

This Agreement between Mr. sharan indrakar ("You") and Elsevier ("Elsevier") consists of your license details and the terms and conditions provided by Elsevier and Copyright Clearance Center.

Print Copy

License Number	5098411430016
License date	Jun 29, 2021
Licensed Content Publisher	Elsevier
Licensed Content Publication	Polymer
Licensed Content Title	Part-A: Synthesis of polyaniline and carboxylic acid functionalized SWCNT composites for electromagnetic interference shielding coatings
Licensed Content Author	T. David,Jyotsna Kiran Mathad,T. Padmavathi,A. Vanaja
Licensed Content Date	Oct 23, 2014
Licensed Content Volume	55
Licensed Content Issue	22
Licensed Content Pages	8
Type of Use	reuse in a thesis/dissertation
Portion	figures/tables/illustrations
Number of figures/tables/illustrations	1
Format	electronic
Are you the author of this Elsevier article?	No
Will you be translating?	No
Title	Doctoral student
Institution name	university of south florida
Expected presentation date	Jan 2022
Portions	Fig 1
Requestor Location	Mr. sharan indrakar [redacted] Attn: university of south florida

Below is copyright permission for Figure 2-15

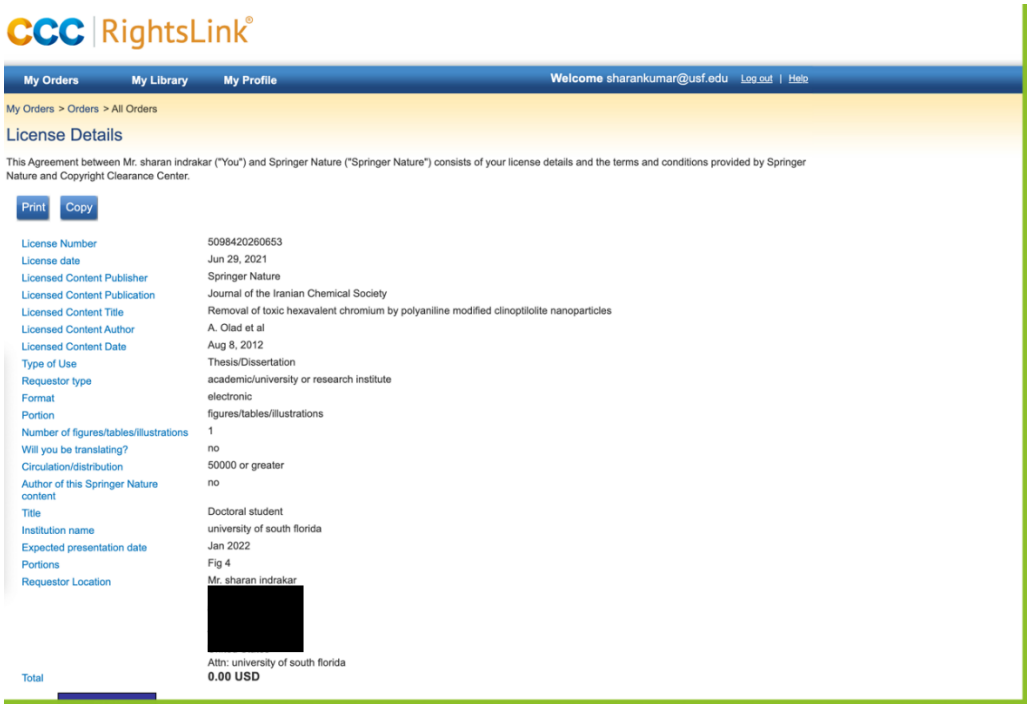

CCC RightsLink

My Orders | My Library | My Profile | Welcome sharankumar@usf.edu | Log out | Help

My Orders > Orders > All Orders

License Details

This Agreement between Mr. sharan indrakar ("You") and Springer Nature ("Springer Nature") consists of your license details and the terms and conditions provided by Springer Nature and Copyright Clearance Center.

Print Copy

License Number	5098420260653
License date	Jun 29, 2021
Licensed Content Publisher	Springer Nature
Licensed Content Publication	Journal of the Iranian Chemical Society
Licensed Content Title	Removal of toxic hexavalent chromium by polyaniline modified clinoptilolite nanoparticles
Licensed Content Author	A. Olad et al
Licensed Content Date	Aug 8, 2012
Type of Use	Thesis/Dissertation
Requestor type	academic/university or research institute
Format	electronic
Portion	figures/tables/illustrations
Number of figures/tables/illustrations	1
Will you be translating?	no
Circulation/distribution	50000 or greater
Author of this Springer Nature content	no
Title	Doctoral student
Institution name	university of south florida
Expected presentation date	Jan 2022
Portions	Fig 4
Requestor Location	Mr. sharan indrakar [redacted] Attn: university of south florida
Total	0.00 USD

Below is copyright permission for Figure 3-7 and Figure 3-8

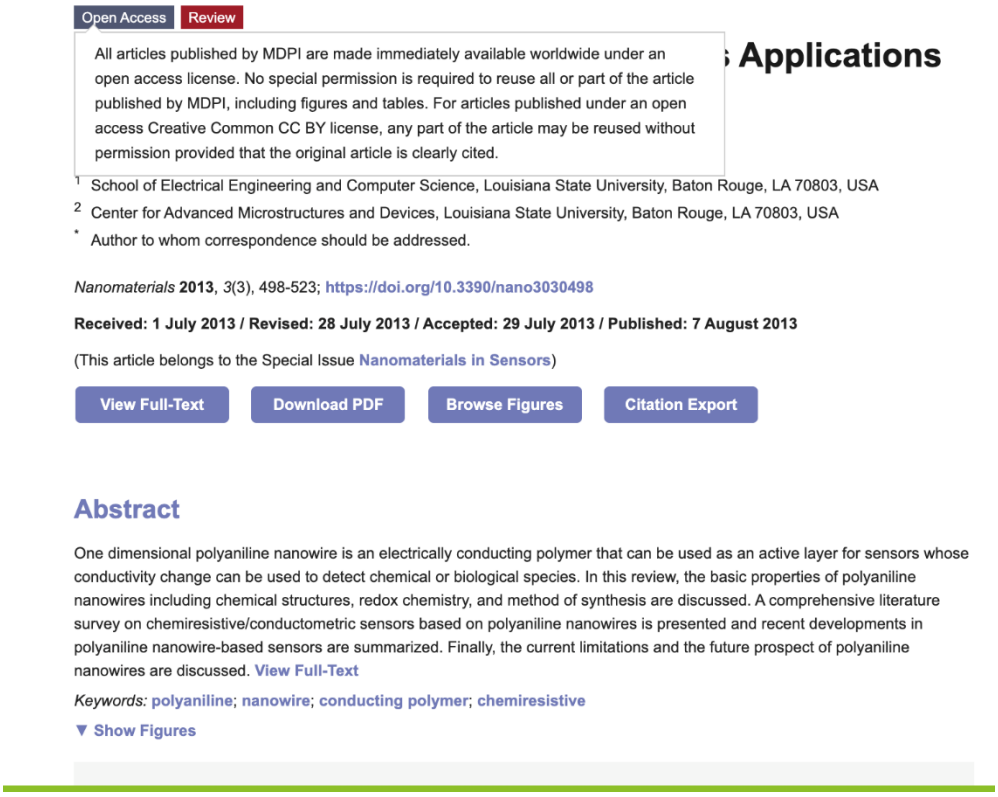

Open Access Review

All articles published by MDPI are made immediately available worldwide under an open access license. No special permission is required to reuse all or part of the article published by MDPI, including figures and tables. For articles published under an open access Creative Common CC BY license, any part of the article may be reused without permission provided that the original article is clearly cited.

Applications

[1] School of Electrical Engineering and Computer Science, Louisiana State University, Baton Rouge, LA 70803, USA

[2] Center for Advanced Microstructures and Devices, Louisiana State University, Baton Rouge, LA 70803, USA

* Author to whom correspondence should be addressed.

Nanomaterials **2013**, *3*(3), 498-523; https://doi.org/10.3390/nano3030498

Received: 1 July 2013 / Revised: 28 July 2013 / Accepted: 29 July 2013 / Published: 7 August 2013

(This article belongs to the Special Issue Nanomaterials in Sensors)

View Full-Text | Download PDF | Browse Figures | Citation Export

Abstract

One dimensional polyaniline nanowire is an electrically conducting polymer that can be used as an active layer for sensors whose conductivity change can be used to detect chemical or biological species. In this review, the basic properties of polyaniline nanowires including chemical structures, redox chemistry, and method of synthesis are discussed. A comprehensive literature survey on chemiresistive/conductometric sensors based on polyaniline nanowires is presented and recent developments in polyaniline nanowire-based sensors are summarized. Finally, the current limitations and the future prospect of polyaniline nanowires are discussed. View Full-Text

Keywords: polyaniline; nanowire; conducting polymer; chemiresistive

▼ Show Figures